

DOE/ET-53088-375

IFSR #375

Nonlinear Self-Focusing of Optical Beams in Plasmas

Taina-Kaisa Susanna Kurki-Suonio

Institute for Fusion Studies
The University of Texas at Austin
Austin, Texas 78712

May 1989

NONLINEAR SELF-FOCUSING OF
OPTICAL BEAMS IN PLASMAS

by

Taina-Kaisa Susanna Kurki-Suonio, LuK, FK

DISSERTATION

Presented to the Faculty of the Graduate School of

The University of Texas at Austin

in partial Fulfillment

of the Requirements

for the Degree of

DOCTOR OF PHILOSOPHY

THE UNIVERSITY OF TEXAS AT AUSTIN

May, 1989

To Olavi and Kaija Rönkkö,
my parents,
and Hannu,
my best friend.

Acknowledgements

There are numerous people, without whom this work would have never been completed. To begin with, I am very grateful for my advisor, Prof. Toshiki Tajima, for providing me with such a fascinating project to work on. And not only that, but he has also showed great foresight and generosity in sending me to various conferences and workshops, where I have been able to get the exposure to the scientific community that is necessary for any graduate student ever wishing to get a job. Last but not least, I also want to thank him for putting up with me.

At the Institute for Fusion Studies there are also other people who have greatly contributed to my progress in plasma physics. Prof. Wendell Horton, Jr., showed great patience in clarifying things to me when I started my studies in plasma physics by taking the relevant classes in the wrong order. I am forever grateful to Prof. Philip Morrison for his infectious enthusiasm, for his unbelievable generosity with his time, and for providing me with a positive kick right when everything appeared so grim to me.

My fellow students deserve a word of honor as well. Dr. Maurice Lebrun has been indispensable in helping me to understand the neurotic personality of computers. He can also take credit for being my favorite enemy — e.g. making faces was perfected to a form of art. Dr. David Booth probably cut my dissertation preparation time in half by letting me freely use his wonderful TEX-macros. He should also take the blame for my spreading rubber roaches around Drexel University. Neil Woodward, nowadays a Navy pilot to be, was

a super friend during the two lonely years in Austin. As a by-product I also learned some ball-room dancing. My officemates, Hamid Ouroua and Dr. Saad Eways deserve a word of thanks for providing a listening ear at the moments of utter frustration.

But the people pushing and pulling me through the graduate school are not limited to IFS. Prof. Bruce Palka (Dept. of Mathematics) and his wife MaryAnn, who had spent a year in Finland, were essential figures in helping us to cope with the cultural shock and adjustments that are unavoidable for students coming from countries like Finland, where the entire population numbers less than many of the U.S. cities. Unforgettable are also those good times we spent with Prof. Richard Matzner (Center for Relativity) and his family; how honored we felt when invited to Deborah's birthday party at the rollerskating rink as the only guests over ten years of age. Neither will the memories of a sailing trip on the not-so-calm Lake Travis fade very easily. I don't know what I would have done without Prof. John Cogdell (Electrical Engineering) and his wife Ann during this past year. Dr. and Mrs. Cogdell cheerfully adopted me as their house-kid every time I needed a place to stay — and those times were many. The love and warmth I felt at their home took me a long way. Prof. Cogdell also did a great favor in translating my fenglish into english.

I am also grateful for the prayer support of my good "god-father" Armond Cosman. (I feel quite committed to find use for that pretty thermal blanket Jo Cosman made for us). And how could I ever forget you, Vento Marme, my horse, who "came and took me"! Dr. Lolly Beaird and her ranch-family provided us with good Texas times filled with animals. The home of

Florence and Charles Freed in Lincoln, Massachusetts, was my safe haven from the big city during my year at M.I.T.

During my studies I have had several wonderful benefactors: My first year in United States was made possible by the generous fellowship from Rotary International. Rotaries did not only provide me with financial support but also with good fellowship. I was frequently invited to Rotary meetings where I was treated like a princess. I have especially fond memories of Dr. and Mrs. Dogerthy, who were my host family during that time. While at the University of Texas, my work has been connected with the Texas Accelerator Center, and I want to thank Dr. Russell Huson for his continuing support and encouragement. During the past two years I have had the honor of receiving the Zonta Amelia Earhart Fellowships. The ladies at Zonta, like the Rotaries, did not limit their support to finances. I have many delightful memories of visits to various Southwestern Zonta Clubs.

During this final year of my graduate studies I have experienced incredible generosity and hospitality at the Department of Physics and Atmospheric Science at Drexel University. I am forever grateful for Prof. Joan Centrella for establishing me as visiting faculty and allowing me to freely use all their wonderful equipment.

Finally, I want to honor the most important people in my life. No word of praise or gratitude could ever add up to express what I feel for them. My parents, Kaija and Olavi Rönkkö, did a remarkable job in trying to bring me up to be a decent person despite my being an only child. It was my father, Olavi

Rönkkö, who planted and cultivated in me the love and curiosity for science and nature. My mother, unfortunately, had her efforts wasted in trying to make me into a fine lady. Then there is Hannu, my husband and my love, without whom this work would have never been started, let alone finished. It is he, who not only never let me give up, but also has contributed most to my understanding of physics. His love, commitment and patience should be stamped on every page of this dissertation.

NONLINEAR SELF-FOCUSING OF OPTICAL BEAMS IN PLASMAS

Publication No. _____

Taina-Kaisa Susanna Kurki-Suonio, Ph.D.
The University of Texas at Austin, 1989

Supervising Professor: T. Tajima

Motivated by the need for a novel, ultra-high energy particle accelerator, the nonlinear interaction between a short optical pulse and plasma is studied. Assuming a steady state in which the ponderomotive force on the electrons is balanced by the electrostatic force, it is found that, for appropriate parameters, the inherent diffraction of a Gaussian beam can be balanced or overcome by plasma lensing brought about by the nonlinear effects. The critical quantity is determined to be the total power of the beam so that for values greater than $P_{cr} \approx 10^{10} (\frac{\omega_0}{\omega_p})^2 W$ the optical beam launched into a plasma will self-focus. A steady asymptotic beam profile solution of a solitary nature is also obtained. A phase-averaged particle simulation code appropriate for studying transport of optical beams in plasmas was developed and is described. The theoretical predictions obtained are tested using this simulation code, and a good qualitative agreement between theory and simulation is obtained.

Table of Contents

I. Introduction	1
1.1 A Brief History of Particle Accelerators	1
1.2 Laser-Plasma Accelerators	9
1.3 Problems In Laser-Plasma Schemes	12
II. Propagation of an electromagnetic wave	15
2.1 A Uniform Plane Wave In Vacuum	15
2.2 A Wave With Gaussian Intensity Profile in Vacuum	16
2.3 A Uniform Plane Wave in Plasma	17
2.4 A Wave With Gaussian Intensity Profile In Plasma	18
III. Self-Trapping of A Laser Beam in Plasma	30
3.1 Introduction	30
3.2 Model For Plasma Response	32
3.3 Evolution Equations for Laser Intensity Profile	33
3.4 Asymptotic Form of the Laser Profile	40
3.5 Hamiltonian Dynamics of Laser Light	52
3.6 Self-Focusing of Laser Light in Plasma	60

3.7 Plasma Fiber Accelerator	74
IV. Numerical Model for Self-Trapping	77
4.1 Motivation for a Numerical Model	77
4.2 Mathematical Formulation	81
4.3 Numerical Algorithm	92
4.4 Testing of the Code: The Rayleigh Spread and Self-Focusing . .	95
V. Numerical Experiments	104
5.1 Introduction	104
5.2 Asymptotic Form of a Self-Focused Laser Beam	105
5.3 Self-Focusing of a Laser Beam	109
5.3. 1 Experiments with Models for Electron Density	109
5.3. 2 Particle Simulation Experiments	116
VI. Summary and Discussion	127
VII. Appendices	132
VIII. References	138

Chapter I

Introduction

1.1 A Brief History of Particle Accelerators

The quest for the fundamental building blocks of matter has led to the birth of an entirely new field in physics, the accelerator physics. As the objects of interest grew smaller, the wavelength of the probe (whether a photon or a particle) also had to be reduced to achieve the required resolution. The wavelength associated with the motion of a particle decreases with increasing energy, and the first devices accelerating subatomic particles were developed in the early 1920's. These particle beams were used to carry out experiments advancing and testing the rapidly developing fields of atomic and nuclear physics.

The first devices were electrostatic accelerators in which a beam of subatomic particles gained energy by passing through a potential difference. The convention of measuring particle energies in units of electron volts (eV) is a relic from this time period: if an electron passes through a 500 Volt potential difference, its energy gain is 500 eV. The upper limit for electrostatic accelerators is set by sparking and material breakdown due to the high voltage. To achieve higher energies than a few MeV one would need to either let the particles traverse several such potential differences in succession, or discharge several high voltage capacitors in sequence across the accelerator tube. The latter scheme carries the name of Cockcroft-Walton generator¹ whereas the first scheme led to the development of the first circular particle accelerator.

In the early 1930's E.O. Lawrence of the University of California introduced the concept of forcing the particles into circular trajectories.^{2,3,4,5} Then, rather than having a long and expensive linear structure with several high voltage fields, only one alternating voltage field is necessary. Based on this idea the first cyclotron was constructed. A cyclotron consists of two D-shaped metal boxes ("dees") connected to the two outputs of a radio-frequency power supply and imbedded in a static magnetic field. The particles are injected from the center of the system. They accelerate in the gap between the dees due to the alternating potential difference, and inside the dees their trajectory is curved by the magnetic field. Thus the particles spiral outward as their energy increases.

The maximum energy gained in a cyclotron is limited by the relativistic effects. For relativistic energies the rate of increase in velocity is slower than the rate of change in energy and so the particles will run out of phase with the alternating voltage field. For heavy particles this does not happen until their energy is up to 20 MeV, but for the light weight electrons the dephasing becomes a problem already at 500 eV.

The first circular accelerator suitable for accelerating electrons was conceived and built by D.W. Kerst^{6,7} in 1940 at the University of Illinois. The device was called a betatron and it operates analogously to a transformer: the windings of an electromagnet act as the primary coil and the electron beam to be accelerated as the secondary coil. The guiding of the electrons on their curvilinear trajectories is provided by the slowly increasing magnetic field. Betatrons provide electrons with energies up to 70 MeV.

To produce even more energetic particle beams, E.M. McMillan⁸ from

the University of California and V.I. Veksler⁹ from the U.S.S.R. came up independently with two ideas for circumventing the relativistic limit on the cyclotron energies. The first idea was to synchronize the rf-voltage in a cyclotron, reducing its frequency according to the rotation frequency of the ion beam. This device was called synchrocyclotron, and the first such device was operated at the University of California in 1946 producing 350-MeV proton beams. The second idea was to increase the guiding magnetic field as a function of time. This resulted in the electron synchrotron. Since electrons with energies of 2 MeV or higher travel at velocities within 2% of the speed of light, they will circulate at practically constant velocity and so no frequency modulation is necessary. These devices have produced electron beams of up to 1 GeV. Combining the ideas of the electron synchrotron with the frequency modulation one obtains a device suitable for ion acceleration, the proton synchrotron. Such devices have produced proton beams of several hundred GeV.

Parallel with the evolution of the circular accelerators the linear accelerators were being developed. R. Wideröe¹⁰ of Germany built the first drift-tube linear accelerator in 1928. In a big glass cylinder he placed up to 30 metal cylinders lined up, with alternate cylinders connected electrically to a radio-frequency power supply. These cylinders are the drift tubes. Within a tube the particles do not feel any force, but between the tubes there is a potential difference and the particles will be accelerated. Because of the increasing velocity of the particles, the drift tubes down the line have to be longer than the first ones in order to phase the particles properly. Due to their inertia heavy ions are thus best suited for this kind of an accelerator.

The major limiting factor for a drift-tube linear accelerator is its phys-

ical size (and thus, its cost). However, the higher the frequency of the power supply, the shorter drift tubes one can have. Thus a significant improvement was obtained by replacing the glass cylinder by a large copper one. Coupling the copper cylinder to a high frequency power supply, it is excited and will act as a resonant cavity reversing the microwave field 200 million times in second. Linear accelerators of this type have been able to produce protons of up to 70 MeV.

In 1934 W.W. Hansen of Stanford, needing energetic electrons for producing x-rays, came up with the idea¹¹ that has persisted as the basic principle for linear accelerators for over fifty years now. Hansen suggested using a high voltage field oscillating at such a high frequency that there would not be time for material breakdown. Coupling a small copper cavity to a high frequency power supply would make the cavity oscillate so that the ends would be oppositely charged and alternate from positive to negative. One would line up these cavities and bore holes at the center of the end caps to let the electrons to fly through. The timing problem was solved by the utilization of a traveling radio wave, as Hansen described: "Now, if a particle be introduced onto the leftmost wave crest with a velocity equal to that of the wave, the particle will feel a steady force to the right and will, therefore, be accelerated. We have assumed that the wave velocity is controllable; let it be adjusted in such a manner that as the particle is accelerated, the wave is also, and at just the same rate, so that the particle will always ride the crest of the wave and will always feel an accelerating force. The particle will then gain energy at the expense of the field, and, if all the above can be made to happen as assumed and the numbers are favorable, we may have a practical means of accelerating charged

particles".¹¹ In 1947 the first Stanford traveling wave electron linear accelerator was in operation producing electrons of up to 6 MeV.

Today the original scheme of Hansen, although the principle is unaltered, is viewed somewhat differently. Currently this accelerator scheme is described as having an electromagnetic wave propagating in a waveguide. Due to the presence of conducting walls the field will have a longitudinal component necessary for particle acceleration. The waveguide is periodically loaded with irises, metal rings extending from the walls, to adjust the phase velocity of the wave which, in the absence of the irises, would be greater than the speed of light. A linear accelerator based on inductive accelerating field similar to the cyclotron is called an induction linac.

In Fig. 1.1¹² the energies available from different machines are shown in the form of a Livingstone diagram. Currently the best performers are seen to be circular accelerators combined with storage rings. Two features emerge clearly from the diagram. First, the envelope shows an exponential trend. During the past forty years or so, the energy of the particles produced by the particle accelerators has increased by a factor of 10^7 . Experimental high energy physics, despite this phenomenal progress, still lags behind theoretical high energy physics. High energy physicists are now dreaming of experiments with projectiles of energies beyond 10 TeV. But the second feature emerging from the diagram is that the energy increase for a specific accelerator scheme is very slow. The exponential envelope has been maintained mostly because of the appearance of new technologies. Thus it appears that, in order to keep up with the exponential trend, the future accelerators should be based on some new ideas. Another observation is that the most current high energy accelerators are colliders, as these achieve much higher energy in comparison with the fixed

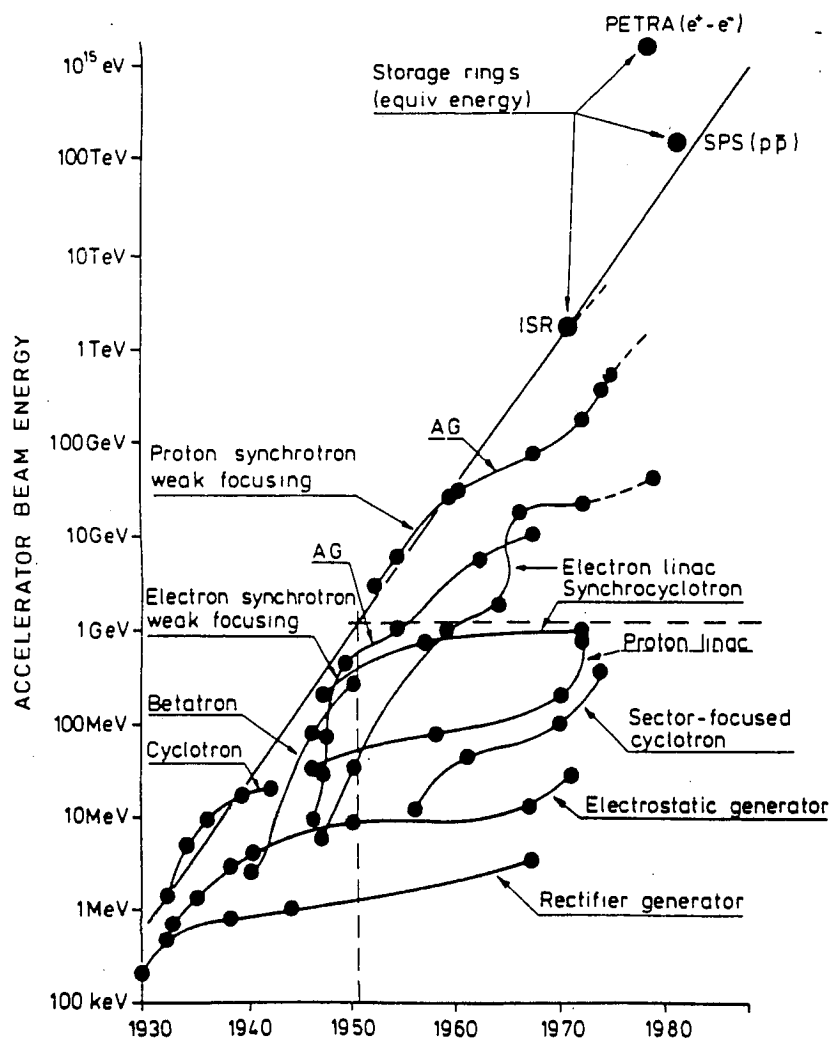


Fig. 1.1 - Livingstone Diagram - - The evolution of the high energy particle accelerators. (Adopted from J.L. Bobin¹²)

target accelerator. The reaction rate of colliders, however, is much smaller than that of fixed target accelerators.

One should also note that in the present energy level the physics of interest is such that lepton accelerators can look directly at the “interesting”

physics as reactions are more elementary, while hadron accelerators have to sift through an overwhelming amount of “garbage” reactions to uncover the interesting ones. Further, because hadrons are composed of constituent elementary particles such as quarks and gluons, the relative colliding energies for the constituent elementary particles are typically considerably less than the nominal hadron colliding energies. These disadvantages of hadron accelerators are compensated for by the fact that it is easier to accelerate hadrons to high energies than to do the same for leptons. The principal reason for this is that leptons are much more radiative than hadrons (and thus lose energy a lot more profusely), as the synchrotron radiation is proportional to the inverse of the fourth power of the mass of the particle. Hadron accelerators can thus be of a circular shape and the present limitation for the final energy in hadron accelerators is given by the strength of magnets and the radius (and the cost) of the accelerator ring. The accelerating gradient is not an issue here. The lepton accelerators, on the contrary, more and more tend to be linear. This is because the synchrotron radiation prevents further increase in the electron energy after 100 GeV or so on a circular trajectory. This upper limit on the electron energy for a circular collider will most probably be reached already in the LEP-2 collider and in TRISTAN. Presently the most important limitation on the energy gained in linear lepton accelerators is set by the accelerating gradient and the length of the devices.

To obtain electrons of energies of the order of 10 TeV or higher, the particle accelerator has to satisfy two requirements: (1) It has to provide a very intense longitudinal electric field (so that the accelerator can be built on a terrestrial scale), and (2) this field has to be able to interact with the electrons for a long time, which implies—in the case of ultra-relativistic particles—that the phase velocity of the accelerating wave has to be very close to the speed

of light (recall the quote from Hansen). The most effective linear accelerator technology at the moment can provide accelerating gradients of the order of $E_L \leq 20$ MV/m. Thus, in order to produce 10 TeV electrons, the length of a conventional accelerator would be at least 500 km. Therefore it is clear that a novel acceleration scheme is necessary before one can reach the desired energy region.

Currently the most intense sources of electromagnetic radiation are provided by lasers. There are, however, limiting factors for the accelerating gradients that can be utilized in a conventional linear accelerator consisting of a large number of resonant cavities. These include

- breakdown of the residual gas in the cavities
- surface heating
- plasma limit (i.e. superficial ionization due to high vacuum fields)

The onset of all the above processes is frequency dependent; the higher the frequency, the higher the acceptable accelerating gradient. Thus the accelerator technology has been slowly moving towards optical frequencies — another reason to consider lasers as a source for accelerating gradients.

Moving up in frequency cannot, however, totally eliminate the problem of material breakdown. If accelerating gradients of the order of 10 GeV/m or higher are ever to be used, that would be equal to $1 \text{ eV}/\text{\AA}$ which is high enough to inevitably modify the electron wavefunctions in the atoms of the surrounding medium thus leading to material breakdown. Apparently there is only one way to avoid the plasma limit and related problems — to start up with a plasma.

Thus, in the quest for an ultra high energy particle accelerator, it is

well worth while to investigate what the laser-plasma combination has to offer. There are various methods proposed;^{13 -21} in some only lasers are used (e.g. an inverse Cerenkov device proposed by Shimoda in 1962, an ink jet device proposed by R. Palmer¹³ in 1972), and in others plasma only is used (e.g. the wakefield accelerator^{15,16,17,18}). In this work, however, we shall concentrate on schemes based on the nonlinear interaction of a laser beam (or beams) with a plasma.

1.2 Laser-Plasma Accelerators

The most developed of the particle accelerator ideas based on the interaction of laser beams and plasma is the beat wave accelerator.^{22,23,24} Besides extensive analytical and numerical work done on the scheme,^{25,26,27,28,29} there is also a fair amount of experimental evidence favoring the soundness of the principle.^{30,31,32} To show at least one possible mechanism of turning the transverse electric field provided by the laser beam into a longitudinal accelerating gradient, we will now briefly present the basic operating principles of a beat wave accelerator .

The plasma we are interested in here consists of two particle species of opposite electric charge, electrons and ions (most likely protons). In equilibrium the densities are uniform and the medium is electrically neutral: $n_i = n_e = n_0$. The electron component of the plasma, due to its minute inertial mass, responds readily to any kind of external electromagnetic perturbation. As a result the electron density will oscillate around the equilibrium value. These oscillations propagate as longitudinal waves with frequency close to the so-called electron plasma frequency, $\omega_p = \sqrt{\frac{4\pi e^2 n_0}{m_e}}$. In what follows we shall call this quantity simply the plasma frequency for brevity, and specify separately if that for the ions is needed. Due to their longitudinal nature, these waves could be used to

accelerate particles.

In a beat wave accelerator the plasma waves are generated by resonant beating of two electromagnetic waves.³³ If the beat frequency and wavenumber,

$$\begin{aligned}\Delta\omega &= \omega_0 - \omega_1 \\ \Delta k &= k_0 - k_1 ,\end{aligned}\tag{1.1}$$

coincide with those characteristic of the plasma wave,

$$\begin{aligned}\Delta\omega &= \omega_p \\ \Delta k &= k_p ,\end{aligned}\tag{1.2}$$

the two laser beams will resonantly excite a plasma wave in the plasma. A rough estimate for the maximum field strength of this wave can be obtained by considering the maximum electron density available for the excitation. Writing the electron density in the form $n_e = n_0 + \delta n_e$, where δn_e is the density perturbation, and assuming that the time scale is short enough to ensure the immobility of the ions ($n_i = n_0$), we may write Gauss' law as

$$k_p E_L = -4\pi e \delta n_e ,\tag{1.3}$$

which yields

$$|E_L| = \frac{m}{ek_p} \omega_p^2 \frac{\delta n_e}{n_0} \approx \frac{mc}{e} \omega_p \frac{\delta n_e}{n_0} ,\tag{1.4}$$

where δn_e is the perturbation in the electron density. The electron density perturbation cannot exceed the equilibrium density and thus the maximum field strength is bounded by the extremum case, $\delta n_e = n_0$:

$$|E_{L,max}| \leq \frac{mc\omega_p}{e} = \left(\frac{\omega_p}{c}\right) \left(\frac{mc^2}{e}\right) = \left(\frac{\omega_p}{c}\right) \times 0.511 \text{ MV} \approx \sqrt{n_0} \frac{V}{cm} ,\tag{1.5}$$

where the electron plasma density n_0 is given in units of cm^{-3} . Therefore the desired accelerating gradient of 1 GeV/m could be attained by using plasma

of density 10^{18} cm^{-3} and, under idealistic conditions, the acceleration distance for electrons with the final energy of the order of 10 TeV would be of the order of ten kilometers.

But as mentioned earlier, a high accelerating gradient is not enough. The second requirement for the future linear accelerator is that the accelerating particles have to be able to phase-lock with the accelerating field so that they can gain energy from the wave over a relatively long distance. The phase velocity of the plasma wave is given by

$$v_{ph} = \frac{\omega_p}{k_p} = \frac{\omega_0 - \omega_1}{k_0 - k_1} . \quad (1.6)$$

If the plasma is sufficiently underdense or, equivalently, the laser frequencies ω_0 and ω_1 are high enough compared to the density-dependent plasma frequency, ($\omega_p/\omega_i \ll 1$ for $i=0,1$), the phase velocity can be brought very close to the speed of light:

$$v_{ph} = \frac{\Delta\omega}{\Delta k} \longrightarrow \frac{d\omega}{dk} = \frac{c}{\sqrt{1 - \frac{\omega_p^2}{\omega_0^2}}} , \quad (1.7)$$

where we have used the dispersion relation for electromagnetic waves in plasma, $\omega_0 = \sqrt{\omega_p^2 + c^2 k_0^2}$. The phase velocity of the plasma wave is thus, under these circumstances, equivalent to the group velocity of the electromagnetic waves.

Assuming now that we have produced a plasma wave with a very large amplitude and moving at phase velocity very close to the speed of light, we shall find what is the maximum energy gained by the electrons accelerated by the wave. This is best done by making a Lorentz-transformation specified by $\beta_p = \frac{v_{ph}}{c} = \sqrt{1 - \omega_p^2/\omega_0^2}$ and $\gamma_p = \frac{\omega_0}{\omega_p}$ to the frame moving with the plasma wave. This is useful because in the laboratory frame the acceleration corresponding to the maximum energy gain takes place over a long distance until the electrons run

out of phase with the wave. In the wave frame, however, this all corresponds to a distance of one half of the laser wavelength during which the electron experiences the maximum potential drop. The maximum potential drop in the laboratory frame is

$$e\varphi_{max} = 2e \int_0^{\lambda_p/2} E_{L,max} dz \approx \frac{m\omega_p c}{e} \lambda_p \approx mc^2, \quad (1.8)$$

which, Lorentz-transformed to the wave frame, yields

$$e\varphi'_{max} = m\gamma_p c^2, \quad (1.9)$$

where the prime stands for the moving frame. This is the maximum energy gained by the electrons in the wave frame, $W'_{max} = e\varphi'_{max}$. The corresponding momentum is

$$p'_{max} = \frac{1}{c} \sqrt{W'^2_{max} - m^2 c^4} = m\beta_p \gamma_p c. \quad (1.10)$$

Thus, transforming back to the laboratory frame,

$$\begin{pmatrix} W_{max} \\ cp_{max} \end{pmatrix} = \begin{pmatrix} \gamma_p & \beta_p \gamma_p \\ \beta_p \gamma_p & \gamma_p \end{pmatrix} \begin{pmatrix} m\gamma_p c^2 \\ m\beta_p \gamma_p c^2 \end{pmatrix} = \begin{pmatrix} m\gamma_p^2 c^2 (1 + \beta_p^2) \\ 2mc^2 \gamma_p^2 \beta_p \end{pmatrix}, \quad (1.11)$$

the maximum energy gained by the electrons is

$$W_{max} = (1 + \beta_p^2) m\gamma_p^2 c^2 \approx 2 \left(\frac{\omega_0}{\omega_p} \right)^2 mc^2, \quad (1.12)$$

and the maximum energy is seen to increase with increasing laser frequency.

1.3 Problems In Laser-Plasma Schemes

The beat wave accelerator scheme, as described above, is a very attractive candidate for an ultra high energy particle accelerator. However, the

'there is no free lunch' -principle applies equally well in physics as in any other field that has a touch-point with real life. The beat wave accelerator , as well as all the other novel accelerator concepts based on plasmas and/or lasers, has some inherent problems^{34,25,26} that need to be addressed.^{35,36} Many of these problems are specific of a certain scenario, but there is one problem that faces all the schemes utilizing lasers: that of the finiteness of the active interaction region of the laser beam and plasma. To produce very high field intensities, the laser beam has to be focused to a very small spot. In free space this spot corresponds to the waist of the beam, and the focusing of the beam would be immediately followed by a defocusing phase. In the case of a beam with a Gaussian intensity profile, $E = E_0 e^{-r^2/w^2}$, this defocusing is characterized in free space by the so-called Rayleigh range, $Z_R = \frac{1}{2} k_0 w_0^2$, after which the beam radius w has increased by a factor of $\sqrt{2}$. Here k_0 stands for the wavenumber of the wave and w_0 is the initial beam radius. This spreading of the beam corresponds to inevitable decrease in the intensity as the beam propagates. In a nonlinear dielectric medium like plasma, however, there is a possibility of self-focusing of the laser beam.

It is this problem of the decaying laser intensity that we wish to address in this dissertation. The analysis is not directly tied to any specific accelerator scheme but the plasma fiber accelerator,³⁷ which will be introduced in the end of Chapter III, seems to emerge naturally from the work. Chapter II serves as an introduction to the problems faced as a finite beam propagates in plasma. In this context we also give a brief summary of the work done earlier on the nonlinear self-focusing of laser beams in plasmas. In Chapter III we study analytically the possible self-focusing of a very short laser pulse with a Gaussian intensity profile in plasma. We also obtain a beam profile that should be stationary (i.e. no diffraction, no self-focusing) as it propagates in plasma. In Chapter IV we

describe a numerical particle simulation code that we constructed to study the transport of laser beams in plasma. In Chapter V the preliminary results from the simulation code, relevant to the earlier work presented here, are presented. Chapter VI consists of conclusions and discussion.

The original work in this dissertation is presented in Chapters 3, 4 and 5.

Chapter II

Propagation of an electromagnetic wave

2.1 A Uniform Plane Wave In Vacuum

An electromagnetic plane wave propagates in vacuum at the speed of light. This, as well as the dispersion relation, follows directly from the relevant Maxwell's equations:

$$\begin{aligned} c\nabla \times \mathbf{E} &= -\frac{\partial \mathbf{B}}{\partial t} \\ c\nabla \times \mathbf{B} &= \frac{\partial \mathbf{E}}{\partial t} . \end{aligned} \quad (2.1)$$

An electromagnetic plane wave in vacuum can be represented in terms of its Fourier components:

$$\mathbf{E}, \mathbf{B} \propto e^{i(k_0 z - \omega_0 t)} , \quad (2.2)$$

where the z -axis is chosen as the direction of propagation, and the electric and magnetic fields are then oriented in the x - and y - directions, respectively. The Maxwell's equations now become

$$\begin{aligned} cik_0 E &= i\omega_0 B \\ -cik_0 B &= -i\omega_0 E , \end{aligned} \quad (2.3)$$

and since, in the Gaussian units we are using, the magnitude of the electric and magnetic field strength is the same, the dispersion relation for electromagnetic plane waves in vacuum is found to be

$$\omega_0 = ck_0 . \quad (2.4)$$

According to the Huygen's principle, every point on the wavefront acts as an instantaneous point source, and since the intensity profile of a plane wave

is flat, all these point sources are uniformly distributed all along the wave front, and the wave will propagate without distortion.

2.2 A Wave With Gaussian Intensity Profile in Vacuum

A more interesting situation arises if the wave propagating in vacuum has a nontrivial intensity profile in the radial direction. For a wave with intensity maximum near the axis of the beam, the point sources in the central region are more intense than those lying further out along the wave front. Therefore the outward component of a spherical wave emitted in the central region will be only partially cancelled by the spherical waves emitted further out, and the phase front will start to curve. This leads to a diverging beam. In the case of a Gaussian intensity profile,

$$I = I_0 e^{-r^2/w_0^2}, \quad (2.5)$$

this diverging is called Rayleigh spreading. We will concentrate here on a Gaussian beam profile because the basic mode of a laser beam is usually represented by a Gaussian beam. Because of the nonuniform initial state, the Fourier analysis used above is not applicable here, and we have to resort to other means to find the behaviour of the beam from the Maxwell's equations. From the wave equation it can be derived (see, *e.g.*, Demtroder³⁸ ; we will go through this derivation later for the two dimensional case) that for Rayleigh spreading the evolution of the beam radius is given by

$$w(z) = w_0 \sqrt{1 + z^2/z_R^2}, \quad z_R \equiv \frac{1}{2} k_0 w_0^2, \quad (2.6)$$

where z_R is the so-called Rayleigh range. The phase shift ψ for Rayleigh spreading is given by

$$\psi = \arctan(z/z_R) - \frac{k_0 r^2}{2R}, \quad R \equiv z(1 + z_R^2/z^2). \quad (2.7)$$

For a non-dissipative system the total power remains invariant: $P_0 \propto I\omega^2$. Therefore the intensity of the wave reduces according to

$$I(t) = \frac{I_0}{1 + z^2/z_R^2} . \quad (2.8)$$

2.3 A Uniform Plane Wave in Plasma

Replacing the vacuum by a medium (in our case a plasma) with non-trivial dielectric properties will add further complexity to the propagation of an electromagnetic beam. The dispersion relation for a plane wave will be modified due to the induced plasma current. The relevant equations are the same as in the vacuum case except that now we have to include a source term due to the plasma current:

$$\begin{aligned} c\nabla \times \mathbf{E} &= -\frac{\partial \mathbf{B}}{\partial t} \\ c\nabla \times \mathbf{B} &= \frac{\partial \mathbf{E}}{\partial t} - 4\pi \mathbf{J} . \end{aligned} \quad (2.9)$$

Taking the curl of the first of Eqs. (2.9) and utilizing the second, we arrive at the wave equation for an electromagnetic wave in plasma:

$$c^2 \nabla \times (\nabla \times \mathbf{E}) = -\frac{\partial^2 \mathbf{E}}{\partial t^2} - 4\pi \frac{\partial \mathbf{J}}{\partial t} . \quad (2.10)$$

Assuming that the electromagnetic wave is a plane wave propagating in a uniform plasma, we can apply the Fourier analysis as we did before:

$$-c^2 \mathbf{k}_0 \times (\mathbf{k}_0 \times \mathbf{E}) = \omega_0^2 \mathbf{E} + 4\pi \frac{\partial \mathbf{J}}{\partial t} , \quad (2.11)$$

and since the electromagnetic field components are transverse to the direction of propagation of the wave, $\mathbf{k}_0 \cdot \mathbf{E} = 0$, the equation simplifies into the form

$$(\omega_0^2 - c^2 k_0^2) \mathbf{E} = 4\pi \frac{\partial \mathbf{J}}{\partial t} . \quad (2.12)$$

A good approximation for the plasma current under the influence of a uniform plane wave is given by keeping only the electric field in the equation for the electron velocity (ions, being very massive, can be taken as stationary in the first approximation):

$$\begin{aligned}\frac{\partial \mathbf{J}}{\partial t} &\approx -en_0 \frac{\partial \mathbf{v}}{\partial t} \\ &\approx \left(\frac{e^2 n_0}{m}\right) \mathbf{E},\end{aligned}\tag{2.13}$$

where e = elementary charge, n_0 = equilibrium plasma density, m = electron mass, and we have assumed non-relativistic electrons. Relativistic effects will be discussed later. The wave equation now becomes

$$(\omega_0^2 - c^2 k_0^2) \mathbf{E} = \left(\frac{4\pi e^2 n_0}{m}\right) \mathbf{E},\tag{2.14}$$

and the requirement for non-trivial solutions ($\mathbf{E} \neq 0$) for the equation leads to the dispersion relation for electromagnetic waves in plasma:

$$\omega_0^2 = \omega_p^2 + c^2 k_0^2,\tag{2.15}$$

where $\omega_p^2 = 4\pi e^2 n_0 / m$ is the electron plasma frequency.

The qualitative difference introduced by the presence of plasma is the appearance of a cut-off frequency at the plasma frequency :

$$\omega_{\text{cut}} = \omega_p,\tag{2.16}$$

so that waves with frequencies less than ω_{cut} will not be able to propagate in plasma but are damped exponentially:

$$E \propto e^{-\kappa z}, \quad \kappa = \frac{\sqrt{\omega_p^2 - \omega_0^2}}{c}.\tag{2.17}$$

2.4 A Wave With Gaussian Intensity Profile In Plasma

Non-linear Self-Focusing

The linearized Maxwell's equations (i.e. taking only the first order contribution of the fields on the plasma current) used above are not appropriate in studying the propagation of a beam with non-uniform intensity profile in plasma because the nonlinear interaction between the beam and the plasma is crucial.³⁹ This can be understood when we look at the electrons of the plasma under the influence of a laser field. An electron located near the beam axis is kicked outward by the large amplitude transverse electric field of the laser beam. As the beam propagates, the direction of the field rotates and soon the electron feels an opposite force pulling it back towards its original position. However, since at this instant the electron is located further away from the intensity maximum, the restoring force is not quite as strong as the one bringing the electron out. Thus there will be a net increase in its outward velocity and the electron will not return back to its original position. Therefore, after several laser oscillation periods, the electron will have drifted outward and the electron density—together with the dielectric properties of the plasma—gets modified.

Mathematically this net drift of electrons can be viewed as a result of a second-order force, called the ponderomotive force,⁴⁰ acting on the electrons. In the case of a circularly polarized electromagnetic wave with nonuniform intensity profile the ponderomotive force is given by (see Appendix A)

$$\mathbf{F}_p = mc^2 \nabla \sqrt{1 + \frac{e^2 E^2}{m^2 \omega_0^2 c^2}}. \quad (2.18)$$

The ponderomotive force does not depend on the sign of the charge of the particle, and thus the ions will eventually follow the electrons provided the

laser pulse is long enough.

The end result of the outward drift of electrons is that a density depression is produced in the central region. According to the dispersion relation for electromagnetic waves in plasma, the phase velocity of the wave depends on the plasma density:

$$v_{ph} = \frac{\omega_0}{k_0} = \frac{\sqrt{\omega_p^2 + c^2 k_0^2}}{k_0} = c \sqrt{1 + \frac{4\pi e^2}{mc^2 k_0^2} n_e}. \quad (2.19)$$

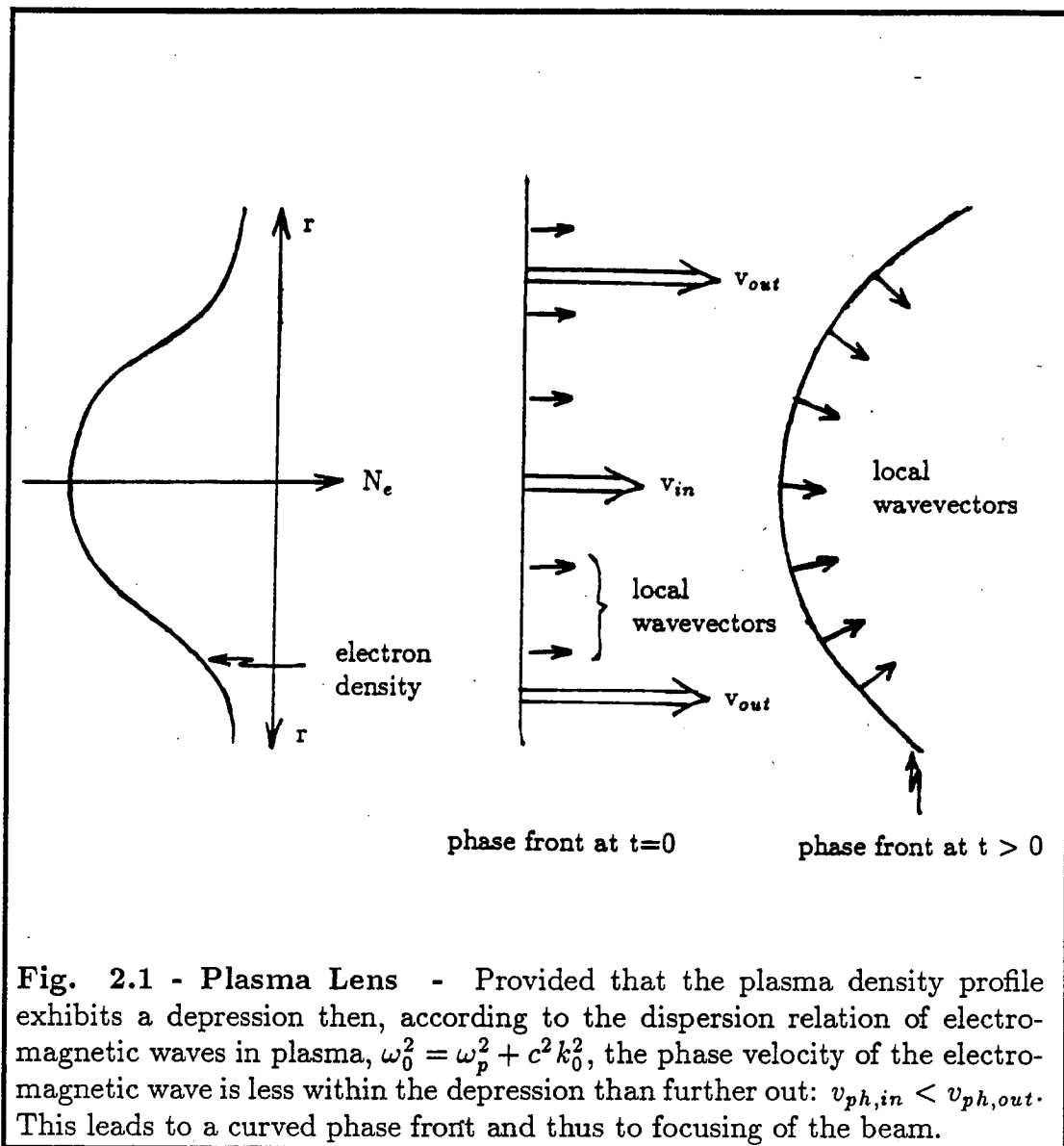
Thus the phase velocity will be lower in the central region, where the electron density is suppressed, than in the outer regions where the density is further enhanced. This leads to a curving wave front as indicated in Fig. 2.1. This curving is directed in opposite direction to that taking place in the Rayleigh spreading, and therefore the nonlinear interaction between the laser beam and the plasma has the potential to lead to focusing of the laser beam. It is called nonlinear self-focusing⁴¹ because it is the laser beam that produces the density perturbation that acts back on the beam.

One way of describing self-focusing mathematically is to say that the dielectric properties of the plasma are altered in such a way that the modified electron density profile acts as a convex lens (sometimes referred to as "plasma lens"). The dielectric function of a plasma is given by

$$\epsilon = 1 - \omega_p^2 / \omega_0^2. \quad (2.20)$$

Since ω_p depends on the electron density, modifying the density profile will also modify the dielectric function of the plasma.

It is important to notice that, although very suggestive, the ponderomotive force is not the only mechanism for self-focusing. Differences in thermal



pressure can modify the electron distribution, leading to thermal self-focusing⁴² in qualitatively the same way as in the ponderomotive self-focusing: An intense electromagnetic wave induces heating in plasma. The temperature increases most in the central region and leads to hydrodynamic expansion there. As in the case of ponderomotive self-focusing, this rarefied region acts as a convex lens focusing the beam.

Furthermore, the plasma frequency depends not only on the electron density but also on the electron mass: $\omega_p^2 \propto 1/m$. Therefore, increasing the electron mass has qualitatively the same effect on the plasma dielectric function as lowering the electron density. This process is called relativistic self-focusing and it is brought about when the electrons oscillating in the laser field are accelerated to relativistic velocities during one oscillation period. Formally this can be seen when we include the relativistic effects in the expression for the plasma current in Eq. (2.13) :

$$\begin{aligned} \frac{d\mathbf{p}}{dt} &\approx -e\mathbf{E}, \quad \mathbf{v} = \frac{\mathbf{p}}{m\gamma}, \gamma = \sqrt{1 + p^2/m^2c^2} \\ \Rightarrow \frac{\partial \mathbf{J}}{\partial t} &\approx \left(\frac{e^2/n_0}{m\gamma} \right) \mathbf{E} \\ \Rightarrow \omega_0^2 &= \frac{\omega_{p0}^2}{\gamma} + c^2 k_0^2, \end{aligned} \tag{2.21}$$

where ω_{p0} is defined using the rest mass of the electrons. Relativistic self-focusing differs qualitatively from the ponderomotive and thermal self-focusing in that it does not require bulk electron motion to modify the plasma dielectric function. Therefore, with appropriate laser and plasma parameters, the relativistic self-focusing can take place almost instantaneously (in the time scale of a laser oscillation period), whereas in ponderomotive and thermal self-focusing there will be a delay before the electron density is reshaped to bring about the lens effect.

Sometimes the self-focusing of an optical beam in plasma is referred to as self-focusing instability because of the feed-back nature of the process. For instance, in the case of ponderomotive self-focusing, the intense beam expels particles from the central region thus modifying the dielectric constant in such a way that the beam starts to focus. The ponderomotive force is thereby reinforced, more particles are expelled, and the dielectric constant is further

severed leading to even more tightly focused beam, and so on. A similar feedback loop takes place in relativistic and thermal self-focusing. This physical picture misled the early investigators to believe that the self-focusing instability would eventually cause the beam to collapse. However, this is not the case. For instance, in the case of ponderomotive self-focusing, as more and more particles are expelled, the beam will eventually be propagating in an evacuated channel where the nonlinear plasma effects necessary for further focusing are absent.^{43,44,45} At that point the beam starts Rayleigh spreading as explained in the beginning of this chapter.

The above, mostly phenomenological and over-simplified introduction to the evolution of a laser beam in plasma can lead one to a conclusion that the problem of non-linear self-focusing of a laser beam is straightforward and well understood. This is, however, not the case. The interaction between a laser beam and plasma is highly nonlinear and even non-local, and the situation is made even worse by the statistical nature of plasma as a many-body system. Therefore, each of papers published on the subject of laser self-focusing in plasmas addresses the problem only under some very specific conditions chosen typically in such a way that only one mechanism producing self-focusing can be considered. We will now briefly present the highlights of the work previously performed on the subject.

F.W. Perkins and E.J. Valeo⁴⁶ addressed the problem of linear thermal self-focusing in both underdense and overdense bounded plasmas by studying the stability of small scale perturbations using linearized fluid equations in slab geometry. It was discovered that thermal self-focusing can take place even for weak incident powers provided that the plasma is highly collisional. R.S. Craxton and R.L. McCrory⁴⁷ carried out a two-dimensional hydrodynamics simu-

lation to study thermal self-focusing of laser beams in plasmas with long scale lengths. They observed whole-beam self-focusing when the beam diameter was less than approximately one-half of the plasma scale length, and in underdense plasma a low density channel was seen to develop. They also concluded that thermal self-focusing is less likely to occur in an initially hot (and thus weakly collisional) plasma.

Self-focusing due to ponderomotive force (as full exponential nonlinearity) was first studied analytically by C.E. Max.⁴³ Using a fluid model (obtained by assuming quasineutrality) for the electron current, and assuming that the beam retains its Gaussian shape at all times, she found that for any incident intensity it is possible to find such a beam radius that self-focusing will take place. The study also indicated that the self-focused beam will oscillate in radius after initial focusing rather than reach a catastrophic focus, as had been speculated earlier. C. Joshi, C.E. Clayton and F.F. Chen³⁰ observed resonant ponderomotive self-focusing of laser light experimentally. The ponderomotive force of a plasma wave is much larger than that of the laser beam, as can be seen from the expression derived for the ponderomotive force in Appendix A:

$$\begin{aligned} F_p(\text{laser}) &= -\frac{1}{2} \frac{e^2}{m\omega_0^2} \frac{1}{\sqrt{1 + \frac{e^2 E_0^2}{m^2 \omega_0^2 c^2}}} \nabla E_0^2 \\ F_p(\text{plasmon}) &= -\frac{1}{2} \frac{e^2}{m\omega_p^2} \frac{1}{\sqrt{1 + \frac{e^2 E_p^2}{m^2 \omega_p^2 c^2}}} \nabla E_p^2 \end{aligned} \quad (2.22)$$

so that for nonrelativistic ($e^2 E^2 / m^2 \omega^2 c^2 \ll 1$) field amplitudes

$$\begin{aligned} F_p(\text{laser}) &\approx -\frac{1}{2} \frac{e^2}{m\omega_0^2} \nabla E_0^2 \\ F_p(\text{plasmon}) &\approx -\frac{1}{2} \frac{e^2}{m\omega_p^2} \nabla E_p^2 \end{aligned} \quad (2.23)$$

where E_0 is the amplitude of the laser wave, and E_p is the amplitude of the plasma wave. From Poisson's equation one obtains an estimate for the plasma wave amplitude in terms of the electron density perturbation δn_e caused by the laser wave:

$$E_p \approx \frac{4\pi e}{k_p} \delta n_e, \quad (2.24)$$

where k_p is the wave number of the plasma wave. Thus the ratio of the ponderomotive force of the plasma wave to the laser ponderomotive force is

$$\left| \frac{F_p(\text{plasmon})}{F_p(\text{laser})} \right| = \frac{\omega_0^2}{\omega_p^2} \left(\frac{4\pi e}{k_p} \right)^2 \frac{\delta n_e^2}{E_0^2} = \left(\frac{\delta n_e}{n_0} \right)^2 \left(\frac{v_\phi}{v_q} \right)^2, \quad (2.25)$$

where $v_\phi \approx c$ is the phase velocity of the plasma wave, and v_q , the so-called quivering velocity, is a measure of the laser intensity, $v_q \equiv \frac{eE_0}{m\omega_0}$, that will be shortly discussed in more detail. Joshi, Clayton and Chen³⁰ noted that this ratio of the ponderomotive forces can be very large; as a representative case they showed that for a density perturbation of $\frac{\delta n_e}{n_0} = 1\%$ and laser with wavelength of $10.6 \mu m$ and intensity of 10^{10} W/cm^2 , the ratio is over a hundred. Thus, to benefit of this enhanced self-focusing, they impinged laser light containing two frequencies, ω_1 and ω_2 , on a plasma and resonantly excited a plasma wave when the plasma density had a proper value to allow for the resonance condition: $\omega_p = \omega_1 - \omega_2$. In their experiment Joshi, Clayton, and Chen observed self-focusing as a dramatic increase (up to 10^5 -fold) in the central intensity.

C.E. Max, J. Arons and A.B. Langdon⁴⁸ addressed the problem of relativistic self-focusing by performing linear stability analysis on the system while treating the plasma as a cold, uniform fluid with fixed ion density. (Notice, that in the studies described above both the electrons and ions were similarly subject to the ponderomotive force as implied by the assumption of quasineutrality. Thus the characteristic time scales in them were long, being dominated by the

ion dynamics). Max, Arons and Langdon⁴⁸ discovered that, under their approximations, even weak $\frac{v^2}{c^2}$ relativistic corrections could produce self-focusing. They also concluded, quite credibly, that at high intensities the ponderomotive effects (when acting on *both* electrons *and* ions as a single fluid) are negligible compared to the relativistic effects. D.A. Jones, E.L. Kane, P. Lalouis, P. Wiles, and H. Hora⁴⁹ constructed a two-dimensional time-dependent laser-plasma interaction code and used it to model the interaction between a 5 psec Nd glass laser pulse of peak power 10^{13} W and a 35 times ionized tin target. The code was based on Maxwell's equations for the electromagnetic fields and the two-fluid conservation equations for the plasma. In addition to a strong modification of the plasma density after the initial (relativistic) self-focusing, they observed acceleration of tin ions up to a maximum energy of 5 GeV. G. Schmidt and W. Horton⁵⁰ investigated self-focusing due to relativistic effects on the oscillating electrons and concluded that the phenomenon has a threshold power of $\frac{9}{2}(\frac{\omega_0}{\omega_p})^2 \times 10^9$ W which the laser has to exceed in order to attain focusing. They also studied the asymptotic state of the light channel produced by self-focusing in slab geometry and arrived at a transverse beam profile having a form of hyperbolic secant with characteristic width of a few collisionless skindepths. The most recent — and most complete — treatment of pure relativistic self-focusing is given by P. Sprangle, C.-M. Tang and E. Esarey.⁵¹ Neglecting the effect of possible phase modulation and assuming that the beam remains Gaussian as it propagates through plasma, they derived an envelope equation describing the radial evolution of a laser beam propagating in plasma, and arrived at a critical power for self-focusing of $17 \times 10^9 (\frac{\omega_0}{\omega_p})^2$ W. For powers exceeding the critical power the beam envelope was found to either oscillate or propagate through plasma with constant radius.

There have also been a few attempts to study the behaviour of the laser

plasma system under the combined effect of relativistic and ponderomotive self-focusing. F.S. Felber⁵² studied analytically the relativistic nonlinear equations governing the steady-state diffraction of intense, circularly polarized electromagnetic beams in warm, quasineutral plasmas. His work thus includes both the relativistic and ponderomotive effects in *quasineutral* regime, and forms a natural continuation to the work by Max described above.⁴³ Assuming that the beam remains Gaussian while propagating in plasma and using paraxial-ray and slowly varying envelope approximations, Felber concluded that, under this set of approximations, the beams cannot self-focus but can self-trap (propagate without diverging) at powers above the threshold power of $2 \times 10^5 (\frac{\lambda_D}{\lambda_0})^2$ MW, where λ_D is the Debye length. Relativistic and ponderomotive self-focusing in another regime, that of a very short laser pulse, was addressed independently by G.-Z. Sun, E. Ott, Y.C. Lee, and P. Guzdar,⁴⁴ and by D.C. Barnes, T. Kurki-Suonio and T. Tajima.⁴⁵ In this regime the ions, due to their great inertia, can be taken as stationary, and only the electrons will respond to the laser fields. Therefore the ponderomotive effects are no longer dominated by the ion time scale — only the electrons are expelled from the central region. The analysis of the evolution of a laser beam in this regime will be described in detail in the next chapter.

More recently two papers have been published on self-focusing of coupled waves. W.B. Mori, C. Joshi, J.M. Dawson, D.W. Forslund and J.M. Kindel studied laser self-focusing using a particle simulation code.⁵³ Carrying out a simulation of two parallel laser beams in very underdense plasma they observed relativistic self-focusing taking place initially, being followed by a “ponderomotive blow-out” and filamentation of the beam at the edge of the channel boundaries. This work will be discussed in more detail in Chapter V. C.J. McKinstrie and D.A. Russell⁵⁴ addressed nonlinear self-focusing of coupled waves more

generally. Unlike all the above mentioned studies, they concentrated on time dependent focusing and performed a spatial averaging. They established the threshold power for self-focusing to be $P_{cr} = 1.7 \times 10^{10} (\frac{\omega_0}{\omega_p})^2$ W.

In the following chapters we will concentrate on collisionless plasma and thus study the ponderomotive and relativistic mechanisms only, leaving out the thermal effects. In the next chapter we will investigate the conditions under which the nonlinear self-focusing of a short laser pulse would be strong enough to overcome the natural diffraction of a laser beam. Evidently, both the severity of the electron density modulation and the strength of the relativistic effect, and hence the total effect of the plasma lens, will be stronger the more intense laser we use. Therefore we anticipate that the deciding factor in determining the qualitative behaviour (i.e., to focus or not to focus) is the laser intensity. A convenient measure for the laser intensity is the so-called quivering velocity, v_q that was already mentioned :

$$v_q \equiv \frac{eE_0}{m_e \omega_0 c} , \quad (2.26)$$

where E_0 is the peak amplitude of the electric field. It is important to notice that, although in the case of weak electric fields v_q is a direct measure of the maximum velocity gained by an electron under the electric field,

$$v_{max} = 0.25v_q, \quad \frac{eE_0}{m_e \omega_0 c}^2 \ll 1 , \quad (2.27)$$

this is *not* the case with very intense laser fields. Strictly speaking the quivering velocity is solely a measure of the laser intensity and can therefore exceed the speed of light. We will be repeatedly using the square of the dimensionless quivering velocity, which we call the normalized intensity:

$$I_n \equiv (\frac{v_q}{c})^2 \equiv (\frac{eE_0}{m_e \omega_0 c})^2 . \quad (2.28)$$

The physical, measurable intensity for a Gaussian laser beam is given by

$$I \equiv \frac{c}{8\pi} E_0^2 e^{-r^2/w_0^2} . \quad (2.29)$$

Therefore the normalized intensity is related to the value of the physical intensity evaluated at the beam axis ($r=0$) by

$$I(r=0) = \frac{m_e \omega_0^2 c^3}{8\pi e^2} I_n \approx 1.37 \times 10^{18} \frac{I_n}{\lambda_0^2} \frac{W}{cm^2} , \quad (2.30)$$

where λ_0 is the wavelength of the laser given in micrometers.

Chapter III

Self-Trapping of A Laser Beam in Plasma

3.1 Introduction

In this chapter we investigate the behavior as well as the conditions for self-trapping of a single short laser pulse. The analysis is analogous to that performed by Felber⁵² but the physical picture is quite different. Felber studied the effect of relativistic and ponderomotive effects assuming a steady state in which the interaction between the plasma and the laser has lasted long enough to assure quasineutrality. The ponderomotive force of the laser light expels plasma from the near-axis region until this repulsive force is balanced by the pressure force of the plasma in the outer regions, and the net result is a low density channel along the beam axis. The plasma density is then represented by a Boltzmann type response,

$$n \sim \exp\left(\frac{e\chi}{T_e}\right) \quad , \quad (3.1)$$

where χ is the ponderomotive potential defined in Appendix A, and T_e is the plasma temperature. Thus the plasma behaves as a single fluid and the time scale of the ponderomotive effects is set by the ions.

The situation is quite different for a very short laser pulse. When the interaction time for the plasma and the laser is short, the ion inertia becomes significant. In a very short time scale the ions can be considered stationary and only the electrons respond to the rapidly oscillating laser electric field. The time scale of the system is therefore essentially that of the electrons, and the system

should be free of instabilities generated by the ion dynamics. Thus we are operating in a region void of parametric instabilities,³⁴ which makes this scenario very attractive for various laser-plasma accelerator concepts. The behavior of the laser-plasma system, as speculated on physical grounds, could be as follows: As described earlier, if the intensity of the laser beam is large enough, the photon (ponderomotive) pressure of the laser beam may blow out the electrons from around the beam axis and thus form a 'vacuum' channel in plasma ('vacuum' in the sense that almost all the electrons are absent). The channel of low electron density that is created by the ponderomotive force of the laser pulse can then act as an optical fiber trapping the laser light. In this chapter we investigate theoretically the behaviour of a short laser pulse launched in a plasma. The main emphasis is on the possible initial self-focusing/defocusing, but in the end we will also make a rough sketch of the later evolution of the beam. (At the same time as this analysis was published in IEEE Transactions for Plasma Science,⁴⁵ there came out a similar work by Sun *et al.*⁴⁴ in Physics of Fluids)

In Section 3.2 we derive a model for the plasma response assuming a very short laser pulse. In Section 3.3 the general evolution equations for the electromagnetic field are developed. A possible asymptotic beam profile is obtained in Section 3.4 using the equations derived in the previous section. In Section 3.5 the dynamical aspects of the beam are addressed using Hamiltonian dynamics, and in Section 3.6 this is carried further with special emphasis on the nonlinear self-focusing. In Section 3.7 possible application of self-focusing to plasma based particle accelerators is discussed.

3.2 Model For Plasma Response

As mentioned above, we consider a short laser pulse so that ions do not have enough time to respond to the laser field and only the electrons respond to the rapidly oscillating electric field. The self-consistency of this assumption will be examined later. Taking ions to be infinitely massive, only the electron density can fluctuate and the ion density remains constant,

$$\begin{aligned} n_e &= n_0 + \delta n_e, \\ n_i &= n_0, \end{aligned} \tag{3.2}$$

where n_0 is the equilibrium density of the plasma and δn_e stands for the electron density fluctuations. Gauss' law can then be written as

$$\nabla \cdot \mathbf{E} = -4\pi e \delta n_e. \tag{3.3}$$

A laser beam has always a radial profile: in the basic mode the intensity peaks at the beam axis and reduces rapidly as one moves away from the axis. Therefore the amplitude of the electric field is non-uniform. This induces the non-linear ponderomotive force, which we introduced in the previous chapter. In Appendix A, for circular polarization the ponderomotive force was found to be given by:

$$\mathbf{F}_p = -\nabla \chi, \tag{3.4}$$

where $\chi = mc^2 \sqrt{1 + I_n}$ and I_n is the normalized intensity introduced in the previous chapter, $I_n = e^2 |\mathbf{E}|^2 / m^2 \omega_0^2 c^2$. Thus, for Gaussian intensity profile,

$$I = I_0 e^{-r^2/w_0^2}, \tag{3.5}$$

the ponderomotive force acting on the electrons is

$$\mathbf{F}_p = \frac{mc^2}{w_0} \frac{r}{w_0} \frac{I_n}{\sqrt{1 + I_n}} \hat{\mathbf{r}}. \tag{3.6}$$

The radial ponderomotive force pushes the mobile electrons outward from the near-axis region leaving a positive net charge there. The consequent charge separation and the associated radial electrostatic field will eventually balance the ponderomotive force so that the net force on the electrons vanishes:

$$\mathbf{F}_p - e\mathbf{E} = 0 \quad . \quad (3.7)$$

Taking a divergence of this force balance equation and using Gauss' law given by Eq.(3.3), we obtain a partial differential equation for the ponderomotive potential:

$$\frac{1}{r} \frac{\partial}{\partial r} r \frac{\partial \chi}{\partial r} + \frac{\partial^2 \chi}{\partial z^2} + \frac{1}{r^2} \frac{\partial^2 \chi}{\partial \theta^2} = 4\pi e^2 \delta n_e \quad . \quad (3.8)$$

Inverting this equation in the case of axisymmetric ($\frac{\partial}{\partial \theta} = 0$) and slowly varying or marginal ($\frac{\partial^2}{\partial z^2} = 0$) variations we get an expression for the electron density fluctuations:

$$\frac{\delta n_e}{n_0} = \left(\frac{c}{\omega_p}\right)^2 \frac{1}{r} \frac{\partial}{\partial r} r \frac{\partial}{\partial r} \sqrt{1 + I_n} \quad . \quad (3.9)$$

The self-consistency of the marginal approximation is discussed later. Under these assumptions the normalized electron density can be written as

$$N_e \equiv \frac{n_e}{n_0} = 1 + \lambda_c^2 \frac{1}{r} \frac{\partial}{\partial r} r \frac{\partial}{\partial r} \sqrt{1 + I_n} \quad , \quad (3.10)$$

where $\lambda_c \equiv \frac{c}{\omega_p}$ is the collisionless skindepth. Here and henceforth the plasma frequency ω_p is defined using the equilibrium density n_0 and the electron rest mass m_e , i.e. no density fluctuations or relativistic mass effects will be hidden in the plasma frequency but will be written out explicitly.

It should be noted that N_e should never be negative, since that would correspond to a situation where the fluctuations in the electron density were greater than the equilibrium density. This restriction is not (yet) built in this particular mathematical model.

3.3 Evolution Equations for Laser Intensity Profile

Having derived a model for the electron density variations, we now turn our attention to the equations governing the evolution of the laser beam. Our starting point is Maxwell's equations and the equation of motion for relativistic electrons:

$$\begin{aligned}
 \nabla \cdot \mathbf{E} &= 4\pi \Sigma e_j n_j \\
 \nabla \cdot \mathbf{B} &= 0 \\
 \nabla \times \mathbf{E} &= -\frac{1}{c} \frac{\partial \mathbf{B}}{\partial t} \\
 \nabla \times \mathbf{B} &= \frac{1}{c} \frac{\partial \mathbf{E}}{\partial t} + \frac{4\pi}{c} \mathbf{J} \\
 \frac{\partial \mathbf{p}}{\partial t} + \mathbf{v} \cdot \nabla \mathbf{p} &= -e \left(\mathbf{E} + \frac{1}{c} \mathbf{v} \times \mathbf{B} \right) \\
 \mathbf{p} &= \frac{m\mathbf{v}}{\sqrt{1 - \frac{v^2}{c^2}}} \quad ,
 \end{aligned} \tag{3.11}$$

where \mathbf{p} and \mathbf{v} are the electron momentum and velocity, respectively. The ions, being infinitely massive, are at rest. The electron pressure gradient is neglected in comparison with the ponderomotive force and the electrons are treated as a cold fluid. (A more detailed justification of this approach appears in the following chapter). The assumption of immobile ions allows us to write, using Eq. (3.2)

$$\begin{aligned}
 \Sigma e_j n_j &= -e\delta n_e \quad \text{and} \\
 \mathbf{J} &= -e(n_0 + \delta n_e)\mathbf{v} \quad .
 \end{aligned} \tag{3.12}$$

We express the electromagnetic fields in terms of the scalar and vector potentials:

$$\begin{aligned}
 \mathbf{E} &= -\frac{1}{c} \frac{\partial \mathbf{A}}{\partial t} - \nabla \Phi \\
 \mathbf{B} &= \nabla \times \mathbf{A} \quad .
 \end{aligned} \tag{3.13}$$

Writing Maxwell's equations in terms of the potentials and combining them we

get the wave equation for electromagnetic waves:

$$\frac{\partial^2 \mathbf{A}}{\partial t^2} - c^2 \nabla^2 \mathbf{A} + c^2 \nabla(\nabla \cdot \mathbf{A}) + c \nabla \frac{\partial \Phi}{\partial t} = 4\pi c \mathbf{J} \quad (3.14)$$

To simplify the form of the equations to come, henceforth we shall use a normalized vector potential: $\mathbf{A} \rightarrow \mathbf{A}_n \equiv \frac{e\mathbf{A}}{mc^2}$. To single out the rapid laser variations we take a trial function of the form

$$\mathbf{A}_n = a_n(\mathbf{r}, t) e^{i(k_0 z - \omega_0 t - \psi(\mathbf{r}, t))} (\hat{\mathbf{x}} + i\hat{\mathbf{y}}) \quad , \quad (3.15)$$

where $a_n(\mathbf{r}, t)$ and $\psi(\mathbf{r}, t)$ are real functions of space and time, k_0 and ω_0 are the (constant) wavenumber and frequency of the laser wave in uniform, unperturbed plasma, and we have chosen the coordinate system such that the z-axis coincides with the direction of propagation. The wave is taken to have circular polarization, as mentioned before. Using this trial function the wave equation becomes

$$\begin{aligned} & \left\{ \frac{1}{c^2} \left\{ \frac{1}{a_n} \left[\frac{\partial^2 a_n}{\partial t^2} - 2i(\omega_0 + \frac{\partial \psi}{\partial t}) \frac{\partial a_n}{\partial t} \right] - (\omega_0 + \frac{\partial \psi}{\partial t})^2 - i \frac{\partial^2 \psi}{\partial t^2} \right\} - \right. \\ & \quad \left. \frac{1}{a_n} \left[\nabla^2 a_n + 2ik_0 \frac{\partial a_n}{\partial z} - 2i(\nabla a) \cdot (\nabla \psi) \right] + (k_0 - \frac{\partial \psi}{\partial z})^2 \right\} \cdot \quad (3.16) \\ & + |\nabla_T \psi|^2 + i \nabla^2 \psi \} \mathbf{A}_n + \frac{e}{mc^3} \nabla \frac{\partial \Phi}{\partial t} = \frac{4\pi e}{mc^3} \mathbf{J} \end{aligned}$$

Next we apply the so-called slowly varying envelope approximation. That is, we assume that the characteristic spatial length of the structure in our system is much greater than the wavelength of the laser wave, and that the characteristic time period involved is much longer than the laser oscillation period. Or mathematically speaking, the amplitude $a_n(\mathbf{r}, t)$ and the phase shift

$\psi(\mathbf{r}, t)$ are slowly varying quantities,

$$\begin{aligned} \left| \frac{\partial a_n}{\partial z} \right| &\ll k_0 a_n \\ \left| \frac{\partial a_n}{\partial t} \right| &\ll \omega_0 a_n, \text{ and} \\ \left| \frac{\partial \psi}{\partial z} \right| &\ll k_0 \\ \left| \frac{\partial \psi}{\partial t} \right| &\ll \omega_0. \end{aligned} \tag{3.17}$$

(Notice that this is consistent with the marginal approximation employed in deriving the model for electron response). The advantage of using a circularly polarized wave here is that for this polarization the intensity $|\mathbf{A}|^2$ does not have any high frequency components (or any phase information, whatsoever):

$$\begin{aligned} \mathbf{A} &= a e^{i\phi} (\hat{\mathbf{x}} + i\hat{\mathbf{y}}) \\ \Rightarrow \mathbf{A} \cdot \mathbf{A} &= a^2 (\cos^2 \phi + \sin^2 \phi) = a^2. \end{aligned} \tag{3.18}$$

Since we are using potentials rather than physical fields, we need to choose an appropriate gauge condition to complete our equations. As discussed earlier, the variation in electron density takes place because of the nonlinear ponderomotive force. The time scale of the electrons drifting under the influence of the ponderomotive force is much slower than the laser oscillation time, as will be shown in the next chapter. Therefore we conclude that the electron density, n_e , is a slowly varying quantity. (This can be seen also formally from the expression derived for n_e : $n_e \sim \nabla a_n^2$, which, according to the Eqs. (3.17) and (3.18) is slowly varying). According to Gauss' law, then, the divergence of the electric field should also be slowly varying:

$$\nabla \cdot \mathbf{E} = -\nabla^2 \Phi - \frac{1}{c} \nabla \cdot \frac{\partial \mathbf{A}}{\partial t} = 4\pi e(n_i - n_e) \quad . \tag{3.19}$$

We will now arrive at very clear separation of the fast and slowly varying parts of the electric field by choosing Coulomb's gauge:

$$\nabla \cdot \mathbf{A} = 0 \quad . \quad (3.20)$$

Then the vector potential disappears altogether from Gauss' law and the scalar potential, Φ , will be purely slowly varying and will stand for the low frequency electrostatic oscillations, whereas the rapid laser oscillations will be entirely given by the vector potential \mathbf{A} . Notice, that had we chosen, say, the Lorentz gauge, this separation would not have been possible.

An expression for the plasma current can be derived by assuming that the equation of motion for electrons is dominated by the transverse laser electric field \mathbf{E}_T :

$$\begin{aligned} \frac{\partial \mathbf{p}}{\partial t} &\approx -e\mathbf{E}_T = -\frac{e}{c} \frac{\partial \mathbf{A}}{\partial t} \\ \Rightarrow \mathbf{p} &= -\frac{e}{c} \mathbf{A} \\ \Rightarrow \mathbf{v} &= \frac{\mathbf{p}}{m\gamma} = \frac{e}{mc} \frac{\mathbf{A}}{\sqrt{1+I_n}} \\ \Rightarrow \mathbf{J} &= -en_e \mathbf{v} = -\frac{\omega_{p0}^2}{4\pi c} \frac{N_e}{\sqrt{1+I_n}} \mathbf{A} \end{aligned} \quad (3.21)$$

and the wave equation becomes

$$\begin{aligned} &\left\{ \frac{1}{c^2} \left\{ \frac{1}{a_n} \left[\frac{\partial^2 a_n}{\partial t^2} - 2i\left(\omega_0 + \frac{\partial \psi}{\partial t}\right) \frac{\partial a_n}{\partial t} \right] - \left(\omega_0 + \frac{\partial \psi}{\partial t}\right)^2 - i \frac{\partial^2 \psi}{\partial t^2} \right\} - \right. \\ &\quad \left. \frac{1}{a_n} \left[\nabla^2 a_n + 2ik_0 \frac{\partial a_n}{\partial z} - 2i(\nabla a_n) \cdot (\nabla \psi) \right] + \left(k_0 - \frac{\partial \psi}{\partial z}\right)^2 \right. \\ &\quad \left. + |\nabla_T \psi|^2 + i \nabla^2 \psi \right\} \mathbf{A}_n + \frac{e}{mc^3} \nabla \frac{\partial \Phi}{\partial t} = \\ &\quad - \frac{1}{\lambda_c^2} \frac{N_e}{\sqrt{1+I_n}} \mathbf{A}_n , \end{aligned} \quad (3.22)$$

where N_e is given by Eq. (3.10). The right-hand side represents all the relevant nonlinearities, i.e. the ponderomotive force (buried in the normalized electron

density N_e) and the relativistic electron mass effects (appearing in the form of the inverse square root factor).

Taking an inner product of the wave equation with the normalized vector potential \mathbf{A}_n gives

$$\begin{aligned}
 & \left\{ \frac{1}{c^2} a_n \left[\frac{\partial^2 a_n}{\partial t^2} - 2i \left(\omega_0 + \frac{\partial \psi}{\partial t} \right) \frac{\partial a_n}{\partial t} \right] - a_n^2 \left[\left(\omega_0 + \frac{\partial \psi}{\partial t} \right)^2 + i \frac{\partial^2 \psi}{\partial t^2} \right] \right\} - \\
 & a_n \left[\nabla^2 a_n + 2ik_0 \frac{\partial a_n}{\partial z} - 2i(\nabla a_n) \cdot (\nabla \psi) \right] + \\
 & a_n^2 \left[\left(k_0 - \frac{\partial \psi}{\partial z} \right)^2 + |\nabla_T \psi|^2 + i \nabla^2 \psi \right] + \frac{e}{mc^3} \mathbf{A}_n \cdot \nabla \frac{\partial \Phi}{\partial t} = \\
 & - \frac{1}{\lambda_c^2} \frac{N_e}{\sqrt{1 + a_n^2}} a_n^2 .
 \end{aligned} \tag{3.23}$$

Since we assume that the modification of the laser beam (and plasma) take place at slow pace compared to the rapid laser oscillations, there will not be any significant development at the time scale of one laser oscillation period. Therefore we can average the wave equation over the laser oscillation period $T_0 = \frac{2\pi}{\omega_0}$. All terms except the one involving the scalar potential remain approximately constant under the averaging integral, and thus can be pulled out from under the integral. The term involving scalar potential is proportional to the rapidly varying phase factor and will thus average to zero. (The scalar potential itself is a slowly varying quantity as a result of the Coulomb's gauge, as was shown above, and is thus pulled out of the integral). Averaging over the laser oscillation period, we thus arrive at an equation describing the slow

evolution of the beam envelope:

$$\begin{aligned}
& \frac{1}{c^2} a_n \left[\frac{\partial^2 a_n}{\partial t^2} - 2i \left(\omega_0 + \frac{\partial \psi}{\partial t} \right) \frac{\partial a_n}{\partial t} \right] - a_n^2 \left[\left(\omega_0 + \frac{\partial \psi}{\partial t} \right)^2 + i \frac{\partial^2 \psi}{\partial t^2} \right] - \\
& a_n \left[\nabla^2 a_n + 2ik_0 \frac{\partial a_n}{\partial z} - 2i (\nabla a_n) \cdot (\nabla \psi) \right] + \\
& a_n^2 \left[\left(k_0 - \frac{\partial \psi}{\partial z} \right)^2 + |\nabla_T \psi|^2 + i \nabla^2 \psi \right] = \\
& - \frac{1}{\lambda_c^2} \frac{N_e}{\sqrt{1 + a_n^2}} a_n^2
\end{aligned} \tag{3.24}$$

Henceforth we shall drop the subscript 'n' for convenience.

Since the amplitude a and the phase shift ψ were chosen to be real quantities, the terms multiplied by the imaginary number 'i' will decouple from the real terms and the wave equation splits into two independent equations; the real terms yield an equation describing the evolution of the amplitude,

$$\begin{aligned}
\frac{\partial^2 a}{\partial t^2} &= a \left(\omega_0 + \frac{\partial \psi}{\partial t} \right)^2 + c^2 \nabla^2 a - \\
& c^2 a \left\{ \left(k_0 - \frac{\partial \psi}{\partial z} \right)^2 + |\nabla_T \psi|^2 \right\} - \omega_{p0}^2 \frac{N_e}{\sqrt{1 + a^2}} a,
\end{aligned} \tag{3.25}$$

and the imaginary terms give a similar equation for the phase shift,

$$\begin{aligned}
\frac{\partial}{\partial t} \left(a^2 \frac{\partial \psi}{\partial t} \right) &= -\omega_0 \frac{\partial a^2}{\partial t} - c^2 k_0 \frac{\partial a^2}{\partial z} + \\
& c^2 (\nabla a^2) \cdot (\nabla \psi) + c^2 a^2 \nabla^2 \psi.
\end{aligned} \tag{3.26}$$

Since we assume that the system has reached a situation where there is no net force acting on the electrons, we will look for a stationary state solution for these equations. Letting the time derivatives equal to zero, the equations become

$$\begin{aligned}
2k_0 \frac{\partial \psi}{\partial z} - \left(\frac{\partial \psi}{\partial r} \right)^2 + \frac{1}{ar} \frac{\partial}{\partial r} r \frac{\partial a}{\partial r} - \frac{1}{\lambda_c^2} \frac{N_e}{\sqrt{1 + a^2}} = \\
- \left(\frac{\omega_0^2}{c^2} - k_0^2 \right) - \frac{1}{a} \frac{\partial^2 a}{\partial z^2} + \left(\frac{\partial \psi}{\partial z} \right)^2,
\end{aligned} \tag{3.27}$$

and

$$-k_0 \frac{\partial a^2}{\partial z} + \frac{\partial a^2}{\partial r} \frac{\partial \psi}{\partial r} + \frac{a^2}{r} \frac{\partial}{\partial r} r \frac{\partial \psi}{\partial r} = -\frac{\partial}{\partial z} \left(a^2 \frac{\partial \psi}{\partial z} \right) , \quad (3.28)$$

where we have also applied the assumption of axial symmetry by taking the transverse Laplacian operator as $\nabla_T^2 \equiv \frac{1}{r} \frac{\partial}{\partial r} r \frac{\partial}{\partial r}$.

3.4 Asymptotic Form of the Laser Profile

To start with, we shall look for a possible asymptotic intensity profile for the laser beam under the combined influence of the ponderomotive and relativistic effects. That is, we shall assume the asymptotic intensity profile to be independent of the variable z . This can be accomplished by choosing the following ansatz for the vector potential:

$$\begin{aligned} a(r, z) &= a(r) , \\ \psi(r, z) &= f(z) + g(r) , \end{aligned} \quad (3.29)$$

where, for generality, we have still allowed for phase modulation in z . The above equations (3.27) and (3.28) become separable under this ansatz: The amplitude equation yields

$$\begin{aligned} -2k_0 \frac{df}{dz} - \Delta_0^2 + \left(\frac{df}{dz} \right)^2 &= C_1 \\ &= \frac{1}{a} \frac{1}{r} \frac{d}{dr} r \frac{da}{dr} - \left(\frac{dg}{dr} \right)^2 - \frac{1}{\lambda_c^2} \frac{N_e}{\sqrt{1+a^2}} , \end{aligned} \quad (3.30)$$

where $\Delta_0^2 \equiv \frac{\omega_0^2}{c^2} - k_0^2$, and C_1 is the separation constant. The phase equation becomes

$$-\frac{d^2 f}{dz^2} = C_2 = \frac{1}{r} \frac{d}{dr} r \frac{dg}{dr} + \frac{1}{a^2} \frac{da^2}{dr} \frac{dg}{dr} \quad (3.31)$$

where C_2 is the separation constant.

According to Eq. (3.31) the z -dependent part of the phase shift ψ can be written in a general form given by

$$f(z) = -\frac{1}{2}C_2 z^2 + C_3 z \quad , \quad (3.32)$$

where C_3 is the integration constant and the (arbitrary) constant phase shift has been neglected. Substituting this expression for $f(z)$ into the z -dependent part of Eq. (3.30) we get

$$-2k_0(-C_2 z + C_3) - \Delta_0^2 + (-C_2 z + C_3)^2 = C_1 \quad . \quad (3.33)$$

For this to be satisfied for all values of z , the coefficients multiplying the different powers of z on the left-hand side have to equal those on the right-hand side. Matching the coefficients in this manner yields

$$\begin{aligned} C_2 &\equiv 0 \\ C_3 &= k_0 \pm \sqrt{k_0^2 + \Delta_0^2 + C_1} \quad , \end{aligned} \quad (3.34)$$

and thus $f(z)$ is given by the linear expression

$$f(z) = k_0 z \pm \sqrt{\frac{\omega_0^2}{c^2} + C_1} z \quad . \quad (3.35)$$

The assumption of slow modulations, $|\frac{\partial \psi}{\partial z}| \ll k_0$, implies that we have to choose square root with the negative sign to retain consistency, and thus $f(z)$ is given by

$$f(z) = k_0 z - \sqrt{\frac{\omega_0^2}{c^2} + C_1} z \quad . \quad (3.36)$$

The radial equations can now be written as

$$\begin{aligned} \frac{1}{a} \frac{1}{r} \frac{d}{dr} r \frac{da}{dr} - \left(\frac{dg}{dr} \right)^2 - \frac{1}{\lambda_e^2} \frac{N_e}{\sqrt{1+a^2}} &= C_1 \quad , \quad \text{and} \\ \frac{1}{r} \frac{d}{dr} r \frac{dg}{dr} + \frac{1}{a^2} \frac{da^2}{dr} \frac{dg}{dr} &= 0 \quad . \end{aligned} \quad (3.37)$$

For simplicity, we will study these equations in slab geometry. Formally this is accomplished by doing the following substitution:

$$\frac{1}{r} \frac{d}{dr} r \frac{d}{dr} \rightarrow \frac{d^2}{dx^2} \quad (3.38)$$

Then the above equations become

$$\begin{aligned} \frac{1}{a} \frac{d^2}{dx^2} a - \left(\frac{dg}{dx} \right)^2 - \frac{1}{\lambda_c^2} \frac{N_e}{\sqrt{1+a^2}} &= C_1, \quad \text{and} \\ a^2 \frac{dg}{dx} &= C_4, \end{aligned} \quad (3.39)$$

where the phase equation was integrated once over x , bringing about the integration coefficient C_4 . Using the expression for the first derivative of the phase factor g , one may write the amplitude equation as

$$\frac{1}{a} \frac{d^2}{dx^2} a - \frac{C_4^2}{a^4} - \frac{1}{\lambda_c^2} \frac{N_e}{\sqrt{1+a^2}} = C_1 \quad (3.40)$$

Recalling from Section 3.1 the expression for the electron density in our model, we will write it here in the form

$$N_e = 1 + \epsilon \frac{1}{\lambda_c^2} \frac{d^2}{dx^2} \sqrt{1+a^2} \quad (3.41)$$

where the perturbation produced by the ponderomotive force is labeled by a parameter $\epsilon = [0, 1]$. This parameterizing is done to facilitate comparisons to earlier works in some of which the ponderomotive force is included ($\epsilon = 1$), whereas in others only the relativistic effects are considered ($\epsilon = 0$). The amplitude equation now becomes

$$\frac{1}{a} \frac{d^2}{dx^2} a - \frac{C_4^2}{a^4} - \frac{1}{\lambda_c^2} \frac{1}{\sqrt{1+a^2}} - \epsilon \frac{1}{\sqrt{1+a^2}} \frac{d^2}{dx^2} \sqrt{1+a^2} = C_1 \quad (3.42)$$

This equation is directly integrable, if one notices the following:

$$\begin{aligned}\frac{d}{dx} \sqrt{1+a^2} &= \frac{aa'}{\sqrt{1+a^2}} \\ \frac{d^2}{dx^2} \sqrt{1+a^2} &= \left(\frac{aa'}{\sqrt{1+a^2}} \right)'.\end{aligned}\quad (3.43)$$

Then, multiplying both sides of the equations by the factor aa' , where the prime stands for differentiation with respect to x , the amplitude equation becomes

$$a''a' - C_4^2 \frac{a'}{a^3} - \frac{1}{\lambda_c^2} \frac{aa'}{\sqrt{1+a^2}} - \epsilon \frac{aa'}{\sqrt{1+a^2}} \left(\frac{aa'}{\sqrt{1+a^2}} \right)' = C_1 aa' \quad . \quad (3.44)$$

This equation is directly integrable yielding

$$a'^2 + C_4^2 \frac{1}{a^2} - \frac{2}{\lambda_c^2} \sqrt{1+a^2} - \epsilon \frac{a^2 a'^2}{1+a^2} - C_1 a^2 = C_5 \quad , \quad (3.45)$$

where C_5 is the integration constant. For the solution given by this first integral of the amplitude equation to be physical, i.e. for the total power of the beam to be finite, both the amplitude and its derivative should vanish at infinity: $a, a' \rightarrow 0$ as $x \rightarrow \infty$. This implies that the coefficients C_4 and C_5 have the following values:

$$\begin{aligned}C_4 &\equiv 0 \\ C_5 &\equiv -\frac{2}{\lambda_c^2} \quad ,\end{aligned}\quad (3.46)$$

and hence the amplitude is given by the first order differential equation

$$a'^2 = \frac{1}{1+a^2(1-\epsilon)} \left[C_1 a^4 + \left(C_1 - \frac{2}{\lambda_c^2} \right) a^2 - \frac{2}{\lambda_c^2} + \frac{2}{\lambda_c^2} (1+a^2)^{\frac{3}{2}} \right] \quad . \quad (3.47)$$

The three-halves power within the expression on the right-hand side of Eq. (3.47) complicates the analytical integration for general values of the amplitude, and thus we start by expanding the right-hand side for nonrelativistic field amplitudes, $a^2 < 1$:

$$a'^2 = \left(C_1 + \frac{1}{\lambda_c^2} \right) a^2 + \left[C_1 + \frac{3}{4\lambda_c^2} - (1-\epsilon) \left(C_1 + \frac{1}{\lambda_c^2} \right) \right] a^4 + O(a^6) \quad . \quad (3.48)$$

Introducing the following shorthand notations,

$$\begin{aligned}\alpha &\equiv \lambda_c^2 C_1 + 1 \\ \beta &\equiv \epsilon\alpha - \frac{1}{4}\end{aligned}\tag{3.49}$$

the equation for the field amplitude becomes

$$\frac{d}{dx}a = \pm \frac{1}{\lambda_c} \sqrt{\alpha a^2 + \beta a^4} \quad , \tag{3.50}$$

or, multiplying the equation on both sides by a , calling $I \equiv a^2$, and moving all the terms involving I to the left hand side, we obtain

$$\frac{dI}{I\sqrt{1 + \frac{\beta}{\alpha}I}} = \pm \frac{2}{\lambda_c} \sqrt{\alpha} dx \quad . \tag{3.51}$$

The expression on the left-hand side has an exact integral⁵⁵ and thus the equation can be integrated to find the amplitude:

$$\ln \left(\frac{\sqrt{1 + \frac{\beta}{\alpha}I} - 1}{\sqrt{1 + \frac{\beta}{\alpha}I} + 1} \right) = \pm 2\sqrt{\alpha} \frac{x}{\lambda_c} + \text{constant} \quad , \tag{3.52}$$

which can be inverted to yield

$$I(x) = 4 \frac{\alpha}{\beta} \frac{C_6 e^{\pm 2\sqrt{\alpha} \frac{x}{\lambda_c}}}{\left(1 - C_6 e^{\pm 2\sqrt{\alpha} \frac{x}{\lambda_c}}\right)^2} \quad . \tag{3.53}$$

This is the nonrelativistic (stationary) solution for the asymptotic field amplitude under the specific assumptions given above.

The solution obtained possesses a curiosity worth noticing. The integration constant C_6 corresponds to merely a shift of the solution along the x-axis. This is evident when we write

$$C_6 e^{2\sqrt{\alpha} \frac{x}{\lambda_c}} \equiv e^{2\sqrt{\alpha} \frac{x}{\lambda_c} + \ln C_6} \quad . \tag{3.54}$$

Thus the general solution consists of a set of identical profiles distributed evenly over the entire x -axis. This "translational invariance" of the solution is actually manifested already in the first-order differential equation for the amplitude; it is seen that the expression for the derivative of a does not depend explicitly on the variable x , and therefore, for a given initial value of the amplitude, the solution will always be the same irrespective of the location on the x -axis. This translational invariance is a consequence of the slab geometry: in cylindrical geometry the z -axis ($r = 0$) has a special significance as the beam axis, whereas in slab geometry there is no reason to have the beam centered around $x = 0$. Formally the difference between these two geometries is manifested already in the second-order differential equation: the Laplacian operator has an explicit reference to the transverse coordinate in cylindrical geometry ($\nabla_T^2 = \frac{1}{r} \frac{\partial}{\partial r} r \frac{\partial}{\partial r} = \frac{1}{r} \frac{\partial}{\partial r} + \frac{\partial^2}{\partial r^2}$), whereas in slab geometry that is not the case ($\nabla_T^2 = \frac{\partial^2}{\partial x^2}$).

To further study the qualitative aspects of the solution we simplify the notation by introducing a dimensionless variable $\xi \equiv \frac{x}{\lambda_c}$. The solution can now be written as

$$I(\xi) = 4 \frac{\alpha}{\beta} \frac{C_6 e^{\pm 2\sqrt{\alpha}\xi}}{(1 - C_6 e^{\pm 2\sqrt{\alpha}\xi})^2} \quad , \quad (3.55)$$

and its first derivative with respect to ξ is given by

$$\frac{dI}{d\xi} = \pm 8 \frac{\alpha}{\beta} C_6 \sqrt{\alpha} e^{\pm 2\sqrt{\alpha}\xi} \frac{1 + C_6 e^{\pm 2\sqrt{\alpha}\xi}}{(1 - C_6 e^{\pm 2\sqrt{\alpha}\xi})^3} \quad . \quad (3.56)$$

From Eq. (3.55) for the intensity profile, it is seen that the integration constant C_6 has to be negative, $C_6 < 0$, because the solution should remain finite for all values of ξ . We therefore replace C_6 by another constant C_7 according to

$$0 < C_7 \equiv -C_6 \quad , \quad (3.57)$$

whence the solution can be written as

$$I(\xi) = -4 \frac{\alpha}{\beta} \frac{C_7 e^{\pm 2\sqrt{\alpha}\xi}}{(1 + C_7 e^{\pm 2\sqrt{\alpha}\xi})^2} , \quad (3.58)$$

and its first derivative as

$$\frac{dI}{d\xi} = \mp 8 \frac{\alpha}{\beta} C_7 \sqrt{\alpha} e^{\pm 2\sqrt{\alpha}\xi} \frac{1 - C_7 e^{\pm 2\sqrt{\alpha}\xi}}{(1 + C_7 e^{\pm 2\sqrt{\alpha}\xi})^3} . \quad (3.59)$$

A good first picture of the solution is obtained by finding the number of extrema of the function. Looking at Eq. (3.56) for the derivative of I , we see that the profile will have one (and only one) extremum only if $C_7 > 0$, a condition that coincides with the one already established above for the finiteness of the solution. The extremum locates at x_m , given by

$$x_m = -\frac{\ln C_7}{2\sqrt{\alpha}} . \quad (3.60)$$

As described above, the general solution consists of a set of profiles covering the x -axis but identical in form. Therefore it is convenient to pin down a single solution that we will be considering. A natural choice is to pick the solution centered around $x = 0$. This implies that we choose $C_7 = 1$, whence the solution is given by

$$\begin{aligned} I(\xi) &= -4 \frac{\alpha}{\beta} \frac{e^{\pm 2\sqrt{\alpha}\xi}}{(1 + e^{\pm 2\sqrt{\alpha}\xi})^2} \\ &= -\frac{\alpha}{\beta} \frac{1}{\cosh^2(\sqrt{\alpha}\xi)} . \end{aligned} \quad (3.61)$$

The intensity of a laser has to be positive, which resritcts the value of α as follows:

$$\frac{\alpha}{\epsilon\alpha - \frac{1}{4}} < 0 . \quad (3.62)$$

A comparison of the solution obtained here to an earlier work performed by Schmidt and Horton⁵⁰ can be done by simply letting the artificial parameter ϵ equal to zero since their work included relativistic effects only. The solution Schmidt and Horton arrived at is given by

$$I(\xi) = 2\alpha_{SH} \frac{1}{\cosh^2(\sqrt{\alpha_{SH}}\xi)} \quad , \quad (3.63)$$

where the constant α_{SH} is given by

$$\alpha_{SH} = 1 + \frac{1}{\omega_{p0}^2}(k^2 c^2 - \omega^2) \quad , \quad (3.64)$$

and the dispersion relation connecting the wavenumber k to the frequency ω is yet to be determined. At the peak of the profile we find the connection of α_{SH} to the maximum (normalized) intensity $I_0 \equiv I(\xi = 0)$:

$$\alpha_{SH} = \frac{1}{2} I_0 \quad . \quad (3.65)$$

From this we can derive the dispersion relation as

$$\omega^2 = \omega_{p0}^2 \left(1 - \frac{1}{2} I_0\right) + c^2 k^2 \quad . \quad (3.66)$$

The complete solution for the asymptotic field amplitude, which Schmidt and Horton chose to present in the form

$$A = A(x)e^{i\varphi} \quad , \quad \varphi \equiv kz - \omega t \quad (3.67)$$

is thus specified by

$$\begin{aligned} I(\xi) \equiv A_n^2(\xi) &= I_0 \frac{1}{\cosh^2(\sqrt{\alpha_{SH}}\xi)} \quad , \quad \alpha_{SH} = \frac{1}{2} I_0 \\ \varphi &= \frac{1}{c} \sqrt{\omega^2 + \omega_{p0}^2 \left(\frac{1}{2} I_0 - 1\right)} z - \omega t \quad . \end{aligned} \quad (3.68)$$

In our approach, we have presented the field amplitude in a general form given by

$$A = A(x)e^{i\varphi} \quad , \quad \varphi \equiv k_0 z - \omega_0 t - \psi(x) \quad , \quad (3.69)$$

where k_0 and ω_0 are the constant wavenumber and frequency connected by the equilibrium dispersion relation, and $\psi(x)$ is the phase shift. The intensity profile for purely relativistic focusing is, as given by Eq. (3.61) with $\epsilon = 0$,

$$I(\xi) = 4\alpha \frac{1}{\cosh^2(\sqrt{\alpha}\xi)} \quad , \quad (3.70)$$

where $\alpha = \lambda_c^2 C_1 + 1$. The constant C_1 can be determined by evaluating the profile at the center of the distribution, as was done in the case studied by Schmidt and Horton:

$$\alpha = \frac{1}{4}I_0 \quad \Rightarrow \quad C_1 = \frac{\omega_{p0}^2}{c^2} \left(\frac{1}{4}I_0 - 1 \right) \quad . \quad (3.71)$$

The phase shift ψ , as recalled from expression (3.36), is given by

$$\begin{aligned} \psi &= \left(k_0 - \sqrt{\frac{\omega_0^2}{c^2} + C_1} \right) z \\ &= \left(k_0 - \sqrt{\frac{\omega_0^2}{c^2} + \frac{\omega_{p0}^2}{c^2} \left(\frac{1}{4}I_0 - 1 \right)} \right) z \quad , \end{aligned} \quad (3.72)$$

and thus the complete solution is specified by

$$\begin{aligned} I(\xi) &= I_0 \frac{1}{\cosh^2(\sqrt{\alpha}\xi)} \quad , \quad \alpha = \frac{1}{4}I_0 \\ \varphi(\xi) &= \frac{1}{c} \sqrt{\omega_0^2 + \omega_{p0}^2 \left(\frac{1}{4}I_0 - 1 \right)} z - \omega_0 t \quad . \end{aligned} \quad (3.73)$$

Therefore, for a given frequency $\omega = \omega_0$, the solution discovered here coincides within a factor of two with the one obtained by Schmidt and Horton. The

difference of the factor of two will be discussed in detail later when we are comparing the critical intensities for self-focusing.

The more interesting case, including the ponderomotive effects, is obtained by letting the parameter ϵ equal to unity. The profile then becomes

$$I(\xi) = -\frac{\alpha}{\alpha - \frac{1}{4}} \frac{1}{\cosh^2(\sqrt{\alpha}\xi)} \quad , \quad (3.74)$$

The condition on α , given by (3.62), is now

$$0 < \alpha < \frac{1}{4} \quad , \quad (3.75)$$

which suggests that we replace the constant α by another constant κ^2 defined by

$$\alpha \equiv \kappa^2, \quad \kappa^2 < \frac{1}{4} \quad . \quad (3.76)$$

The intensity profile can now be written in terms of a single parameter κ as:

$$I(\xi) = \frac{\kappa^2}{\frac{1}{4} - \kappa^2} \frac{1}{\cosh^2(\kappa\xi)} \quad . \quad (3.77)$$

The interpretation of κ is obvious: it is the inverse of the beam width in units of the collisionless skindepth.

The parameter κ is found to be directly related to the peak intensity of the profile at $\xi = 0$. Evaluating the intensity at $\xi = 0$ we obtain

$$I(\xi = 0) \equiv I_0 = \frac{\kappa^2}{\frac{1}{4} - \kappa^2} \quad , \quad (3.78)$$

which can be inverted to yield

$$\kappa^2 = \frac{1}{4} \frac{I_0}{1 + I_0} < \frac{1}{4} \quad , \quad (3.79)$$

which is consistent with the definition of κ given earlier. The total power of the beam can be expressed in terms of κ , too. If we define a normalized power, P_n of the laser beam by

$$P_n \equiv \int_{-\infty}^{+\infty} I(\xi) d\xi \quad , \quad (3.80)$$

then, for the profile derived above in terms of the parameter κ , it becomes

$$\begin{aligned} P_n &= \frac{\kappa^2}{\frac{1}{4} - \kappa^2} \int_{-\infty}^{+\infty} \frac{1}{\cosh^2(\kappa\xi)} \\ &= \frac{\kappa}{\frac{1}{4} - \kappa^2} \quad . \end{aligned} \quad (3.81)$$

The profile we have thus derived bears a close resemblance to a soliton: for a soliton with a sech^2 - profile, if the width of it scales as $\frac{1}{\kappa}$, the intensity scales as κ^2 . For the profile obtained here the intensity scales as $\frac{\kappa^2}{\frac{1}{4} - \kappa^2}$.

It is also important to notice that phase modulation is necessary for a nontrivial solution: If one assumes no phase modulation, $\psi \equiv 0$, the profile one arrives at is that of a plane wave, $I(\xi) = \text{const.}$ This is because no phase modulation implies $\kappa^2 = 0$.

As a final consideration of the asymptotic profile we will investigate how the profile looks for relativistic amplitudes, $a^2 \geq 1$. It could be quite plausible that the qualitative behaviour of the profile could be different at these amplitudes. We shall here include both the relativistic and the ponderomotive effects and thus set the parameter ϵ equal to unity in the differential equations for the amplitude. The first order differential equation for a general value of amplitude, as recalled from Eq. (3.47), can be rewritten as

$$\begin{aligned} \frac{da}{d\xi} &= \pm \sqrt{[(\kappa^2 - 1)a^2 - 2](1 + a^2) + 2(1 + a^2)^{3/2}} \\ &= \pm \sqrt{[(\kappa^2 - 1)a^2 + 2(\sqrt{1 + a^2} - 1)](1 + a^2)} \quad . \end{aligned} \quad (3.82)$$

Changing variable according to⁵⁶

$$u(\xi)^2 = a(\xi)^2 + 1 , \quad (3.83)$$

the equation becomes

$$\begin{aligned} \frac{du}{d\xi} &= \pm \sqrt{(u^2 - 1)[(\kappa^2 - 1)u^2 + 2u - (1 + \kappa^2)]} \\ &= \pm \sqrt{(u^2 - 1)(u + 1)[(\kappa^2 - 1)u + (1 + \kappa^2)]} . \end{aligned} \quad (3.84)$$

Introducing yet another variable defined as⁵⁶

$$y(\xi) = u(\xi) - 1 , \quad (3.85)$$

the differential equation can be written as

$$\frac{dy}{d\xi} = \pm \sqrt{(\kappa^2 - 1)y^2 + 2(2\kappa^2 - 1)y + 4\kappa^2} \, y , \quad (3.86)$$

which can be recognized as an elementary quadrature and which, upon integration, yields

$$\begin{aligned} \xi + C_8 &= -\frac{1}{2\kappa} \ln \left| \frac{1}{y} \{ 2\sqrt{4\kappa^2[(\kappa^2 - 1)y^2 + 2(2\kappa^2 - 1)y + 4\kappa^2]} \right. \\ &\quad \left. + 8\kappa^2 + 2(2\kappa^2 - 1)y \} \right| . \end{aligned} \quad (3.87)$$

Defining $E \equiv \exp(-2\kappa(\xi + C_8))$ and inverting the relation we obtain an implicit expression for y :

$$\pm Ey = 4\kappa \sqrt{(\kappa^2 - 1)y^2 + 2(2\kappa^2 - 1)y + 4\kappa^2} + 8\kappa^2 + 2(2\kappa^2 - 1)y . \quad (3.88)$$

The solution to this equation is given by

$$y = \frac{\pm 16\kappa^2 E}{E^2 \mp 4E(2\kappa^2 - 1) + 4} . \quad (3.89)$$

Unraveling the changes of variables made on the way the solution for the intensity becomes

$$I_n = a_n^2 = \frac{\pm 32(E \pm 2)^2 \kappa^2 E}{[(E \pm 2)^2 \mp 8\kappa^2 E]^2} . \quad (3.90)$$

Since the intensity has to be positive, and the variable E is positive definite, we have to choose the upper sign in the expression for the intensity. As in the nonrelativistic case, we want to center the profile at $\xi = 0$. The maximum of the profile takes place at $E = 2$ corresponding to the integration constant $C_8 = -\frac{1}{2\kappa} \ln 2$. The amplitude profile centered at $\xi = 0$ thus becomes

$$a_n = \frac{4\kappa e^{-\kappa\xi} (e^{-2\kappa\xi} + 1)}{(e^{-2\kappa\xi} + 1) - 4\kappa^2 e^{-2\kappa\xi}} , \quad (3.91)$$

which can be rewritten in terms of sech-function as

$$a_n = \frac{2\kappa \operatorname{sech}(\kappa\xi)}{1 - \kappa^2 \operatorname{sech}^2(\kappa\xi)} . \quad (3.92)$$

The profile is seen to coincide with that derived for the nonrelativistic amplitudes when both profiles are evaluated for $\kappa^2 \ll 1$. The important feature of the solution for general amplitudes is that it is qualitatively similar to that obtained for the nonrelativistic case, i.e. the profile has only a single 'hump'. Figure 3.1 shows the profiles for various values of maximum amplitude a_m .

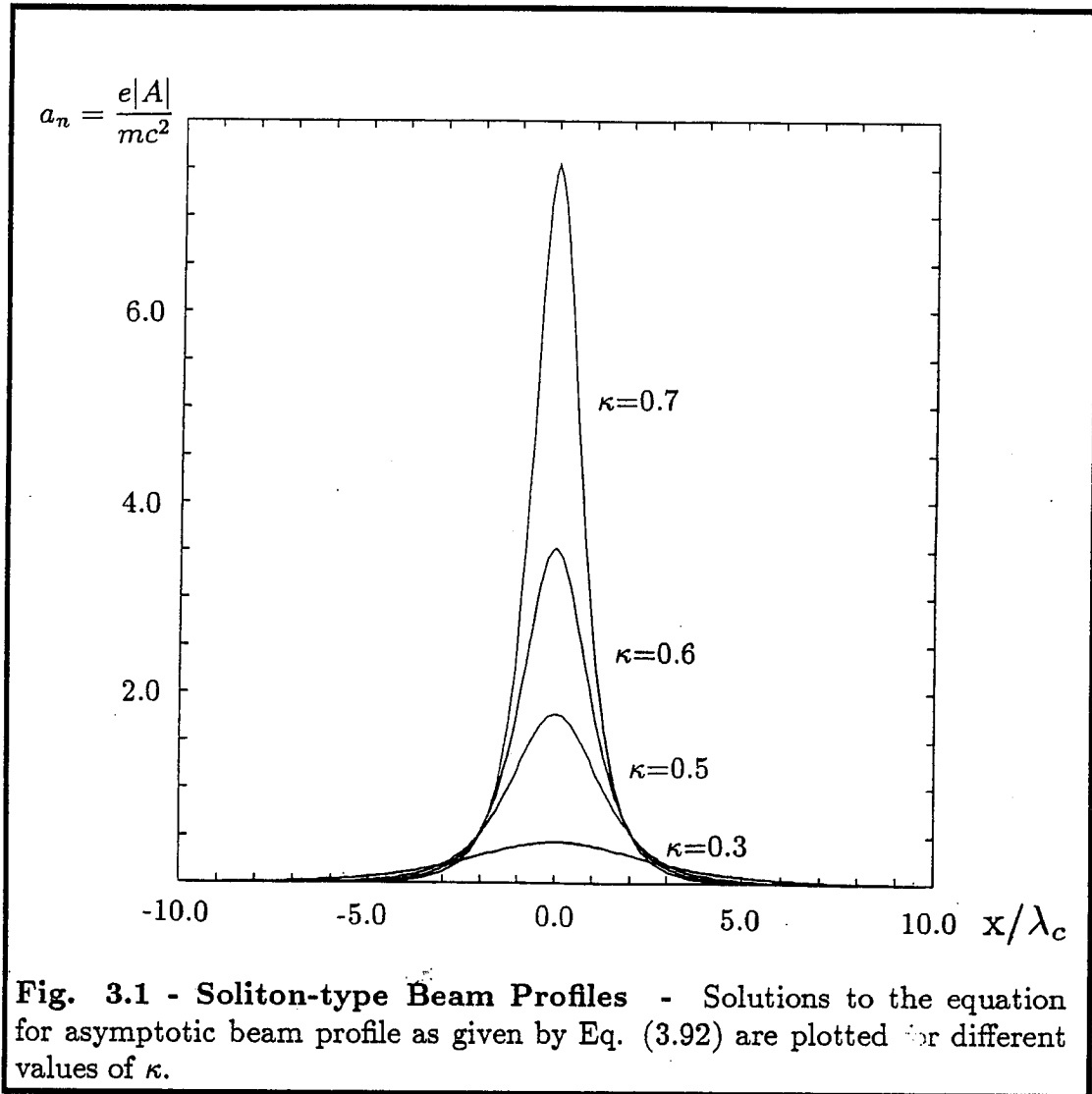
Rewriting the basic differential equation, Eq. (3.82), in the form

$$\left(\frac{da}{d\xi} \right)^2 + V(a) = 0 , \quad (3.93)$$

we obtain an expression for the characteristic potential for the system:

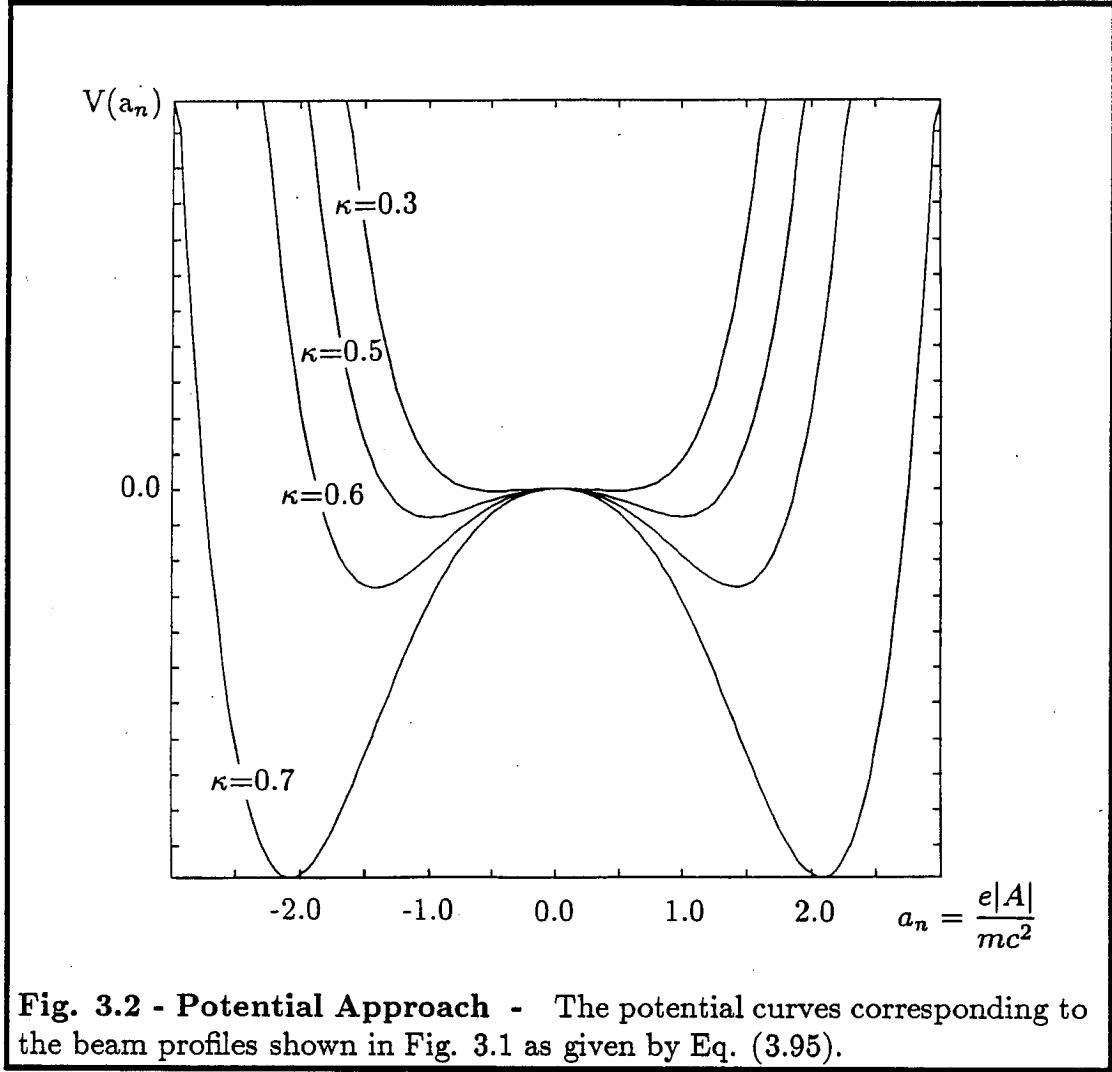
$$V(a) = -(1 + a^2) [(\kappa^2 - 1)a^2 + 2(\sqrt{1 + a^2} - 1)] . \quad (3.94)$$

In Fig. 3.2 this potential is plotted for various values of the beam parameter κ . It is seen that for all possible values of κ there exists a homoclinic orbit. This homoclinic orbit corresponds to the soliton-type profile we derived analytically above. The other possible orbits most probably correspond to multisolitons.⁵⁷



3.5 Hamiltonian Dynamics of Laser Light

In this section we shall allow variation in the direction of propagation (which in our model has been chosen parallel to the z -axis). We then wish to study the dynamics (in the direction of propagation) of the laser light under the combined influence of relativistic and ponderomotive effects. We still assume that the system has reached a stationary state where there will be no net force acting on the electrons so that we can use the model for electron response



derived in Section 3.2.

As our starting point we use the basic evolution equations (3.27) and (3.28) derived for the laser beam in Section 3.3:

$$\begin{aligned}
 2k_0 \frac{\partial \psi}{\partial z} - \left(\frac{\partial \psi}{\partial r} \right)^2 + \frac{1}{a_n r} \frac{\partial}{\partial r} r \frac{\partial a_n}{\partial r} - \frac{1}{\lambda_c^2} \frac{N_e}{\sqrt{1 + a_n^2}} = \\
 - \left(\frac{\omega_0^2}{c^2} - k_0^2 \right) - \frac{1}{a_n} \frac{\partial^2 a_n}{\partial z^2} + \left(\frac{\partial \psi}{\partial z} \right)^2,
 \end{aligned} \tag{3.95}$$

and

$$-k_0 \frac{\partial a_n^2}{\partial z} + \frac{\partial a_n^2}{\partial r} \frac{\partial \psi}{\partial r} + \frac{a_n^2}{r} \frac{\partial}{\partial r} r \frac{\partial \psi}{\partial r} = -\frac{\partial}{\partial z} \left(a_n^2 \frac{\partial \psi}{\partial z} \right) \quad (3.96)$$

As with the model for electron density, also here we assume marginal variations and disregard all second-order derivatives in the z -direction. Equations (3.95) and (3.96) then become

$$\begin{aligned} -2k_0 \frac{\partial \psi}{\partial z} + \left(\frac{\partial \psi}{\partial r} \right)^2 - \frac{1}{a_n r} \frac{\partial}{\partial r} r \frac{\partial a_n}{\partial r} + \frac{1}{\lambda_c^2} \frac{N_e}{\sqrt{1 + a_n^2}} = \\ \left(\frac{\omega_0^2}{c^2} - k_0^2 \right) \end{aligned} \quad (3.97)$$

and

$$-k_0 \frac{\partial a_n^2}{\partial z} + \frac{\partial a_n^2}{\partial r} \frac{\partial \psi}{\partial r} + \frac{a_n^2}{r} \frac{\partial}{\partial r} r \frac{\partial \psi}{\partial r} = 0 \quad (3.98)$$

The zeroth-order solution corresponds to a situation where all the derivatives can be neglected:

$$\begin{aligned} a_n &\equiv \text{constant} \equiv a_0 \\ \psi &\equiv \text{constant} \equiv \psi_0 \quad , \end{aligned} \quad (3.99)$$

i.e., to a plane wave. From Eq. (3.10) it is seen that a uniform plane wave does not excite net fluctuations in electron density:

$$N_e \equiv 1 \quad .$$

Therefore the zeroth-order solution yields the familiar dispersion relation for electromagnetic waves in plasma:

$$\begin{aligned} \frac{1}{\lambda_c^2} \frac{1}{\sqrt{1 + a_0^2}} &= \frac{\omega_0^2}{c^2} - k_0^2 \\ \Rightarrow \omega_0^2 &= \frac{\omega_{p0}^2}{\sqrt{1 + a_0^2}} + c^2 k_0^2 \quad , \end{aligned} \quad (3.100)$$

in agreement with our initial definition of ω_0 and k_0 . The square root factor dividing the plasma frequency is due to the mass increase of the electrons that follow the oscillating field:

$$\begin{aligned}
 p_{osc} &= -\frac{eE}{\omega_0} = \frac{eA}{c} \\
 \Rightarrow \gamma_{osc} &= \sqrt{1 + \frac{p_{osc}^2}{m^2 c^2}} = \sqrt{1 + \frac{e^2 A^2}{m^2 c^4}} \\
 &= \sqrt{1 + a_n^2} \\
 \Rightarrow m_{rel} &= \gamma_{osc} m = \sqrt{1 + a_n^2} m \quad .
 \end{aligned} \tag{3.101}$$

Using the zeroth-order dispersion relation, we write the first order amplitude equation in the form

$$\begin{aligned}
 -\frac{\partial \psi}{\partial z} + \frac{1}{2k_0} \left\{ \left(\frac{\partial \psi}{\partial r} \right)^2 - \frac{1}{a_n r} \frac{\partial}{\partial r} r \frac{\partial a_n}{\partial r} + \right. \\
 \left. \frac{1}{\lambda_c^2} \left[\frac{N_e}{\sqrt{1 + a_n^2}} - \frac{1}{\sqrt{1 + a_0^2}} \right] \right\} = 0 \quad .
 \end{aligned} \tag{3.102}$$

Equation (3.102) has the form of the Hamilton-Jacobi equation,

$$\frac{\partial S}{\partial t} + H = 0 \quad , \tag{3.103}$$

when we identify :

$$\begin{aligned}
 \text{action } S &\rightarrow -\psi \quad , \\
 \text{time } t &\rightarrow z \quad ,
 \end{aligned} \tag{3.104}$$

and

$$\begin{aligned}
 \text{Hamiltonian } H &\rightarrow \frac{1}{2k_0} \left\{ \left(\frac{\partial \psi}{\partial r} \right)^2 - \frac{1}{a_n r} \frac{\partial}{\partial r} r \frac{\partial a_n}{\partial r} + \right. \\
 &\left. \frac{1}{\lambda_c^2} \left[\frac{N_e}{\sqrt{1 + a_n^2}} - \frac{1}{\sqrt{1 + a_0^2}} \right] \right\} \quad .
 \end{aligned} \tag{3.105}$$

The canonical momentum is then given by

$$p_r = -\frac{\partial \psi}{\partial r} \quad , \tag{3.106}$$

and the Hamiltonian can be alternatively written as

$$H = \frac{1}{2k_0} \left\{ p_r^2 - \frac{1}{a_n r} \frac{\partial}{\partial r} r \frac{\partial a_n}{\partial r} + \frac{1}{\lambda_c^2} \left[\frac{N_e}{\sqrt{1+a_n^2}} - \frac{1}{\sqrt{1+a_0^2}} \right] \right\} \quad (3.107)$$

Applying Hamilton's equations, with z corresponding to "time",

$$\begin{aligned} \frac{dr}{dz} &= \frac{\partial H}{\partial p_r} \\ \frac{dp_r}{dz} &= -\frac{\partial H}{\partial r} \end{aligned} \quad (3.108)$$

the relation between the canonical variables r and p_r is found to be

$$\frac{dr}{dz} = \frac{1}{k_0} p_r \quad (3.109)$$

and Eq. (3.98) for phase will give the conservation of beam power. The beam power is defined by

$$\begin{aligned} P &\equiv \int \mathbf{I} \cdot d\mathbf{S} = 2\pi \int I r dr = \frac{c}{4} \int |E|^2 r dr \\ &= \frac{\omega_0^2}{4c} \int a^2 r dr \end{aligned} \quad (3.110)$$

Thus (aside from a constant factor) the rate of change of the beam power in variable z is

$$\begin{aligned} \frac{dP}{dz} &\propto \int \frac{da^2}{dz} r dr + a^2 r \frac{dr}{dz} \\ &= \int \left\{ \frac{da^2}{dz} + \frac{1}{r} \frac{\partial}{\partial r} \left(a^2 r \frac{dr}{dz} \right) \right\} r dr \\ &= \int \left\{ \frac{da^2}{dz} + \frac{\partial a^2}{\partial r} \frac{dr}{dz} + \frac{a^2}{r} \frac{\partial}{\partial r} \left(r \frac{dr}{dz} \right) \right\} r dr \\ &= \int \left\{ \frac{da^2}{dz} + \frac{1}{k_0} \frac{\partial a^2}{\partial r} p_r + \frac{a^2}{k_0 r} \frac{\partial}{\partial r} (r p_r) \right\} r dr \end{aligned} \quad (3.111)$$

On the other hand, with the Hamilton-Jacobi formalism the phase equation (3.98) can be written in form

$$\begin{aligned} & -k_0 \frac{\partial a^2}{\partial z} - \frac{\partial a^2}{\partial r} p_r - \frac{a^2}{r} \frac{\partial}{\partial r} (r p_r) = 0 \\ \Leftrightarrow & \frac{\partial a^2}{\partial z} + \frac{1}{k_0} \frac{\partial a^2}{\partial r} p_r + \frac{a^2}{k_0 r} \frac{\partial}{\partial r} (r p_r) = 0 \end{aligned} \quad (3.112)$$

But according to this equation the integrand in the expression for the rate of change of power is seen to vanish, and thus the beam power is, under these approximations, conserved:

$$\frac{dP}{dz} = 0 \quad (3.113)$$

From Hamilton's equations we can also derive an equation of motion for the beam rays:

$$\begin{aligned} \frac{d^2 r}{dz^2} &= \frac{1}{k_0} \frac{dp_r}{dz} \\ &= -\frac{1}{k_0} \frac{\partial H}{\partial r} \\ &= -\frac{1}{2k_0^2} \frac{\partial}{\partial r} \left\{ \frac{1}{\lambda_c^2} \frac{N_e}{\sqrt{1+a^2}} - \frac{1}{ar} \frac{\partial}{\partial r} \left(r \frac{\partial a}{\partial r} \right) \right\} \end{aligned} \quad (3.114)$$

In order to discuss the global properties of the optical beam, from hereafter we assume the form of the solution near the beam axis to be Gaussian:

$$a = a_m e^{-\frac{1}{2} \frac{r^2}{w^2}}, \quad r \leq w \quad (3.115)$$

where a_m , the value of the amplitude on the beam axis, and w , the width of the beam, are slowly varying functions of z . This assumption allows us to carry out the calculations analytically, but at the expense of reduced accuracy. The solutions obtained using paraxial approximation are somewhat different from the solutions for the wave equation using the full slowly varying envelope

approximation (see discussion in Ref. 52). This discrepancy arises because the paraxial approximation forces the beam into Gaussian shape at all times.

Substituting the paraxial (Gaussian) trial function into the ray equation Eq. (3.114) we obtain

$$\begin{aligned} \frac{d^2 r}{dz^2} = \frac{1}{2k_0^2} \{ & 2 \frac{r}{w^4} - \frac{1}{\lambda_c^2} \frac{r}{w^2} \frac{a^2}{(1+a^2)^{3/2}} [1 - \frac{\lambda_c^2}{w^2} \frac{a^2}{\sqrt{1+a^2}} \times \\ & \left(2 - 2 \frac{r^2}{w^2} + \frac{r^2}{w^2} \frac{a^2}{1+a^2} \right)] \\ & + \frac{1}{w^2} \frac{a^2}{1+a^2} \times \\ & [-4 \frac{r}{w^2} + 2 \frac{r}{w^2} \frac{a^2}{1+a^2} + r \left(-2 \frac{r}{w^2} + \frac{r}{w^2} \frac{a^2}{1+a^2} \right)^2 \\ & - 2 \frac{r}{w^2} \left(2 - \frac{a^2}{1+a^2} \right) - 4 \frac{r^2}{w^4} \frac{a^2}{1+a^2} \left(1 - \frac{a^2}{1+a^2} \right)] \} . \end{aligned} \quad (3.116)$$

Our primary interest is not in what happens in the outer skirts of the beam but rather in what takes place near the beam axis. Therefore we shall evaluate the ray equation, Eq. (3.116) in the near-axis region by letting

$$r = \epsilon w \quad , \quad \epsilon \ll 1 \quad , \quad (3.117)$$

and neglect the second-, or higher-order terms in ϵ . Expanding the Gaussian intensity profile in this manner we see that the first term is sufficient:

$$a(r = \epsilon w) = a_m + O(\epsilon^2) \quad . \quad (3.118)$$

The ray equation now becomes

$$\begin{aligned} \epsilon \frac{d^2 w}{dz^2} = \frac{\epsilon}{2k_0^2} \{ & \frac{2}{w^3} - \frac{1}{\lambda_c^2 w} \frac{a_m^2}{(1+a_m^2)^{3/2}} [1 - 2 \frac{\lambda_c^2}{w^2} \frac{a_m^2}{\sqrt{1+a_m^2}}] \\ & + \frac{1}{w^3} \frac{a_m^2}{1+a_m^2} [-4 + 2 \frac{a_m^2}{1+a_m^2} - 2 \left(2 - \frac{a_m^2}{1+a_m^2} \right)] \} \\ & + O(\epsilon^2) \quad . \end{aligned} \quad (3.119)$$

Reintroducing the normalized intensity, $I \equiv a_m^2$, and rearranging the terms, we can write the equation in a more simplified form:

$$\begin{aligned} \frac{d^2 w}{dz^2} = \frac{1}{k_0^2} \left\{ \frac{1}{w^3} - \frac{1}{2\lambda_c^2 w} \frac{I}{(1+I)^{3/2}} \right. \\ \left. - \frac{2}{w^3} \frac{I}{1+I} \left[1 + \frac{1}{1+I} \right] + \frac{1}{w^3} \left(\frac{I}{1+I} \right)^2 \right\} , \end{aligned} \quad (3.120)$$

which is formally the equation of motion for the beam radius, $w(z)$. The terms on the right-hand side of the equation represent the forces acting on the beam radius. The first term stands for the diffraction of the beam due to the non-uniform radial profile. The other terms represent plasma lens effects.

3.6 Self-Focusing of Laser Light in Plasma

In the limit when the intensity goes to zero, the inherent diffraction of the beam overcomes the plasma focusing (which is, of course, what happens also in the absence of plasma, when all but the diffraction term disappear) and we recover pure Rayleigh spreading. In this limit the equation of motion, Eq. (3.120) becomes

$$\frac{d^2 w}{dz^2} = \frac{1}{k_0^2 w^2} , \quad (3.121)$$

which upon integration in z yields

$$w^2 = w_0^2 \left(1 + \frac{z^2}{R_L^2} \right) , \quad (3.122)$$

where $R_L \equiv \frac{1}{2} k_0 w_0^2 = \pi w_0 \left(\frac{w_0}{\lambda_0} \right)$ is the Rayleigh length, $z=0$ was chosen as the location for the beam waist: $w(z=0) = w_0$, and the initial divergence was assumed to vanish. As the intensity increases, the effect of the plasma focusing becomes more and more important until it equals in magnitude the effect of the Rayleigh spreading term. This situation corresponds to zero force in the equation of motion, and thus to a constant beam radius, $w(z) = \text{const.}$

Self-focusing occurs when the "total force" acting on the beam radius is negative in Eq. (3.120). From Eq. (3.120) this happens when

$$1 - 2I < \frac{1}{2} \frac{w^2}{\lambda_c^2} I \sqrt{1 + I} \quad , \quad (3.123)$$

or, removing the normalization and rearranging terms,

$$\sqrt{1 + \frac{e^2 E^2}{m^2 \omega_0^2 c^2}} \geq 2 \frac{\lambda_c^2}{w^2} \left[\left(\frac{m \omega_0 c}{e E} \right)^2 - 2 \right] \quad . \quad (3.124)$$

Equation (3.124) defines the critical intensity as a function of plasma and laser parameters, $I_{cr}(\frac{\lambda_c}{w})$, above which the self-focusing dominates defocusing. That is, if the initial intensity of a laser beam is higher than the critical intensity, the beam will start to focus as it enters the plasma.

It is instructive to carry the particle analogy of the ray dynamics further and calculate the effective potential responsible for the defocusing/self-focusing of the beam. We let $P_n \equiv I w^2$ be the power at the entrance to the plasma, and, according to Eq. (3.113), we assume it to be practically constant: $P_n(z) \approx P_n(0)$. Integrating the force term in Eq. (3.120), we write the equation of motion in the form

$$\frac{d^2 w}{dz^2} = -\frac{\partial V}{\partial w} \quad , \quad (3.125)$$

where

$$V(w) = \frac{1}{k_0^2} \left\{ \frac{3}{2} \frac{1}{P_n + w^2} - \frac{1}{P_n} \ln \left(1 + \frac{P_n}{w^2} \right) + \frac{1}{2} \frac{1}{\lambda_c^2} \frac{1}{\sqrt{1 + \frac{P_n}{w^2}}} + \text{constant} \right\} \quad (3.126)$$

is the Sagdeev potential for the beam radius. It is important to notice that this potential cannot be applied as such for all values of beam radius — the potential diverges as the beam radius goes to zero, $V(w \rightarrow 0) = -\infty$. This

feature can be traced back to the model for electron density:

$$N_e(r \rightarrow 0) = 1 - 2 \left(\frac{\lambda_c}{w} \right)^2 \frac{I}{\sqrt{1+I}} + O(\epsilon^2) \quad (3.127)$$

From this expression it is seen that the model describes the early stages of the laser-plasma system correctly. As the beam narrows and the laser intensity accordingly increases, the electron density near the beam axis is depleted eventually reaching zero for sufficiently high intensity (sufficiently narrow beam). For intensities higher than this, the electron density should remain zero. In the model, however, the electron density will become negative for these intensities, corresponding to an unphysical situation as described in the end of Section 3.2. This fault in the model results from the assumption of immobile ions — in reality, by the time the electrons are depleted, the ions start following them.

We find the intensity I_v and corresponding beam radius w_v at which the depletion of electrons near the axis happens:

$$\begin{aligned} N_e &= 0 \\ \Rightarrow \frac{w_v^2}{\lambda_c^2} \sqrt{1+I_v} &= 2I_v \quad , \end{aligned} \quad (3.128)$$

where $I_v = \frac{P_2}{w_v^2}$. The beam radius corresponding to vacuum formation is plotted as a function of the invariant beam power in Fig. 3.3. For $w < w_v$ the equation of motion as given by Eq. (3.120) is not valid as such. As the vacuum is formed in the axial region, the plasma lens terms should disappear and we should recover pure Rayleigh spreading. This defect of the model can be remedied by writing the equation of motion, Eq. (3.120) in two parts:

$$\begin{aligned} \frac{d^2 w}{dz^2} &= -\frac{1}{k_0^2} \left\{ \frac{4}{w^3} \frac{I}{1+I} \left[1 + \frac{1}{1+I} \right] - \frac{2}{w^3} \left(\frac{I}{1+I} \right)^2 \right. \\ &\quad \left. + \frac{1}{\lambda_c^2 w} \frac{I}{(1+I)^{\frac{3}{2}}} - \frac{2}{w^3} \right\} \quad \text{for } w > w_v \quad , \end{aligned} \quad (3.129)$$

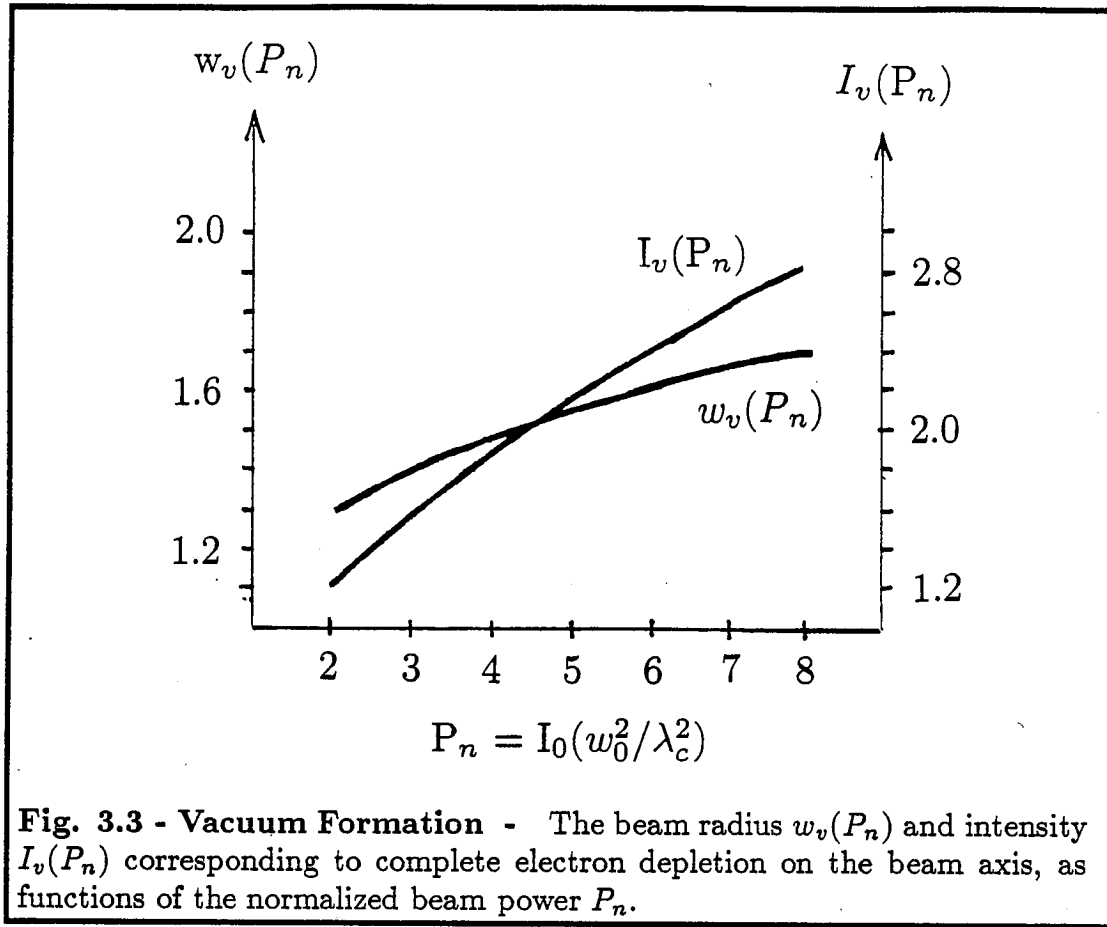


Fig. 3.3 - Vacuum Formation - The beam radius $w_v(P_n)$ and intensity $I_v(P_n)$ corresponding to complete electron depletion on the beam axis, as functions of the normalized beam power P_n .

and

$$\frac{d^2 w}{dz^2} = \frac{1}{k_0^2 w^3} \quad \text{for } w < w_v \quad (3.130)$$

where the plasma effect is absent once the electron density becomes zero in Eq. (3.127). Equation (3.130) contains only the vacuum Rayleigh diffraction. Integrating the right hand side of Eqs. (3.129) and (3.130) with respect to w , the potential becomes

$$V(w) = \frac{1}{k_0^2} \left\{ \frac{3}{2} \frac{1}{P_n + w^2} - \frac{1}{P_n} \ln \left(1 + \frac{P_n}{w^2} \right) + \frac{1}{2} \frac{1}{\lambda_c^2} \frac{1}{\sqrt{1 + \frac{P_n}{w^2}}} - \frac{1}{2\lambda_c^2} \right\} \quad \text{for } w > w_v \quad (3.131)$$

and

$$V(w) = \frac{1}{k_0^2} \left(\frac{1}{2} \frac{1}{w^2} + C \right) \quad \text{for } w < w_v, \quad (3.132)$$

where

$$C \equiv \frac{1}{2} \frac{1}{w_v^2} \frac{2 - I_v}{1 + I_v} - \frac{1}{P_n} \ln(1 + I_v) + \frac{1}{2} \frac{1}{\lambda_c^2} \left[\frac{1}{\sqrt{1 + I_v}} - 1 \right], \quad (3.133)$$

and the constant of integration has been chosen such that the potential vanishes at infinity.

To see the qualitative nature of the potential, we look for its extrema by setting the first derivative equal to zero. This leads to an equation for the extremum radius, w_e ,

$$\frac{P_n}{\lambda_c^2} \sqrt{1 + \frac{P_n}{w_e^2}} = 2 \left(1 - 2 \frac{P_n}{w_e^2} \right), \quad (3.134)$$

from which it follows that an extremum exists only if the normalized power satisfies the condition

$$P_n \leq P_{cr} \equiv 2\lambda_c^2. \quad (3.135)$$

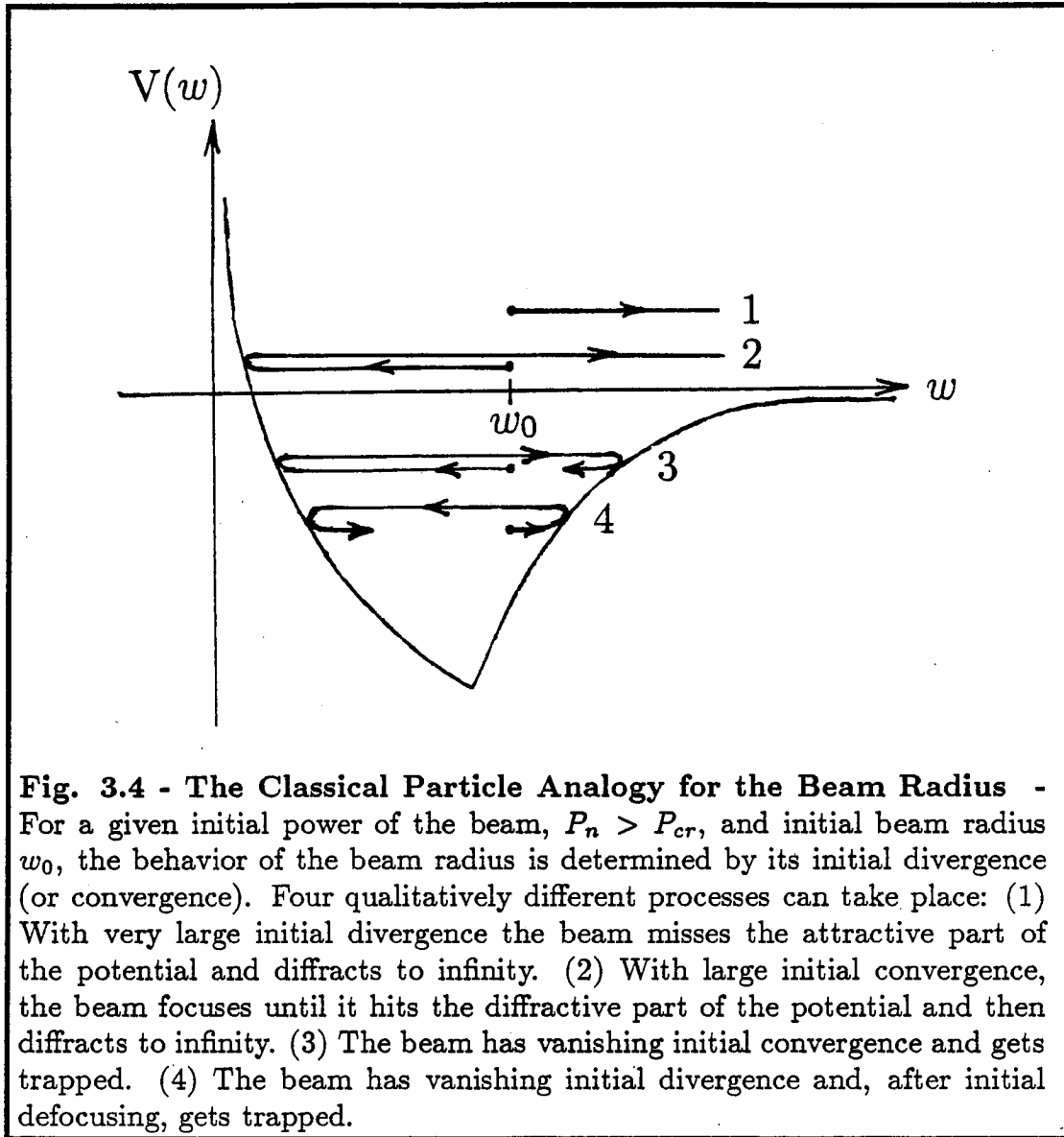
Calculating the second derivative of the potential we determine that the extremum corresponds to a maximum, and for $P_n > P_{cr}$ the potential behaves qualitatively as shown in Fig. 3.4. The qualitatively different cases for the beam radius are also indicated. It is important to note that the cusp in the potential at $w = w_v$ is a mathematical artifact arising from our model when $N_e \rightarrow 0$.

Thus the condition for self-focusing is

$$P_n \geq P_{cr} \equiv 2\lambda_c^2. \quad (3.136)$$

or, in terms of the normalized intensity,

$$I_n \geq 2 \frac{\lambda_c^2}{w^2}. \quad (3.137)$$



Defining the beam power by

$$P = c \int \frac{E(r)^2}{8\pi} 2\pi r dr = \frac{c}{8} E_m^2 w^2, \quad (3.138)$$

where E_m is the field amplitude on the axis: $E_m \equiv E(r=0)$, the critical power

is given by

$$P_{cr} = \frac{c}{4} \left(\frac{mc^2}{e} \right) \frac{\omega_0^2}{\omega_{p0}^2} \approx 10^{10} \frac{\omega_0^2}{\omega_{p0}^2} W \quad (3.139)$$

The threshold power obtained here compares favorably with work done earlier on the subject. As mentioned earlier, Schmidt and Horton⁵⁰ addressed the possible self-focusing of a laser beam in plasma including relativistic effects only. They found that the focusing effects dominate over the diffractive effects once a threshold given by the normalized power,

$$P_{n,SH} = \lambda_c^2 \quad (3.140)$$

is exceeded. If we repeat the analysis given above for relativistic effects only, we find that our threshold power remains unaltered:

$$P_{n,rel} = 2\lambda_c^2 \quad (3.141)$$

Therefore, aside from a factor of two, the result obtained by Schmidt and Horton agrees with the one yielded by the analysis given here. The difference of the factor of two is in this case actually a difference of three factors of two combined: First, as mentioned earlier, Schmidt and Horton used linearly polarized wave whereas a circularly polarized one was used in this work accounting for one factor of two. Secondly, Schmidt and Horton expanded the relativistic gamma before obtaining the expression for the threshold power thus introducing another factor of two. And thirdly, Schmidt and Horton never assumed any specific form for the profile (e.g. Gaussian, as was chosen here). Therefore, what they call the width of the beam w_{SH} is somewhat arbitrary. In deriving the threshold power they replace the transverse part of the Laplacian (in slab geometry) by the inverse of the width squared,

$$\frac{d^2}{dx^2} A \rightarrow \frac{1}{w_{SH}^2} A \quad , \quad (3.142)$$

whereas in our case, evaluating the (cylindrical) Laplacian near the beam axis we obtain

$$\frac{1}{r} \frac{\partial}{\partial r} r \frac{\partial}{\partial r} A \rightarrow \frac{2}{w^2} A \quad , \quad (3.143)$$

and the third factor of two is revealed.

An important consequence we wish to emphasize is that the threshold power for self-focusing is entirely defined by the relativistic effects. This seems quite reasonable because, as discussed in Chapter II, the relativistic effects are practically instantaneous whereas it will take a finite time before the ponderomotive effects can produce the lensing effect necessary for the self-focusing.

The analysis carried out by Felber⁵² who assumed quasineutrality and an equilibrium in which the ponderomotive force is balanced by the thermal pressure, yielded the following threshold power for the self-focusing:

$$P_{n,F} = 4\lambda_D^2 \quad , \quad (3.144)$$

where λ_D is the Debye length. It is formally similar to the condition obtained by Schmidt and Horton and us, but the scale length of Felber's system is the Debye length rather than the collisionless skindepth. This implies a strong temperature dependence of the plasma response, which could cause thermally unstable plasma profiles in the quasineutral regime.

Another comparison can be made with the filamentation mode.⁵⁸ Felber and Chernin⁵⁹ have found that laser light in a plasma goes unstable with respect to filamentation when

$$C \equiv \frac{1}{2} \epsilon_1 k_0^2 w^2 > \frac{1}{2} \quad , \quad (3.145)$$

where

$$\begin{aligned}
 k_0 &= \text{unperturbed wavenumber of the laser field,} \\
 \epsilon_1 &= \frac{I_n}{\epsilon_0} \frac{d\epsilon}{dI_n} \text{ evaluated near the beam axis,} \\
 &\text{where the electric field can be approximated by a plane wave,} \quad (3.146) \\
 \epsilon &= \text{scalar dielectric constant of the plasma, and} \\
 \epsilon_0 &= \text{dielectric constant evaluated near the beam axis.}
 \end{aligned}$$

In the short pulse regime (immobile ions) the plasma response may be described by the dielectric constant

$$\epsilon = 1 - \left(\frac{\omega_p}{\omega_0} \right)^2 \frac{N_e}{\sqrt{1 + I_n}}, \quad (3.147)$$

where N_e is defined by equation (3.10). This gives

$$C = \frac{1}{2} \left(\frac{w}{\lambda_c} \right)^2 \left[\frac{1}{2} \frac{I_n}{(1 + I_n)^{3/2}} + 2 \left(\frac{\lambda_c}{w} \right)^2 \frac{I_n}{(1 + I_n)^2} \right] \quad (3.148)$$

The condition for a plasma to go unstable against filamentation in Eq. (3.145) is now equivalent to :

$$I_n \sqrt{1 + I_n} > 2 \left(\frac{\lambda_c}{w} \right)^2 (1 + I_n^2), \quad (3.149)$$

which, for nonrelativistic amplitudes ($I \ll 1$), resembles the condition for the self-focusing given by Eq. (3.123). Thus the self-trapping of the laser light seems to be closely related to the filamentation instability, at least for nonrelativistic amplitudes.

After addressing the question “to focus or not to focus”, we shall now study what happens to the beam after initial self-focusing.

According to our analysis above, provided that the beam power (or intensity — notice that for $P_n > P_{cr}$ also the condition (3.123) for intensity is

satisfied) is high enough, and that the initial divergence, $\frac{dw}{dz}$, is small enough (in our analysis the initial divergence was assumed to be zero), the beam entering the plasma will self-focus. In our model there are two possible mechanisms to halt this focusing. Either (1) the self-focusing continues until the intensity reaches a high enough value for electron evacuation to take place (cf. Eq. (3.128)), after which the central beam is propagating in vacuum and will thus Rayleigh spread, or, (2) the natural diffraction of the beam, which increases with decreasing beam radius, takes over the focusing as the beam shrinks to small enough radius. The equation of motion for the beam radius, Eq. (3.120) shows that the net force guiding the evolution of the beam radius is still negative for the evacuation intensity I_v given by Eq. (3.128). Therefore we conclude that, within the framework of our model (including the assumption of vanishing initial divergence) the electron depletion (and thus the vacuum duct formation) will always take place once the self-focusing has begun. If the beam has a substantial initial divergence, it is possible that the diffraction takes over before the electron depletion occurs.

After the beam has shrunk enough to bring about the electron depletion, it will thus propagate in vacuum and start to diverge. The diverging beam will encounter ever increasing electron density outside the central vacuum duct. The beam will now have two options depending on the initial divergence, which in the classical particle analogy plays the role of the kinetic energy. If the initial divergence was large enough, the beam will diffract forever. However, in the case of vanishing initial divergence, the plasma lens effects brought about by the increasing electron density will eventually dominate, and the beam will start to focus again. These different cases are illustrated with the help of the classical particle analogy in Fig. 3.4.

In what follows we study the behavior of the system in the situation where the potential has an attractive part (i.e. $P > P_{cr}$) and the initial divergence of the beam is vanishing. Then, according to our model, the beam will self-trap, i.e. the beam radius will oscillate around an equilibrium value corresponding to the minimum of the potential. The oscillations are not, however, symmetric since the potential is not symmetric across the minimum. This asymmetry arises because the physical mechanism responsible for the self-focusing is not the same as the mechanism that causes defocusing; self-focusing is due to the nonlinear interaction between the laser wave and the plasma, whereas defocusing is due to the absence of plasma. Thus the forces responsible for the different phases are necessarily different.

The equation of motion, Eq. (3.120) in the neighborhood of the minimum of the potential, $w_0 \equiv w_v$, can be rewritten as

$$\begin{aligned} \frac{d^2 w}{dz^2} &\approx -\left\{ \frac{\partial V}{\partial w} \Big|_{w_0} + \frac{\partial^2 V}{\partial w^2} \Big|_{w_0} (w - w_0) \right\} \\ \Rightarrow \frac{d^2 \xi}{dz^2} + \kappa^2 \xi &= -\beta \quad , \end{aligned} \tag{3.150}$$

where

$$\begin{aligned} \xi &\equiv w - w_0 \quad , \\ \beta &\equiv \frac{\partial V}{\partial w} \Big|_{w_0} \quad , \quad \text{and} \\ \kappa^2 &\equiv \frac{\partial^2 V}{\partial w^2} \Big|_{w_0} \quad . \end{aligned}$$

Equation (3.150) has to be applied separately in the defocusing and self-focusing regions, because the quantities κ and β have different values in these regions. We shall denote the quantities related to self-focusing and defocusing phases by subscripts 1 and 2 , respectively.

Consider now a laser beam with initial radius w_i and initial divergence w'_i . Assuming that the intensity of the beam is high enough and w'_i is weak

enough, the beam starts self-focusing as it enters the plasma and the solution for this phase is given by

$$\xi_1(z) = \frac{\Delta'_0}{\kappa_1} \sin(\kappa_1 z) + \left(\Delta_0 + \frac{\beta_1}{\kappa_1^2} \right) \cos(\kappa_1 z) - \frac{\beta_1}{\kappa_1^2} , \quad (3.151)$$

where $\Delta_0 \equiv w_i - w_0$, $\Delta'_0 \equiv w'_i$, $\kappa_1^2 \equiv \frac{3}{k_0^2 w_0^4}$, and $\beta_1 \equiv \frac{1}{k_0^2 w_0^8}$. After half of the period, at $z = z_0 = \frac{\pi}{\kappa_1}$, self-focusing gives way to defocusing and the beam starts to obey the second solution

$$\xi_2(z) = A \sin(\kappa_2 z) + B \cos(\kappa_2 z) - \frac{\beta_2}{\kappa_2^2} , \quad (3.152)$$

where

$$\kappa_2^2 \equiv \frac{1}{k_0^2 w_v^4} \frac{3 - 5I_v^2 - 11I_v}{(1 + I_v)^3} \quad \text{and}$$

$$\beta_2 \equiv \frac{1}{k_0^2} \left\{ \frac{2}{w_v^3} \frac{2I_v - 1}{(1 + I_v)^2} + \frac{1}{\lambda_c^2 w} \frac{I_v}{(1 + I_v)^{\frac{3}{2}}} \right\} .$$

Matching the two solutions at $z = z_0$ we obtain the amplitudes A and B, and the solution can be written in the form

$$\xi_2(z) = \left\{ \frac{\beta_2}{\kappa_2^2} - 2 \frac{\beta_1}{\kappa_1^2} - \Delta_0 \right\} \cos\left(\frac{\kappa_2}{\kappa_1} \pi - \kappa_2 z\right) + \left(\frac{\Delta'_0}{\kappa_2} \right) \sin\left(\frac{\kappa_2}{\kappa_1} \pi - \kappa_2 z\right) - \frac{\beta_2}{\kappa_2^2} . \quad (3.153)$$

The behaviour of the beam radius in the case of self-trapping is sketched in Fig. 3.5.

The shortcomings of our model are now obvious from the expressions for the beam radius. For $w = w_v$ to be a true equilibrium value, the constant terms in the expressions for the beam radius should disappear since they correspond to the first derivative of the potential at that point. The problem lies again in the model for the electron density and in the fact that, in order to prevent the electron density from getting negative, we wrote the potential in two parts.

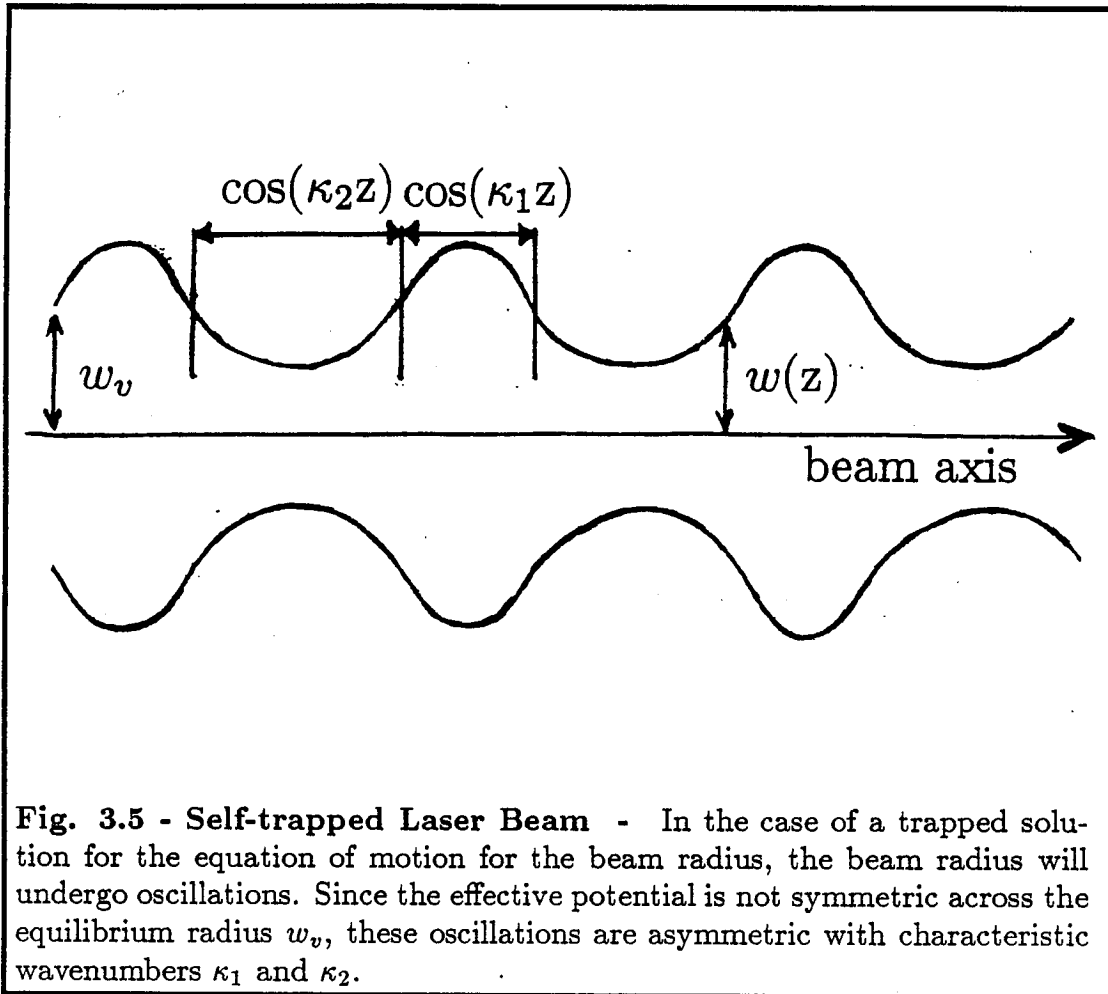


Fig. 3.5 - Self-trapped Laser Beam - In the case of a trapped solution for the equation of motion for the beam radius, the beam radius will undergo oscillations. Since the effective potential is not symmetric across the equilibrium radius w_v , these oscillations are asymmetric with characteristic wavenumbers κ_1 and κ_2 .

Therefore the equilibrium radius w_v is a forced one, located at the kink of the potential. The true form of the potential at $w = w_v$ should, of course, be smooth. Despite of this weakness of the model, this analysis gives us a qualitative picture of the behaviour of the beam as well as an approximation for the equilibrium beam radius w_v .

For very high powers it is not correct to treat the ions as infinitely massive because in reality they start following the electrons. For the present model to be self-consistent the characteristic time t_i for ions has to satisfy $t_i \gg t_{pulse}$, where t_{pulse} is the laser pulse length.

The equation of motion for ions gives the acceleration:

$$\dot{v}_i \approx \frac{eE_r}{M} \quad , \quad (3.154)$$

where M is the ion mass and the radial electric field is given by Gauss' law:

$$\frac{1}{r} \frac{\partial}{\partial r} (rE_r) = -4\pi e \delta n_e \quad .$$

Using Eq. (3.10) for the fluctuations in the electron density we obtain

$$E_r = 4\pi e n_0 \left(\frac{\lambda_c}{w} \right)^2 r \frac{I_n}{\sqrt{1 + I_n}} \quad . \quad (3.155)$$

(The integration constant was set to zero in order to make the electric field vanish at infinity). The electric field is seen to vanish on the beam axis, and since we are looking for the maximum value of the electric field, we have to evaluate Eq. (3.155) away from the axis. Because of the exponential radial dependence of the intensity, we can approximate $\sqrt{1 + I_n} \approx 1$ and obtain

$$E_r \approx \frac{mc^2}{ew^2} r I_0 e^{-r^2/w^2} \quad , \quad (3.156)$$

where we have used the definition of the collisionless skindepth, $\lambda_c = \frac{c}{\omega_p}$. The maximum electric field is found at $r^2 = \frac{1}{2}w^2$:

$$E_{r,max} \approx 0.4 I_0 \frac{mc^2}{ew} \quad , \quad (3.157)$$

or, equivalently, recalling that $I_0 = \frac{v_g^2}{c^2} < 1$,

$$\frac{eE_{r,max}}{m\omega_p c} = 0.4 \frac{\lambda_c}{w} \frac{v_g^2}{c^2} \quad . \quad (3.158)$$

Using this value for the electric field in expression (3.154) we find

$$\dot{v}_i \approx 0.4 \frac{m}{M} \frac{1}{w} \frac{v_g^2}{c^2} c^2 \quad . \quad (3.159)$$

Taking all the electrons to be displaced by the vacuum channel radius w_v , given by $\frac{w_v^2}{\lambda_c^2} \sqrt{1 + (\frac{v_q}{c})^2} = 2(\frac{v_q}{c})^2$, we get a rough approximation for the ion oscillation time:

$$\begin{aligned} t_i &\approx \sqrt{2 \frac{w_v}{v_i}} \approx \sqrt{\frac{M}{0.2m}} \frac{w_v}{\lambda_c} \frac{c}{v_q} \frac{1}{\omega_p} \\ \Rightarrow t_i &\approx \sqrt{10 \frac{M}{m}} \frac{1}{\omega_p} \approx 140 \frac{1}{\omega_p} , \end{aligned} \quad (3.160)$$

for a hydrogen plasma. The laser pulse length should be sufficiently shorter than t_i given by Eq. (3.160).

3.7 Plasma Fiber Accelerator

The picture of laser self-focusing given in the preceding sections appears very suitable for the plasma fiber accelerator scheme.³⁷ Assume we have produced a rarefied channel around the beam axis in the manner described above. This channel acts as an effective plasma waveguide thus providing a longitudinal component of the electric field. Letting k_{\parallel} denote the wavenumber of the wave parallel to the waveguide, we have the familiar result for the phase velocity of an electromagnetic wave in a waveguide:

$$v_{ph} = \frac{\omega_0}{k_{\parallel}} > c . \quad (3.161)$$

Thus, although the plasma waveguide provides the longitudinal component of the electric field necessary for particle acceleration, the phase velocity of the field is too high for efficient coupling to the particles.

If, however, the walls of the waveguide are rippled instead of straight as shown in Fig. 3.5, the system provides a slow wave structure of electromagnetic waves:⁶⁰

$$v_{ph} = \frac{\omega}{k_{\parallel} + \kappa} , \quad (3.162)$$

where κ is the wavenumber of the ripples. (The ripples are called irises in accelerator physics, and a "rippled" waveguide is called a loaded waveguide). By varying the parameters of the laser-plasma system we can adjust the wavenumber of the ripples and can, at least in principle, provide ideal coupling between the wave and the particles:

$$v_{ph} = v_{particle} \approx c \quad . \quad (3.163)$$

The proper wavenumber of the ripples κ for this case can be obtained using the dispersion relation, $\omega_0^2 = c^2(k_0^2 + k_T^2)$,

$$\begin{aligned} c &= \frac{\omega}{k_0 + \kappa} = \sqrt{k_0^2 + \frac{\pi^2}{w_v^2} \frac{c}{k_0 + \kappa}} \\ \Rightarrow \kappa &\approx \frac{\pi}{4} \frac{\lambda_0}{w_v^2} \quad . \end{aligned} \quad (3.164)$$

Using this expression we can check the self-consistency of both the marginal and the eikonal approximation. In the radial direction, from the Eq. (3.128) for the radius of the vacuum channel it is seen that it satisfies the condition for eikonal approximation:

$$w_v \ll \lambda_c \ll \lambda_0 \quad . \quad (3.165)$$

Therefore

$$L_{ripple} = \frac{1}{\kappa} \approx \left(\frac{w_v}{\lambda_0} \right) w_v \gg \lambda_0 \quad , \quad (3.166)$$

and the eikonal approximation is valid also in the z-direction. Furthermore, since

$$L_{ripple} \gg w_v \quad , \quad (3.167)$$

the marginal approximation is self-consistent.

The parallel electric field available for accelerating particles is roughly given by⁶¹

$$\frac{E_{\parallel}}{E_T} = \frac{1}{2} \frac{\pi}{k_0 w} \frac{\delta \omega_p^2}{\omega_p^2} \leq \frac{1}{2} \frac{\pi}{k_0 w} \quad , \quad (3.168)$$

where $\frac{\delta \omega_p^2}{\omega_p^2}$ describes the fraction of plasma density that forms the ripples, and E_T is the transverse laser field.

Chapter IV

Numerical Model for Self-Trapping

4.1 Motivation for a Numerical Model

The theoretical study of the previous chapter provides us with great promises: it seems that the problem of reduction of laser intensity due to diffraction can be overcome with the help of nonlinear self-focusing, and the phase mismatch between the laser fields and the particles to be accelerated can be eliminated by a rippled plasma wave guide. However, the laser-plasma system is extremely complex and so, in deriving these predictions, we were forced to employ several approximations. Therefore it is desirable to have a means to verify the validity of these predictions. Many potential disasters can be avoided and valuable insight gained if, before setting up elaborate experiments with real plasmas, the problem is further explored with computer simulations.

The interrelation between high frequency electromagnetic waves and plasma oscillations has been an active area of research, and computational efforts are fairly well documented.^{22,24,23} However, the investigation of the beam dynamics over longer time scales and larger spatial extent is less developed. Some attempts have been made but these tend to lack self-consistency.²⁶ It is of vital importance, therefore, to develop a numerical model that encompasses time scales much longer than the radiation time scale and that can follow the overall dynamics (i.e. transport) of the optical beam. Only with such a model one can fully study, for example, the long time scale evolution and transport of the beam in applications to the beat wave accelerator²² and the plasma fiber

accelerator.³⁷

Most numerical studies of laser self-trapping have been attempts to numerically integrate the field equations using various models for the plasma response. There are very few papers reporting studies of self-trapping using a particle simulation code.^{53,62,63} The difficulty in using a conventional particle simulation code to simulate the self-focusing of a laser beam including the ponderomotive effects lies in the disparity of time and spatial scales of the problem. The electromagnetic radiation has typically very high frequency (unless it is in resonance or propagates in an overdense plasma), $\omega_0 \sim ck_0$, where k_0 is the wavenumber of the wave and c is the speed of light, and so, in order to resolve the rapid oscillations, the time step of a conventional particle simulation code has to be minute. The ponderomotive modulations, on the other hand, take place in a time scale much longer than the laser oscillation period. An estimate for the ponderomotive effects is obtained by finding the approximate time it takes for the electron density to get deformed, *i.e.*, how long it takes for an electron to drift a characteristic distance, say, the beam radius w_0 . As described in the earlier chapters, the electron will experience net drift outward due to the nonuniform intensity profile of the laser. Assuming that the electron is at rest on the axis when the laser electric field starts acting on it, it will accelerate during the first quarter of the oscillation period, $T_0 = 2\pi/\omega_0$, to a maximum velocity roughly given by (for non-relativistic case)

$$|v_{max}| \leq \left| \frac{e}{m} \int_0^{T_0/4} E_0 \cos \omega_0 t dt \right| = \frac{e}{m\omega_0} E_0 \quad (4.1)$$

During the second quarter of the oscillation period the laser field will, after reversing its direction, slow the electron down to rest again. Thus the average

velocity of the electron is, during the first half of the oscillation period

$$\langle v \rangle \simeq \frac{1}{2} \frac{e}{m\omega_0} E_0 \quad (4.2)$$

and the distance it has moved in this time is

$$\Delta x_{out} \approx \langle v \rangle \frac{T_0}{2} = \frac{cT_0}{4} \sqrt{I_n}, \quad (4.3)$$

where $I_n \equiv (e^2 E_0^2 / m^2 \omega_0^2 c^2)$ is the normalized intensity introduced in Chapter II. The electron will then experience a force pulling it back towards the axis and thus it reverses its motion. Since the electron is now displaced from the axis by Δx_{out} , the electric field acting on the electron is smaller than the field bringing it out. The electric field accelerating the electron inward is given by

$$E_{in} = E_0 e^{-\Delta x_{out}^2 / w_0^2} \cos \omega_0 t \quad (4.4)$$

and so, repeating the simple calculation performed above, the distance the electron traverses during the latter half of the oscillation period is given by

$$\Delta x_{in} \approx \frac{cT_0}{4} \sqrt{I_n} e^{-\Delta x_{out}^2 / w_0^2} = \frac{cT_0}{4} \sqrt{I_n} e^{-\frac{1}{16} \left(\frac{\lambda_0}{w_0}\right)^2 I_n}, \quad (4.5)$$

where we have used $cT_0 \approx \lambda_0$ in the expression for Δx_{out} . Noticing that for realistic beams $\lambda_0 \ll w_0$ and, recalling that we assumed the beam to be non-relativistic, $I_n < 1$, we estimate the net outward drift of the electron during one oscillation period to be

$$\Delta x_{out} - \Delta x_{in} \approx \frac{cT_0}{4} \sqrt{I_n} \left[1 - \left(1 - \frac{1}{16} \left(\frac{\lambda_0}{w_0} \right)^2 I_n \right) \right] = \frac{cT_0}{64} \left(\frac{\lambda_0}{w_0} \right)^2 I_n^{3/2}. \quad (4.6)$$

So the fraction of the beam radius w_0 that the electron traverses in one oscillation period is given by

$$\frac{\Delta x_{out} - \Delta x_{in}}{w_0} \approx \frac{1}{64} \left(\frac{\lambda_0}{w_0} \right)^3 I_n^{3/2}. \quad (4.7)$$

Thus, for nonrelativistic beams with realistic beam parameters ($\lambda_0/\omega_0 \lesssim 0.1$) the time it takes for an electron to drift across one beam radius is of the order of $10^4 T_0$! (This is actually not quite accurate since the electron will also have a net increase in its outward velocity after each oscillation, as mentioned earlier. Nonetheless, the fact remains that this second-order drift is very slow compared to the laser oscillations).

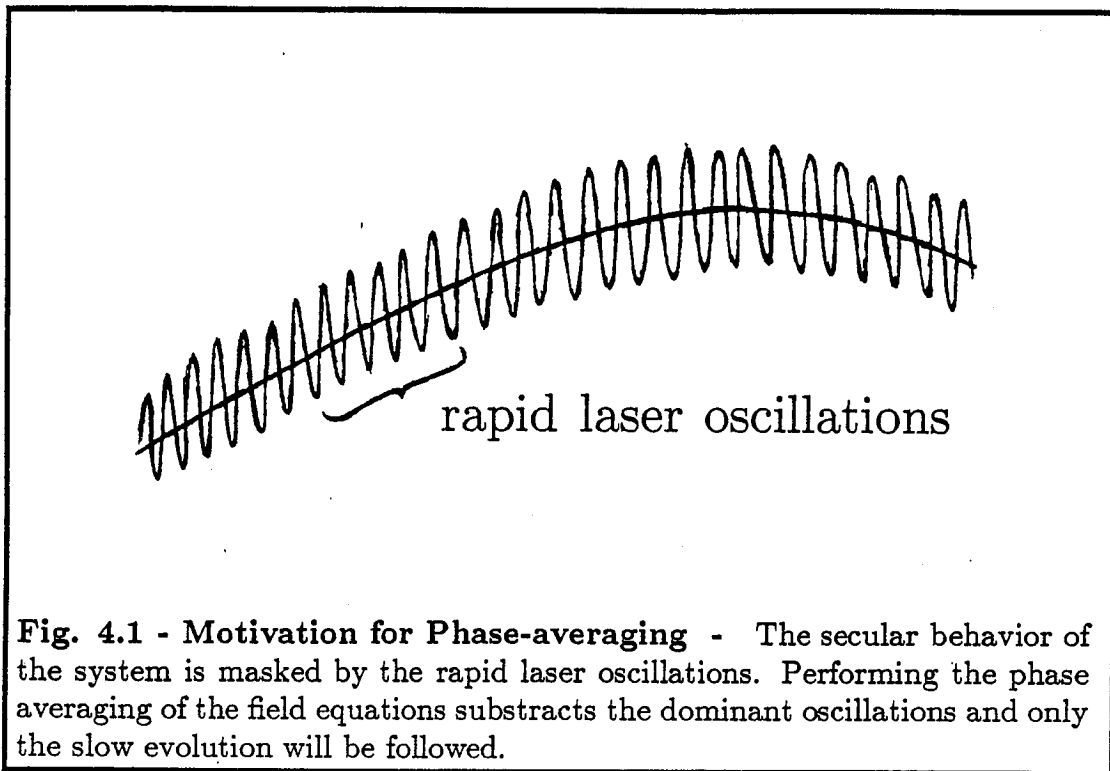
Although it is not necessary for the electrons to drift quite this long distances in order to produce a density perturbation significant enough to re-fract the beam, an enormous number of time steps is required in order to *both* observe the evolution of the beam under the ponderomotive effects *and* resolve the rapid laser oscillations. The laser oscillation period and the ponderomotive effects are not the only time scales present in the plasma laser system. Plasma oscillations involve the electron plasma frequency $\omega_p = \sqrt{\frac{4\pi n e^2}{m}}$ which is typically much smaller than the photon frequency ω_0 in an underdense plasma. In what follows we concern ourselves primarily with underdense plasmas. There are also time scales associated with ions (such as the ion plasma frequency ω_{pi} , and ion acoustic frequency $k_0 c_s$, with c_s being the sound speed) and those associated with the transport of the optical beam (including diffusion, diffraction, scattering and dissipation (depletion)).

A similar hierarchy of spatial scales can be discerned as well. They are the electromagnetic wavelength, the plasma wavelength associated with the plasma frequency and the Debye length, the dimensions of the optical beam (the width and the length), and the transport length such as the depletion length. The grid cell size is restricted by the wavelength of the laser, which is much less than the characteristic length in the problem, say the beam radius. Therefore,

in order to simulate self-focusing including ponderomotive effects using a conventional, $2\frac{1}{2}$ dimensional, fully electromagnetic particle simulation code, we would need an immense grid and an unacceptable number of time steps.

Since a particle simulation is much closer to a real plasma experiment than a mere numerical solution of the equations, we have pursued ways of avoiding the practical problems mentioned above. In this chapter we present a scenario conceived to circumvent the severe limitations imposed by the rapid laser oscillations.

The present effort of model development may be regarded as an electromagnetic counterpart to the Zakharov model⁶⁴ of electrostatic pulses and to the subsequent numerical calculations.^{65,66} In Section 4.2 we present our model of time-averaged (or phase-averaged) equations. The equations governing the evolution of the electromagnetic fields and the particle dynamics are averaged over the rapid laser oscillations as was done in the previous chapter. This way only the secular changes in field quantities will be followed. Also, since typically the amplitude of the modulation is much smaller than the amplitude of the electromagnetic oscillations, this scheme has the additional advantage of making the signal cleaner by averaging out the masking dominant oscillations, see Fig. 4.1. In Section 4.3 computational algorithmic considerations are discussed. Test results of the code are discussed in Section 4.4. The field solver is tested by using the code to propagate a Gaussian laser beam in vacuum. The soundness of the particle solver is then tested by following the propagation of a plane wave in plasma. To test the particle pusher we use a nonuniform field and monitor the collective behavior of the electrons.



4.2 Mathematical Formulation

The basic idea in developing the mathematical model for computation is to average the equations evolving the electromagnetic field and the equations governing the electron motion (the ions are assumed to be stationary in this first version) over the short laser oscillation period. That way we eliminate the fast time scale of the uninteresting rapid oscillations and follow only the slower time scales associated with the net changes in quantities of interest as illustrated in Fig. 4.1. The averaging in space and time can be carried out simultaneously provided the ansatz is chosen appropriately.

Consider the wave equation for the vector potential instead of the set of Maxwell's equations for the electric and magnetic fields. This is done because averaging Maxwell's equations over the laser oscillation period would lead to a

set of trivial identities. Further, if we had chosen to study the wave equation in terms of either electric or magnetic field, the plasma contribution would appear as the time derivative of the plasma current, whereas with the vector potential the plasma current as such appears in the wave equation. Writing the electric and magnetic fields in terms of their potentials,

$$\mathbf{E} \equiv -\nabla\Phi - \frac{1}{c} \frac{\partial \mathbf{A}}{\partial t}, \quad \mathbf{B} \equiv \nabla \times \mathbf{A}, \quad (4.8)$$

and choosing the Coulomb gauge (for justification, see previous chapter),

$$\nabla \cdot \mathbf{A} = 0, \quad (4.9)$$

the wave equation, rewritten from Eq. (3.14), becomes

$$\frac{1}{c^2} \frac{\partial^2 \mathbf{A}}{\partial t^2} - \nabla^2 \mathbf{A} + \frac{1}{c} \nabla \frac{\partial \Phi}{\partial t} = \left(\frac{4\pi}{c} \right) \mathbf{J}. \quad (4.10)$$

As in the previous chapter, the electromagnetic fields are assumed to have circular polarization and the vector potential is written in the form

$$\mathbf{A}(\mathbf{x}, t) = a(\mathbf{x}, t) \exp \{ i k_0 z - i \omega_0 t - i \psi(\mathbf{x}, t) \} (\hat{\mathbf{x}} + i \hat{\mathbf{y}}), \quad (4.11)$$

where amplitude $a(\mathbf{x}, t)$ and phase shift $\psi(\mathbf{x}, t)$ are slowly varying (compared to the laser oscillations), real quantities:

$$\begin{aligned} \left| \frac{\partial \psi}{\partial t} \right| &\ll \omega_0 & \left| \frac{\partial \psi}{\partial z} \right| &\ll k_0 \\ \left| \frac{\partial a}{\partial t} \right| &\ll \omega_0 a & \left| \frac{\partial a}{\partial z} \right| &\ll k_0 a \end{aligned} \quad (4.12)$$

The averaging over laser oscillations now becomes straightforward for most terms in the wave equation:

$$\begin{aligned} \frac{1}{T_0} \int |\mathbf{A}|^2 dt &= \frac{1}{2} \mathbf{A} \cdot \mathbf{A}^* = a(\mathbf{x}, t)^2 \\ \frac{1}{\lambda_0} \int |\mathbf{A}|^2 dz &= \frac{1}{2} \mathbf{A} \cdot \mathbf{A}^* = a(\mathbf{x}, t)^2, \end{aligned} \quad (4.13)$$

where \mathbf{A}^* is the complex conjugate of \mathbf{A} . If we use Eq. (4.11) for the vector potential and multiple the wave equation by the complex conjugate of \mathbf{A} , the real part of the wave equation yields an averaged partial differential equation for the amplitude, $a(\mathbf{x}, t)$, and the imaginary part yields an averaged equation for the phase shift, $\psi(\mathbf{x}, t)$:

$$\begin{aligned} \frac{\partial^2}{\partial t^2} a = & c^2 \nabla^2 a + a \left[\left(\frac{\partial \psi}{\partial t} \right)^2 - c^2 |\nabla \psi|^2 \right] + (\omega_0^2 - c^2 k_0^2) a \\ & + 2a \left[\omega_0 \frac{\partial \psi}{\partial t} + c^2 k_0 \frac{\partial \psi}{\partial z} \right] + \left(\frac{4\pi}{c} \right) \text{Re}(\mathbf{J} \cdot \mathbf{A}^*) \end{aligned} \quad (4.14)$$

and

$$\frac{\partial}{\partial t} \left(a^2 \frac{\partial \psi}{\partial t} \right) = c^2 \nabla \cdot (a^2 \nabla \psi) - 2a \left(\omega_0 \frac{\partial a}{\partial t} + c^2 k_0 \frac{\partial a}{\partial z} \right) - \left(\frac{4\pi}{c} \right) \text{Im}(\mathbf{J} \cdot \mathbf{A}^*), \quad (4.15)$$

where use was made of the fact found in Chapter III that the term involving scalar potential does not survive the averaging integral. Equations (4.14) and (4.15) are essentially the same equations as Eqs. (3.25) and (3.26).

In deriving an expression for the plasma current we assume that the ions, being much heavier than the electrons, can be regarded as stationary over the period of interest. This is motivated by our desire to operate in a regime void of parametric instabilities. In applications to the beat wave accelerator or the plasma fiber accelerator it is important to make the length of the optical beam sufficiently short so that it does not induce instabilities related to ionic responses. This simplifies the experimental situations along with the computational considerations. In what follows we confine ourselves to these circumstances only. With the assumption of immobile ions the current can be written in the form:

$$\mathbf{J} \approx \sum_{\alpha} q_{\alpha} n_{\alpha} \mathbf{v}_{\alpha} \approx -en_e \mathbf{v}_e. \quad (4.16)$$

The electrons are treated as a fluid when deriving an expression for the electric current in the averaged wave equation. The electron contribution to the plasma current is obtained by using the relativistic equation of motion:

$$n_e \frac{\partial}{\partial t} \mathbf{p} + n_e \mathbf{v} \cdot \nabla \mathbf{p} = -en_e \mathbf{E} - \left(\frac{en_e}{c} \right) \mathbf{v} \times \mathbf{B} - \nabla P$$

$$\mathbf{p} = m\gamma \mathbf{v} \quad , \quad \gamma = \sqrt{1 + \frac{p^2}{m^2 c^2}},$$
(4.17)

where P is the pressure of the electron fluid. (The subscript ‘e’ has now been dropped from the electron velocity). We will expand the electron velocity (as well as momentum) in terms of the normalized quivering velocity $a_n \equiv \frac{ea}{mc^2} < 1$ introduced in the previous chapter. In order to include the ponderomotive and relativistic effects consistently, it is necessary to keep terms up to the second order in a_n . To incorporate the effects due to the electron density depression we need to keep terms up to the third order in a_n . Keeping terms up to the third order only we can drop the pressure term, because it is of the fourth order in a_n :

$$|\nabla P| \sim T_e \nabla \delta n_e \sim v_{th}^2 \nabla \delta n_e \sim \left(\frac{v_{th}}{v_q} \right)^2 a_n^2 \nabla \delta n_e, \quad (4.18)$$

where v_q is the quivering velocity introduced in the second chapter. As recalled from the previous chapter, δn_e is of the order of a_n^2 , and so

$$|\nabla P| \sim \left(\frac{v_{th}}{v_q} \right)^2 O(a_n^4). \quad (4.19)$$

The equation of motion for electrons, therefore, can be written as

$$\begin{aligned} \frac{\partial}{\partial t} (\mathbf{p}_1 + \mathbf{p}_2 + \mathbf{p}_3) + \mathbf{v}_1 \cdot \nabla (\mathbf{p}_1 + \mathbf{p}_2) + \mathbf{v}_2 \cdot \nabla \mathbf{p}_1 \\ = e \nabla \Phi + \left(\frac{e}{c} \right) \frac{\partial \mathbf{A}}{\partial t} + \left(\frac{e}{c} \right) (\mathbf{v}_1 + \mathbf{v}_2) \times (\nabla \times \mathbf{A}), \end{aligned} \quad (4.20)$$

and the plasma current as

$$\mathbf{J} \approx -en_0(\mathbf{v}_1 + \mathbf{v}_2 + \mathbf{v}_3) - e\delta n_e \mathbf{v}_1. \quad (4.21)$$

Here the subscript i indicates the order of the quantity so that, for instance p_1 is the electron momentum first order in a_n .

It is important to notice that even though the thermal velocity of the electrons does not contribute to the plasma current explicitly, it still affects the current through the relativistic mass increase of the electrons:

$$\gamma = \sqrt{1 + \frac{(\mathbf{p}_0 + \mathbf{p}_1 + \mathbf{p}_2 + \mathbf{p}_3)^2}{m^2 c^2}}, \quad (4.22)$$

where \mathbf{p}_0 denotes the momentum corresponding to the thermal velocity. For a cool plasma the effect of \mathbf{p}_0 is, of course, negligible.

The electron momenta in different orders, as obtained from the relativistic equation of motion, are given by:

$$\begin{aligned} \mathbf{p}_1 &= \left(\frac{e}{c}\right) \mathbf{A}, \\ \frac{\partial}{\partial t} \mathbf{p}_2 &= \mathbf{v}_1 \cdot \nabla \mathbf{p}_1 + e \nabla \Phi - \left(\frac{e}{c}\right) \mathbf{v}_1 \times (\nabla \times \mathbf{A}), \\ \frac{\partial}{\partial t} \mathbf{p}_3 &= \mathbf{v}_1 \cdot \nabla \mathbf{p}_2 + \mathbf{v}_2 \cdot \nabla \mathbf{p}_1 - \left(\frac{e}{c}\right) \mathbf{v}_2 \times (\nabla \times \mathbf{A}). \end{aligned} \quad (4.23)$$

In order to express the momenta in terms of the field quantities only, we need to define the different order electron velocities \mathbf{v}_i , $i = 1, 2, 3$. This may be done by expanding the relativistic gamma in powers of a_n :

$$\begin{aligned} \mathbf{v} &\equiv \frac{\mathbf{p}}{m\gamma}, \\ \frac{1}{\gamma} &= \frac{1}{\sqrt{1 + \frac{p^2}{m^2 c^2}}} \\ &= \frac{1}{\sqrt{1 + \frac{p_0^2}{m^2 c^2}}} \left[1 + \frac{2\mathbf{p}_0 \cdot \mathbf{p}_1 + p_1^2 + 2\mathbf{p}_0 \cdot \mathbf{p}_2 + 2\mathbf{p}_0 \cdot \mathbf{p}_3 + 2\mathbf{p}_1 \cdot \mathbf{p}_2}{m^2 c^2 + p_0^2} \right]. \end{aligned} \quad (4.24)$$

With a short hand notation $\gamma_0 \equiv \sqrt{1 + \frac{p_0^2}{m^2 c^2}}$, the expansion gives

$$\frac{1}{\gamma} \approx \frac{1}{\gamma_0} \left[1 - \frac{1}{m^2 c^2 \gamma_0^2} (\mathbf{p}_0 \cdot \mathbf{p}_1 + \frac{1}{2} p_1^2 + \mathbf{p}_0 \cdot \mathbf{p}_2 + \mathbf{p}_0 \cdot \mathbf{p}_3 + \mathbf{p}_1 \cdot \mathbf{p}_2) \right]. \quad (4.25)$$

Using this expression for gamma we can now write down the different order electron velocities:

$$\begin{aligned}
 \mathbf{v}_1 &= \frac{1}{m\gamma_0} \left[\mathbf{p}_1 - \left(\frac{1}{m\gamma_0} \right)^2 (\mathbf{p}_0 \cdot \mathbf{p}_1) \mathbf{p}_0 \right] \\
 \mathbf{v}_2 &= \frac{1}{m\gamma_0} \left\{ \mathbf{p}_2 - \left(\frac{1}{m\gamma_0} \right)^2 \left[(\mathbf{p}_0 \cdot \mathbf{p}_1) \mathbf{p}_1 + \left(\frac{1}{2} p_1^2 + \mathbf{p}_0 \cdot \mathbf{p}_2 \right) \mathbf{p}_0 \right] \right\} \\
 \mathbf{v}_3 &= \frac{1}{m\gamma_0} \left\{ \mathbf{p}_3 - \left(\frac{1}{m\gamma_0} \right)^2 \left\{ (\mathbf{p}_0 \cdot \mathbf{p}_1) \mathbf{p}_2 + \left(\frac{1}{2} p_1^2 + \mathbf{p}_0 \cdot \mathbf{p}_2 \right) \mathbf{p}_1 + \right. \right. \\
 &\quad \left. \left. (\mathbf{p}_0 \cdot \mathbf{p}_3 + \mathbf{p}_1 \cdot \mathbf{p}_2) \mathbf{p}_0 \right\} \right\} .
 \end{aligned}$$

But the thermal velocity cannot contribute to the macroscopic plasma current because its particle average is zero. Therefore, for our purposes, we can neglect the terms involving \mathbf{p}_0 ; hence the velocities contributing to the plasma current are:

$$\begin{aligned}
 \mathbf{v}_1 &= \left(\frac{\mathbf{p}_1}{m\gamma_0} \right) \\
 \mathbf{v}_2 &= \left(\frac{\mathbf{p}_2}{m\gamma_0} \right) \\
 \mathbf{v}_3 &= \left(\frac{1}{m\gamma_0} \right) \left[\mathbf{p}_3 - \frac{1}{2} \left(\frac{1}{m\gamma_0} \right)^2 p_1^2 \mathbf{p}_1 \right] .
 \end{aligned} \tag{4.26}$$

where the terms with odd powers of the thermal velocity have vanished. Using these expressions for the electron velocity, we can now write all the different order electron momenta in terms of the field quantities:

$$\begin{aligned}
 \mathbf{p}_1 &= \left(\frac{e}{c} \right) \mathbf{A} , \\
 \frac{\partial}{\partial t} \mathbf{p}_2 &= e \nabla \Phi - \left(\frac{e^2}{2m\gamma_0 c^2} \right) \nabla a^2 \quad \text{and} \\
 \frac{\partial}{\partial t} \mathbf{p}_3 &= - \left(\frac{e}{m\gamma_0 c} \right) [\mathbf{A} \cdot \nabla \mathbf{p}_2 + (\nabla \mathbf{A}) \cdot \mathbf{p}_2] ,
 \end{aligned} \tag{4.27}$$

where we have used the fact that for a circularly polarized wave given by expression (4.11):

$$\mathbf{A} \cdot \mathbf{A} = a^2. \quad (4.28)$$

The expression for the second-order momentum consists of only slowly varying terms (Φ and a) and it will be kept in the differential form. In the code we will store \mathbf{p}_2 as a grid quantity and advance it explicitly. The third-order momentum, however, consists of both slowly and rapidly varying terms, and we find an expression for \mathbf{p}_3 by approximating the behavior of rapidly varying terms by $\exp(-i\omega_0 t)$:

$$\mathbf{p}_3 \approx -i \left(\frac{e}{m\gamma_0 c \omega_0} \right) [\mathbf{A} \cdot \nabla \mathbf{p}_2 + (\nabla \mathbf{A}) \cdot \mathbf{p}_2]. \quad (4.29)$$

The different order electron velocities are now given by

$$\begin{aligned} \mathbf{v}_1 &= \left(\frac{e}{m\gamma_0 c} \right) \mathbf{A} \\ \mathbf{v}_2 &= \left(\frac{1}{m\gamma_0} \right) \mathbf{p}_2 \\ \mathbf{v}_3 &= - \left(\frac{e}{m^2 \gamma_0^2 c} \right) \left\{ \frac{1}{2} \left(\frac{e^2}{2m\gamma_0 c^4} \right) a^2 \mathbf{A} + \left(\frac{i}{\omega_0} \right) [\mathbf{A} \cdot \nabla \mathbf{p}_2 + (\nabla \mathbf{A}) \cdot \mathbf{p}_2] \right\}. \end{aligned} \quad (4.30)$$

Having expressed everything in the plasma current in terms of the field potentials, we can now average over the rapid laser oscillations. As in the case of the left-hand side of the wave equation, this is done by multiplying the plasma current by the complex conjugate of the vector potential and averaging over the laser oscillation period. The first-order current is

$$\begin{aligned} \mathbf{J}_1 &= -en_0 \mathbf{v}_1, \quad \text{and so} \\ \left(\frac{1}{T_0} \right) \int \mathbf{J}_1 \cdot \mathbf{A}^* dt &= -2 \left(\frac{e^2 n_0}{m\gamma_0 c} \right) a^2. \end{aligned} \quad (4.31)$$

The second-order current is slowly varying and therefore it vanishes upon averaging.

$$\begin{aligned}\mathbf{J}_2 &= -en_0\mathbf{v}_2 \\ \Rightarrow \frac{1}{T_0} \int \mathbf{J}_2 \cdot \mathbf{A}^* dt &\approx \frac{1}{T_0} \mathbf{J}_2 \cdot \int \mathbf{A}^* dt = 0.\end{aligned}$$

The third-order current calls for special care. It contains terms that are not proportional to the vector potential. Therefore, if we multiply it by the complex conjugate of the vector potential, unphysical terms will arise due to phase mixing. To avoid this, the term not proportional to \mathbf{A} must be averaged using real representation. The third order current is given by

$$\begin{aligned}\mathbf{J}_3 &= -e(n_0\mathbf{v}_3 + \delta n_e\mathbf{v}_1) = \\ &- \left(\frac{en_0}{m\gamma_0} \right) \left[\mathbf{p}_3 - \frac{1}{2} (mc\gamma_0)^2 p_1^2 \mathbf{p}_1 \right] - e\delta n_e\mathbf{v}_1.\end{aligned}\quad (4.32)$$

The two latter terms, being proportional to \mathbf{A} , can be averaged using complex notation:

$$\begin{aligned}\left(\frac{1}{T_0} \right) \int \delta n_e\mathbf{v}_1 \cdot \mathbf{A}^* dt &\approx 2 \left(\frac{e\delta n_e}{mc\gamma_0} \right) a^2, \\ \left(\frac{1}{T_0} \right) \int p_1^2 \mathbf{p}_1 \cdot \mathbf{A}^* dt &\approx 2 \left(\frac{e}{c} \right)^3 a^4.\end{aligned}\quad (4.33)$$

Averaging the first term in the expression for \mathbf{J}_3 we return to real notation.

Recall the expression for \mathbf{p}_3 :

$$\mathbf{p}_3 = -i \left(\frac{e}{mc\gamma_0\omega_0} \right) [\mathbf{A} \cdot \nabla \mathbf{p}_2 + (\nabla \mathbf{A}) \cdot \mathbf{p}_2]. \quad (4.34)$$

Carrying out the averaging term by term using the real components of these quantities, we find

$$\begin{aligned}\left(\frac{1}{T_0} \right) \int \mathbf{A} \cdot [\mathbf{A} \cdot \nabla \mathbf{p}_2] dt &= \left(\frac{1}{T_0} \right) \int A_j A_i \partial_i p_{2j} dt \\ &\approx \partial_i p_{2j} \left(\frac{1}{T_0} \right) \int A_i A_j dt \\ &= \partial_i p_{2j} \left(\frac{1}{2} a^2 \delta_{i,j} \right) \quad \text{for } i, j = x, y \\ &= \frac{1}{2} a^2 \nabla_T \cdot \mathbf{p}_2,\end{aligned}\quad (4.35)$$

where $\nabla_T \equiv \hat{x} \frac{\partial}{\partial x} + \hat{y} \frac{\partial}{\partial y}$, and

$$\begin{aligned} \left(\frac{1}{T_0}\right) \int \mathbf{A} \cdot [(\nabla \mathbf{A}) \cdot \mathbf{p}_2] dt &= \left(\frac{1}{T_0}\right) \int \mathbf{A} \cdot \left[\left(\frac{1}{a}\right) \nabla a + i \nabla \varphi \right] \mathbf{A} \cdot \mathbf{p}_2 dt \\ &\approx \left[\left(\frac{1}{a}\right) \partial_j a + i \partial_j \varphi \right] p_{2j} \left(\frac{1}{T_0}\right) \int A_i A_i dt \\ &= \frac{1}{2} \left[\frac{1}{2} (\mathbf{p}_2 \cdot \nabla_T a^2) + i a^2 \mathbf{p}_2 \cdot \nabla_T \varphi \right], \end{aligned} \quad (4.36)$$

where $\varphi \equiv k_0 z - \omega_0 t - \psi$. Thus the averaged value of the first term in the expression for \mathbf{J}_3 is

$$\begin{aligned} \left(\frac{1}{T_0}\right) \int \mathbf{p}_3 \cdot \mathbf{A}^* dt &= - \left(\frac{e}{m c \gamma_0 \omega_0}\right) \left\{ a^2 \mathbf{p}_2 \cdot \nabla_T \psi + \right. \\ &\quad \left. i \left[a^2 \nabla_T \cdot \mathbf{p}_2 + \frac{1}{2} \mathbf{p}_2 \cdot \nabla_T a^2 \right] \right\}, \end{aligned} \quad (4.37)$$

where we have used $\nabla_T \varphi \equiv -\nabla_T \psi$, and have multiplied the term requiring averaging in real representation by a factor of two. This is necessary to compensate for the difference arising from the two averaging schemes (see e.g. Eqs. (4.28) and (4.35)). The averaged third-order current can now be written as

$$\begin{aligned} \left(\frac{1}{T_0}\right) \int \mathbf{J}_3 \cdot \mathbf{A}^* dt &\approx \left(\frac{e^2 n_0}{m \gamma_0 c}\right) \left\{ a^2 \left[\left(\frac{ea}{m \gamma_0 c}\right)^2 - 2 \frac{\delta n_e}{n_0} \right] \right. \\ &\quad \left. + \left(\frac{1}{m \gamma_0 \omega_0}\right) \left[a^2 \mathbf{p}_2 \cdot \nabla_T \psi + i \left(a^2 \nabla_T \cdot \mathbf{p}_2 + \frac{1}{2} \mathbf{p}_2 \cdot \nabla_T a^2 \right) \right] \right\}, \end{aligned} \quad (4.38)$$

and the total current is given by

$$\begin{aligned} \left(\frac{1}{T_0}\right) \int \mathbf{J} \cdot \mathbf{A}^* dt &\approx \left(\frac{e^2 n_0}{m \gamma_0 c}\right) \left\{ a^2 \left[\left(\frac{ea}{m \gamma_0 c}\right)^2 - 2 N_e \right] \right. \\ &\quad \left. + \left(\frac{1}{m \gamma_0 \omega_0}\right) \left[a^2 \mathbf{p}_2 \cdot \nabla_T \psi + i \left(a^2 \nabla_T \cdot \mathbf{p}_2 + \frac{1}{2} \mathbf{p}_2 \cdot \nabla_T a^2 \right) \right] \right\}, \end{aligned} \quad (4.39)$$

where $N_e \equiv 1 + \frac{\delta n_e}{n_0}$. Using this expression we can now write the amplitude and phase equations from Eqs. (4.14) and (4.15) as

$$\begin{aligned} \frac{\partial^2}{\partial t^2} a = & c^2 \nabla^2 a + a \left[\left(\frac{\partial \psi}{\partial t} \right)^2 - c^2 |\nabla \psi|^2 \right] + 2a \left(\omega_0 \frac{\partial \psi}{\partial t} + c^2 k_0 \frac{\partial \psi}{\partial z} \right) \\ & + \frac{1}{2} \left(\frac{\omega_p^2}{\gamma_0} \right) a \left[\left(\frac{ea}{m\gamma_0 c^2} \right)^2 - 2N_e + \left(\frac{1}{m\gamma_0 \omega_0} \right) \mathbf{p}_2 \cdot \nabla_T \psi \right] \end{aligned} \quad (4.40)$$

and

$$\begin{aligned} \frac{\partial}{\partial t} \left(a^2 \frac{\partial \psi}{\partial t} \right) = & c^2 \nabla \cdot (a^2 \nabla \psi) - 2a \left(\omega_0 \frac{\partial a}{\partial t} + c^2 k_0 \frac{\partial a}{\partial z} \right) \\ & - \frac{1}{2} \left(\frac{\omega_0}{\omega_p} \right)^2 \left(\frac{\omega_0}{m\gamma_0^2} \right) \left[a^2 \nabla_T \cdot \mathbf{p}_2 + \frac{1}{2} \mathbf{p}_2 \cdot \nabla_T a^2 \right]. \end{aligned} \quad (4.41)$$

The explicit electrons in the simulation code are needed for calculating the electron density, N_e , appearing in the amplitude equation. The equation of motion for electrons under the influence of an external electromagnetic field is

$$\frac{d}{dt} \mathbf{p} = -e\mathbf{E}_S - e \left(\mathbf{E}_M + \frac{1}{c} \mathbf{v} \times \mathbf{B} \right), \quad (4.42)$$

where \mathbf{E}_S is the electrostatic field due to the (possible) induced charge separation, \mathbf{E}_M is the external electric field, and \mathbf{B} is the external magnetic field. In the case when the external electromagnetic field is that of a powerful laser, the external electric field dominates the other terms in the equation. We can thus facilitate the phase averaging of the equation of motion for electrons by again evaluating the electron momentum in different orders. As a matter of fact, this was already done in the second chapter and, recalling the results derived in Appendix A, the phase-averaged equation of motion for electrons can be written as

$$\frac{d}{dt} \mathbf{p} = -e\mathbf{E}_S - mc^2 \nabla \sqrt{1 + a_n^2}. \quad (4.43)$$

where we also recalled from Chapter III that the electrostatic field is a slowly varying quantity. Thus the phase-averaged equation of motion for the electrons

consists of two terms: the electrostatic force and the ponderomotive force, which are both second order in the quivering velocity.

Equations (4.40), (4.41) and (4.43), consisting of the phase averaged wave equation in terms of the field potentials and the equation of motion for the electrons averaged similarly over the rapid oscillations, constitute the basic set of equations for our system in the slow time scale. As we remarked earlier, they may be considered as the electromagnetic counterpart of the Zakharov equations⁶⁴ in electrostatics. In the following we shall try to solve these basic equations.

4.3 Numerical Algorithm

From the form of the field equations one notices that the direction of the beam propagation singles out. Furthermore, the transverse directions appear only in terms involving inner products. This allows us to represent the transverse dimensions by one scalar variable (instead of a two-dimensional vector), which we will call 'x'. The direction of beam propagation is labeled by 'y'. With these conventions the amplitude and phase equations are as follows:

$$\begin{aligned} \frac{\partial^2}{\partial t^2} a = & c^2 \nabla^2 a + a \left[\left(\frac{\partial \psi}{\partial t} \right)^2 - c^2 |\nabla \psi|^2 \right] + 2\omega_0 a \left[\frac{\partial \psi}{\partial t} + c \frac{\partial \psi}{\partial y} \right] \\ & + \frac{1}{2} \left(\frac{\omega_p^2}{\gamma_0} \right) a \left[\left(\frac{ea}{m\gamma_0 c^2} \right) - 2N_e + \left(\frac{1}{m\gamma_0 \omega_0} \right) p_{2x} \frac{\partial \psi}{\partial x} \right] \end{aligned} \quad (4.44)$$

and

$$\begin{aligned} \frac{\partial}{\partial t} \left(a^2 \frac{\partial \psi}{\partial t} \right) = & c^2 (a^2 \nabla^2 \psi + \nabla a^2 \cdot \nabla \psi) - 2\omega_0 a \left(\frac{\partial a}{\partial t} + c \frac{\partial a}{\partial y} \right) \\ & - \frac{1}{2} \left(\frac{\omega_0}{\omega_p} \right)^2 \left(\frac{\omega_0}{m\gamma_0^2} \right) \left[a^2 \frac{\partial p_{2x}}{\partial x} + \frac{1}{2} p_{2x} \frac{\partial a^2}{\partial x} \right], \end{aligned} \quad (4.45)$$

where $\nabla \equiv \hat{x} \frac{\partial}{\partial x} + \hat{y} \frac{\partial}{\partial y}$.

The code solves for the four interdependent quantities, a , a_t , ψ , and ψ_t by the standard leap-frog integration over the four first-order partial differential equations obtained from Eqs. (4.44) and (4.45). In addition the electrons are pushed according to Eq. (4.43) and the electron density updated at every time step. The structure of the code is as follows:

- initialize fields
- initialize particles
- loop over the main program:
 - push particle positions
 - accumulate charge density and compute electrostatic field
 - update the amplitude and the time derivative of phase shift
 - calculate total force on particles and advance the grid momentum by half time step
 - update the phase shift and the time derivative of amplitude
 - update grid momentum and particle momentum

The boundary conditions are chosen to be periodic in both longitudinal (y) and transverse (x) directions. This implies that we are simulating an infinite number of identical, parallel beams. The width of the simulation system has to be chosen large enough compared to the width of Gaussian beam so that the parallel beams do not interact significantly with each other during the run.

The spatial differentiation could be performed using fast Fourier transforms to retain as high accuracy as possible.⁶⁷ Unfortunately, the theoretical

behavior of the phase shift, ψ , is such that at the edges in the transverse direction there is a discontinuity in the spatial derivative of ψ . This discontinuity is, of course, an artifact of the model due to the finite simulation box, but fortunately it takes place in the region where it should have no significance (the amplitude, having Gaussian profile, has dropped to practically zero). However, with Fourier transform this effect will no longer be localized, but the sharp, unphysical structures will be instantaneously reflected all over the grid. For this reason we have adopted finite differencing for the spatial differentiation.

To further suppress the artifacts arising from the finiteness of the simulation box, in the outer skirts of the beam (about 15% of the total width of the box) where the intensity has dropped off to practically zero, we use a binomial filter on the phase shift and its time derivative to smooth out the sharp structures arising from the discontinuity of the spatial derivative. The filter is not applied at every time step but every fifth or tenth time step appears to be sufficient to remove the unphysical high wavenumber components from the system.

Furthermore, it is important to notice that whenever the amplitude vanishes, the phase information is lost. This is reflected in the leap-frog equations in that the calculation for ψ_t involves division by a^2 , an operation that diverges as a vanishes. To circumvent this problem that has arisen from our choice of independent variables (amplitude and phase instead of field components) and equations (wave equation instead of the set of Maxwell's equations), we introduce a ghost factor in evaluating the time derivative of the phase shift:

$$\psi_t = \frac{(a^2 \psi_t)}{a^2} \rightarrow \frac{a^2 (a^2 \psi_t)}{a^4 + \epsilon^2}, \quad (4.46)$$

where ϵ^2 is a very small number (typically we have used $\epsilon^2 = (0.0001 \cdot a_0^2 - (0.001 \cdot a_0)^2)$). The ghost factor will have a negligible effect in the computation

when the amplitude is finite, and it will prevent a divergence without altering the value of phase shift when the amplitude vanishes.

Despite of these nice features of the ghost factor, one should be careful in interpreting the simulation output in the outer skirts of the beam where the ghost has a noticable effect. It is important to keep those regions as small as possible. Thus we are in a situation where good compromises are necessary. In order to prevent the parallel beams from overlapping we would like to have as wide a simulation box as our resources would permit, but on the other hand it is necessary to minimize the physically insignificant area in the outer skirts of the beam, which not only doesn't provide us with any interesting physics but also can be a source of all kind of numerical trouble. Experimenting with different widths has proven to be the best guide in making these decisions.

In accumulating the charge density on the grid we have chosen to use area weighing. This was done because the SUD-method ordinarily used in many electromagnetic particle simulation codes produces unphysical spikes near the edges of the simulation box where the situation is already troubled.

Initially the electrons and ions are loaded uniformly on top of each other so that, since the ions are taken as stationary, the initial electron distribution can be used for the constant ion density during the simulation run.

4.4 Testing of the Code: The Rayleigh Spread and Self-Focusing

We started the testing of the code by first testing the field solver separately. This can be accomplished by removing the plasma altogether from the code, thus simulating an electromagnetic wave in vacuum.

A nontrivial, meaningful test is produced by launching a beam with a

Gaussian intensity profile:

$$a(t=0) = a_0 e^{-x^2/w_0^2}, \quad (4.47)$$

where a_0 is the initial amplitude and w_0 the initial radius of the beam. The initial conditions for the other field variables are thus (see Appendix B):

$$\begin{aligned} a_t(t=0.5\Delta t) &= -a_0 \frac{t}{T_R} \left(1 + \frac{t^2}{T_R^2}\right)^{-9/4} \left(\frac{1}{2} + 2\frac{r^2}{w_0^2} + \frac{1}{2}\frac{t^2}{T_R^2}\right) e^{-x^2/w_0^2} \\ \psi(t=0.5\Delta t) &= \frac{1}{2} \arctan(t/T_R) - \frac{k_0}{2R} x^2, \text{ and} \\ \psi_t(t=0) &= \frac{1}{2T_R} - \frac{1}{2} k_0 \frac{x^2}{cT_R^2}, \end{aligned} \quad (4.48)$$

where the initial values are properly staged.

The evolution of a Gaussian beam is reasonably well understood theoretically. In a stationary state, the behavior of the beam radius is given by the Rayleigh spreading (for derivation in a two dimensional case, see Appendix B),

$$w(y)^2 = w_0^2 \left[1 + \frac{y^2}{y_R^2}\right], \quad (4.49)$$

where $y_R \equiv \frac{1}{2} k_0 w_0^2$ is the Rayleigh range. In the code, instead of assuming a stationary state ($\frac{\partial}{\partial t} = 0$), we give initially a beam uniform in y ($\frac{\partial}{\partial y} = 0$). In doing this, the roles of time and direction of propagation get interchanged and we expect to see Rayleigh spreading in time rather than in space:

$$w(t)^2 = w_0^2 \left[1 + \frac{t^2}{T_R^2}\right], \quad (4.50)$$

where T_R is the Rayleigh time corresponding to the Rayleigh range, $T_R \equiv \frac{1}{2} \omega_0 \frac{w_0^2}{c^2}$. Instead of monitoring the beam radius, $w(t)$, which would involve complicated evaluations, we monitor the central amplitude, which can be simply

looked up. The theoretical behavior of the central amplitude can be obtained by noting that the total power is invariant:

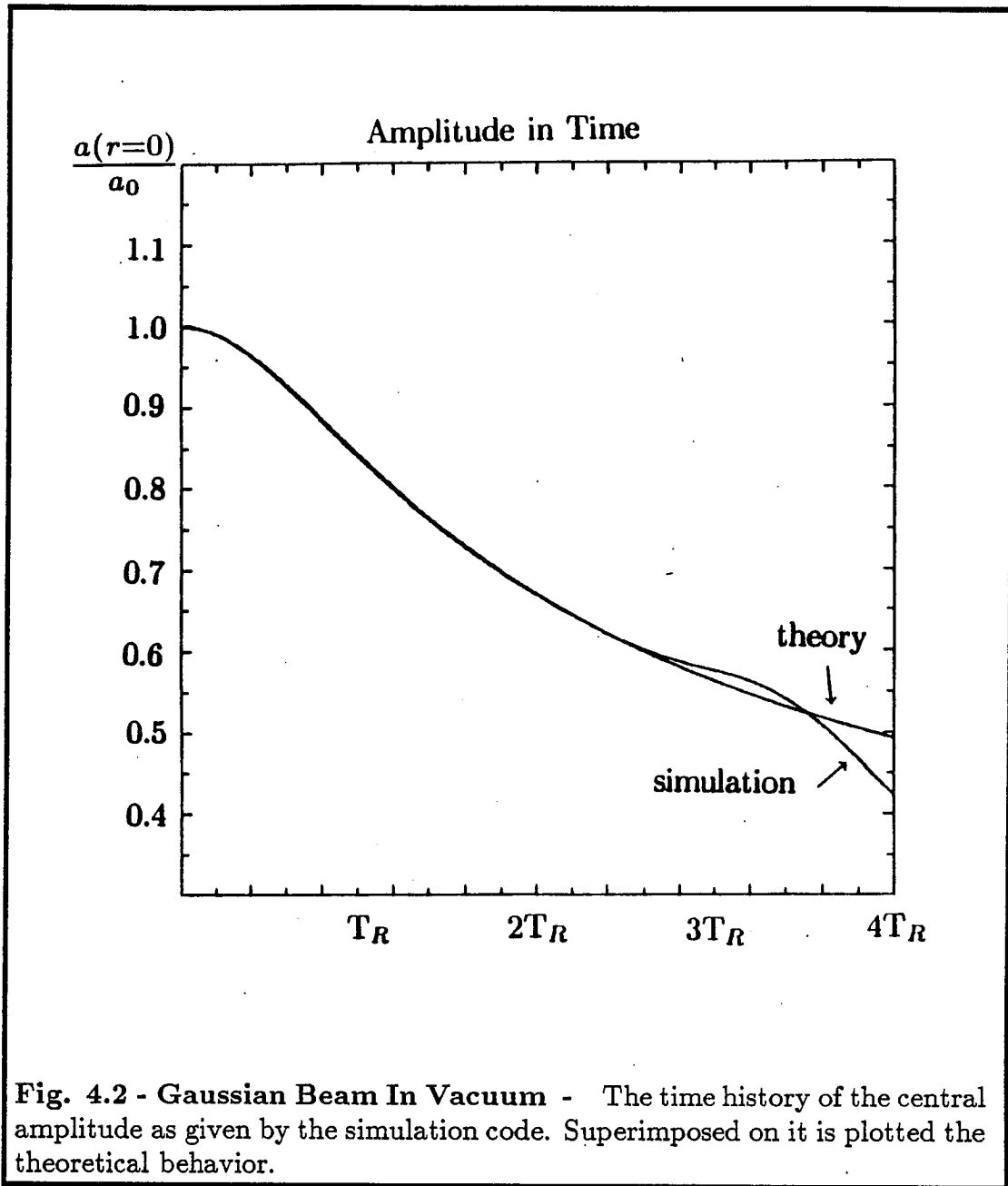
$$P_3 \equiv a_0^2 w_0^2 = a(t)^2 w(t)^2 \quad \text{in 3 dimensions}$$

$$P_2 \equiv a_0^2 w_0 = a(t)^2 w(t) \quad \text{in 2 dimensions .}$$

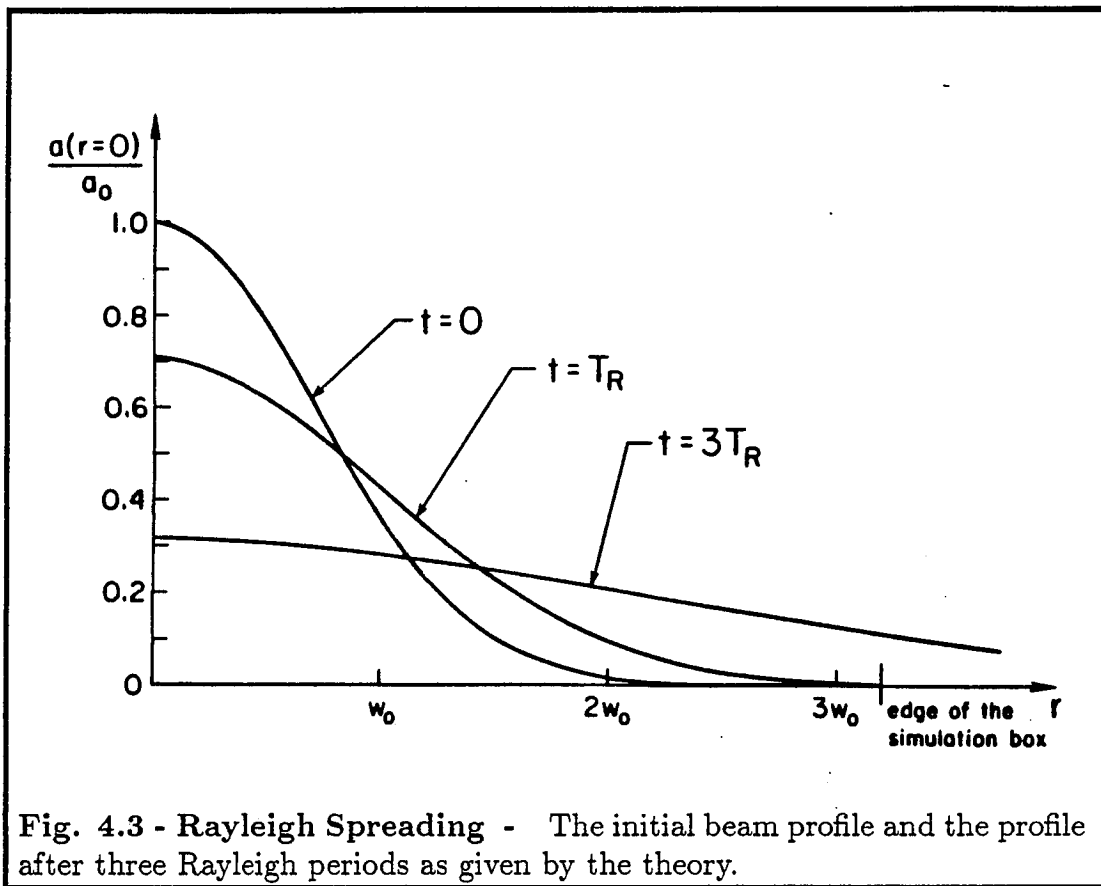
The behavior of the central amplitude is thus completely specified by the behavior of the beam radius, and so we can equally well follow the evolution of the amplitude.

We launched a Gaussian beam in a simulation where the radius (or waist) of the beam was $w_0 = 4\lambda_c$, the width of the simulation box was $L_x = 25.6\lambda_c$, the number of the grid points was $N_g = 128$, and the time step was $\Delta t = 0.01\omega_{pe}^{-1}$. In Fig. 4.2 we have plotted the time behavior of the peak amplitude obtained from the simulation run, together with the theoretical curve. The two curves are identical until after about three Rayleigh times they start to diverge. This is due to the significant overlapping at the skirts of the beam we are monitoring with the identical beams parallel to it (see Fig. 4.3) that exist outside the simulation box due to the choice of the periodic boundary conditions.

Having a reasonably good verification for the soundness of the field solver, we now turn to test the particle solver. No major complications are expected because the particle solver is basically the standard one used in most particle simulation codes — only in the equation of motion the effect of the electromagnetic fields is represented by the ponderomotive force (see Eq.(4.43)) rather than the field components. To make sure, however, we tested the full particle simulation code by launching a uniform plane wave. Since the profile of the ‘beam’ is now uniform, it should propagate unaltered through the plasma, if the code is working correctly. This is exactly what was observed. In Fig. 4.4(a)



we have plotted the initial and final profiles demonstrating that, besides the fluctuations characteristic of any particle simulation, the wave is propagating without a net distortion. In Fig. 4.4(b) is plotted the time history of the total energy showing that the system does not possess any sources or sinks of energy



but that the total energy is conserved.

A test with a uniform plane wave can convince us that the particle pusher does not have any absurd features, but it does not really show if the particle pusher will do its job as expected. This is because the ponderomotive force term in the pusher will never get activated. To test the ponderomotive part of the pusher we have to launch a beam with a nonuniform intensity profile. We will here concentrate on the particle dynamics and will not address the behavior of the laser beam since that will be the topic of the following chapter. In Fig. 4.5 are plotted the kinetic and electrostatic energies of the system as given by the simulation when a Gaussian beam is launched into a plasma. The beam has identical parameters with the beam used in testing the Rayleigh

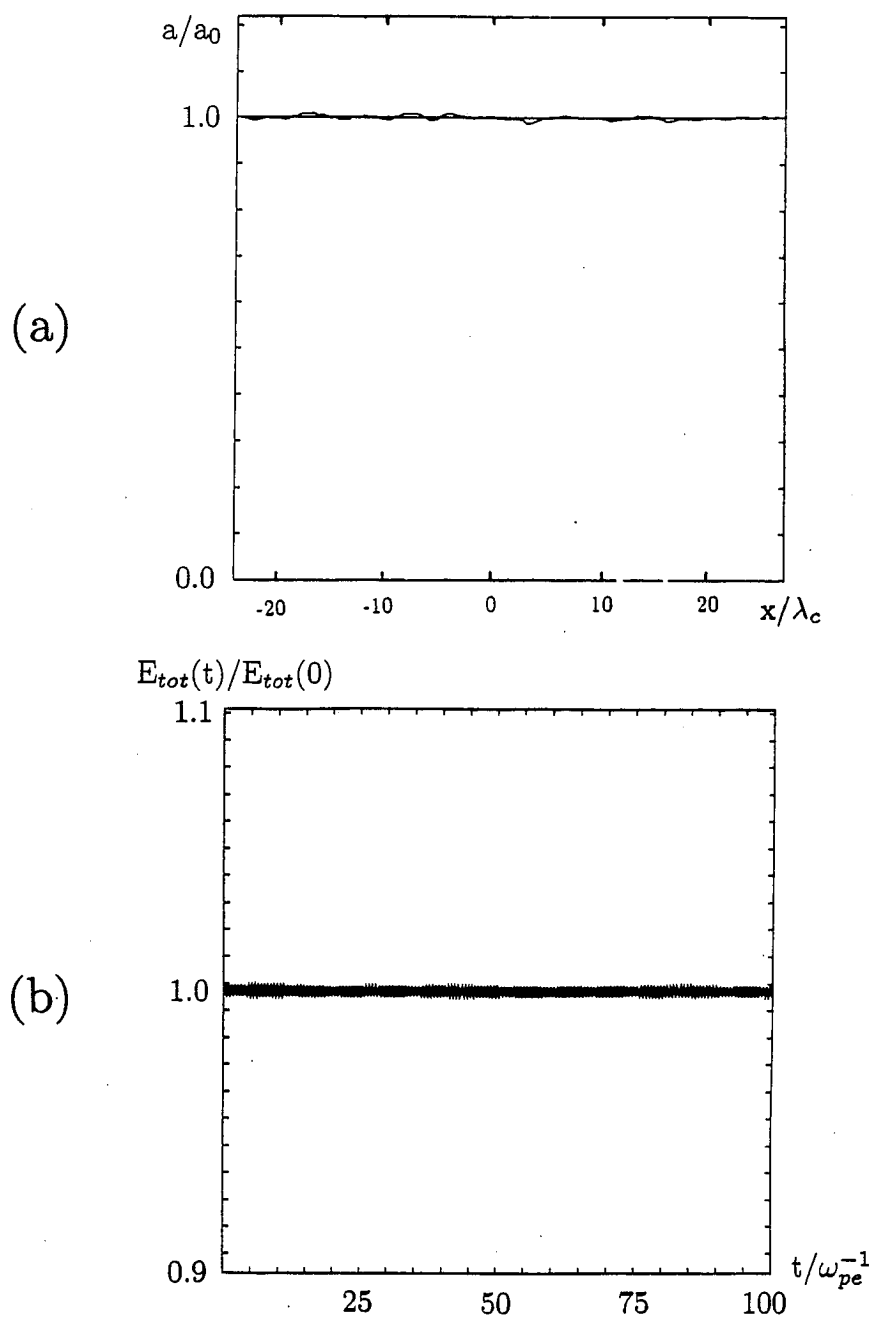


Fig. 4.4 - A Plane Wave In Plasma - (a) The initial ($t=0$) and final ($t=50\omega_p^{-1}$) beam profile plotted on top of each other. (b) The total energy of the system as a function of time.

spreading in vacuum. The grid had 128 cells and there were 100 electrons per grid cell. The thermal velocity of the electrons was taken to be one-tenth of the speed of light, corresponding to the plasma temperature of $T_e = 5$ keV. If the particle pusher is operating properly, the ponderomotive force due to the radially nonuniform intensity profile should first kick the electrons outward corresponding to an increase in not only the kinetic energy but also in the electrostatic energy because of the induced charge separation. Eventually the electrostatic field due to the charge separation should balance out and overcome the ponderomotive force, the electrons should start to decelerate, and the kinetic energy should start to drop. The electrostatic energy, however, continues to increase since the electrons are still moving away from the axis. It is only when the electrons come to a complete stop and reverse the direction of their motion to that of the prevailing laser electric field that the electrostatic energy starts to drop. At that time the kinetic energy starts to grow again. Therefore, both the kinetic and the electrostatic energies are expected to oscillate — the former at a frequency twice as large as the latter. This behavior is very clearly manifested in Figs. 4.5(a) and (b), respectively.

A closer look at the time histories (particularly Fig. 4.4(b)) reveals that superimposed on the expected behavior there are high frequency oscillations with very small amplitude. The amplitude of these oscillations is completely insensitive to reductions in the size of the time step or increases in the grid density. Thus they are probably not due to numerical inaccuracies of the integration scheme itself. Notice also that the oscillations are present from the very beginning and that the amplitude of the oscillations does not grow or diminish but retains a constant value.

The amplitude of the oscillations is, however, extremely sensitive to

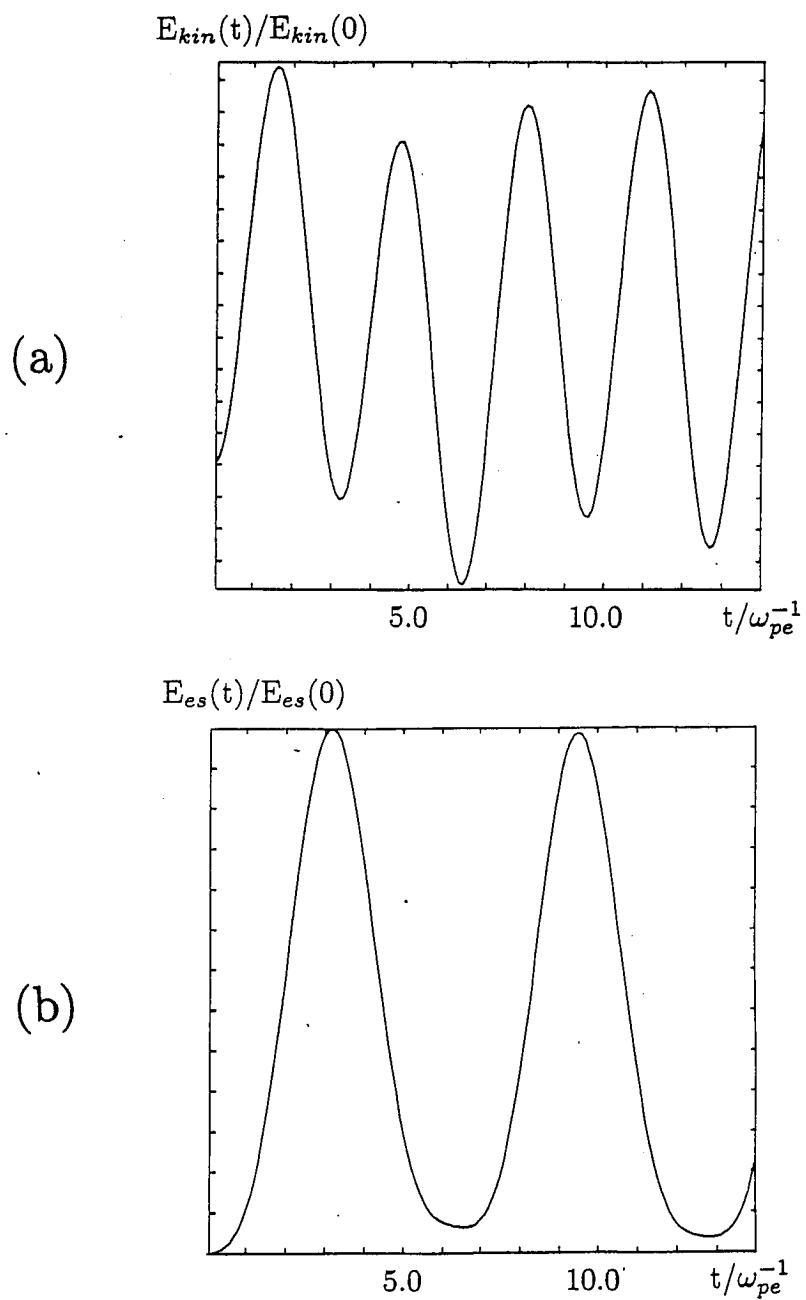


Fig. 4.5 - Gaussian Beam In Plasma - (a) Kinetic energy as a function of time. (b) Electrostatic energy as a function of time.

the initial conditions. This suggests that we should look at how accurately we know the initial conditions of the beam-plasma system we are simulating. The theoretical forms for the time derivative of the amplitude and the phase shift and its derivative that are used in the field initialization are derived in Appendix B. The derivation is based on the assumption that the amplitude and phase shift were slowly varying quantities compared to the laser oscillations, and thus only the first order derivatives are retained. The characteristic time scale for the amplitude modulations is the Rayleigh spreading time, $T_R = \frac{\pi w_0}{c\lambda_0}$, and so an appropriate smallness parameter is $\epsilon = 1/\omega_0 T_R \propto \frac{1}{k_0^2 w_0^2}$. Thus the errors in the initialization of the fields in the code are of the order of $\epsilon^2 \approx \frac{1}{k_0^4 w_0^4}$. Therefore, by comparing the relative amplitude of the small oscillations for simulation runs with different parameters, we should be able to decide if the inaccuracies in the initial conditions are the source of these oscillations. In particular, carrying out two simulation runs with identical parameters except that the beam waist of one is set to be twice the beam waist of the other, we should see a difference of a factor of $2^4 = 16$ when comparing the amplitudes of the small oscillations as observed in the two cases. That is, this should be the case if our hypothesis of the origin of the oscillations is correct. We ran the simulation for a laser beam with frequency $\omega_0 = 5\omega_{pe}$ and beam waist first set at $w_0 = 4\lambda_c$ and later at $w_0 = 8\lambda_c$. The ratio of the small oscillations observed in the two runs was about 13, which is quite close to the theoretical estimate, considering the crudeness of the measurement of the amplitudes from the plots. Thus we conclude that the small amplitude oscillations observed on top of the theoretical behaviour are most exproably due to the inaccuracies in the initial conditions.

Chapter V

Numerical Experiments

5.1 Introduction

In this chapter we shall reinvestigate the problems studied in Chapter III, this time using the computer simulation code described in the previous chapter. A computer simulation can provide not only solutions to nonlinear problems but also the temporal evolution. Obtained numerical solutions may thus inspire the physicist to look into more relevant regimes and behaviors. Also, a computer simulation can prove the existence of a certain set of solutions, as the theory often has to assume their existence to begin with.

In Section 5.2 the soliton-type profile of a self-focused laser beam derived in Section 3.3 will be tested. Running the profile through a particle simulation should give a good indication whether or not this specific profile is a feasible candidate for an asymptotic profile. In Section 5.3 we study the dynamical behavior of a self-focusing beam. In particular, the threshold intensity for self-focusing will be determined/confirmed from these numerical experiments, but also the later evolution of the beam profile will be investigated. Comparisons to the theoretical results of Section 3.4 will be made. In Section 5.3.1 the plasma response is incorporated using various theoretical models for the plasma density rather than explicit particles. This way we can turn off some mechanisms if that is desired, and we can thereby study the self-focusing due to a single process. In Section 5.3.2 the self-focusing is studied under the influence of the full, phase-averaged electron dynamics.

Most of the simulation runs presented here are carried out using the same value for the laser frequency, $\omega_0 = 5\omega_{pe}$. This is not because we have not run the code with other values for ω_0 , but because this specific value for the frequency is convenient. For instance, the Rayleigh spreading time as given by Eq. (4.51) increases as the frequency increases. Therefore, in order to see significant spreading of the beam, we need to run the code longer for larger value of ω_0 . Although we do not have an analytic expression for the time scale for self-focusing, running the code with various values of ω_0 has shown that this is the case for self-focusing, too. Thus we do not want to choose the laser frequency too high. On the other hand, choosing the frequency of the laser smaller than $5\omega_{pe}$, we are getting close to the quarter critical density region ($\omega_0 = 2\omega_{pe}$), where the parametric instabilities could pose a problem as far as application to particle accelerators is concerned.

An important feature of the approach we have adopted in this work is that the magnitude of the laser frequency does not enter in the critical quantities. Since we use the vector potential rather than the field components of the electromagnetic field, the laser frequency disappears from the expression for the quivering velocity of the laser beam, and thus the dimensionless intensity as well as the power are independent of the laser frequency. Therefore the threshold power/intensity for self-focusing should be independent of the frequency of the laser. We are thus not sacrificing generality by running most of the simulations using a fixed value of ω_0 .

5.2 Asymptotic Form of a Self-Focused Laser Beam

In this section we wish to find out how realistic the asymptotic beam

profile derived in Section 3.3 is. That is, if such a profile is formed in a plasma, does it indeed propagate without distortion of its shape? In particular, this beam profile should not be subject to either defocusing or self-focusing.

The work leading to the specific profile obtained in Section 3.3 did not incorporate any assumptions on the dynamics that would produce such an asymptotic profile as its final state. Therefore we have to prepare an initial state where the beam has already attained the presumed asymptotic form. If this profile is indeed an asymptotic one, it should then propagate without distortion even when we shall allow for the full electromagnetic interaction between the beam and the plasma in the numerical experiment.

As mentioned in the previous chapter, the interdependent field quantities to be evolved in the code are the magnitude and time derivatives of the amplitude and the phase shift. The initial conditions for these variables can be obtained from Section 3.3. As in the test case, we shall here replace the stationary state by a state uniform in the direction of propagation. This implies that the z -coordinate in the expressions of Section 3.3 will be replaced by the time t according to $z = ct$, and the dynamics will take place in time rather than in the direction of propagation since we are effectively simulating an infinite beam. This replacement is simply a change of variables and not a Lorentz transformation. Because the profile is supposedly asymptotic, the initial conditions for the amplitude and its time derivative are:

$$\begin{aligned} a(x, t = t_0) &= \frac{2 \operatorname{sech}^2(\delta\xi)}{1 - \operatorname{sech}^2(\delta\xi)} \\ a_t(x, t = t_0) &= 0 . \end{aligned} \tag{5.1}$$

The initial conditions for the phase shift and its time derivative are, from

Eq. (3.72)

$$\begin{aligned}\psi(x, t = t_0) &= \left(ck_0 - \sqrt{\omega_0^2 + \omega_{p0}^2 \left(\frac{1}{4} I_0 - 1 \right)} \right) t_0 \\ \psi_t(x, t = t_0) &= \left(ck_0 - \sqrt{\omega_0^2 + \omega_{p0}^2 \left(\frac{1}{4} I_0 - 1 \right)} \right) .\end{aligned}\tag{5.2}$$

The run using this set of initial conditions will be referred to as FDFBCOSH. The proper staging of the variables implies that, if the amplitude is specified at $t_0 = 0$, the phase shift and the time derivative of the amplitude have to be specified at $t = \frac{1}{2} \Delta t$, and the time derivative of the phase shift is specified at $t_0 = 0$.

We tested a soliton-type profile with the inverse beam width set at $\kappa = 0.2 \lambda_c^{-1}$. This corresponds, according to Eq. (3.83), to the normalized peak intensity of $I_0 = 0.16$. The frequency of the beam was $\omega_0 = 5 \omega_{pe}$. The width of the simulation box was set at $L_x = 51.2 \lambda_c$ and the total number of grid points was $N_g = 256$. There were 100 electrons per grid cell, and the thermal velocity of the electrons was chosen to be $v_{th} = 0.1c$, corresponding to the plasma temperature of $T_e = 5$ keV.

To facilitate the interpretation of the simulation results, we also carried out the same simulation runs using a Gaussian intensity profile. A Gaussian beam with a form closest to the solitary profile described above, has peak intensity of $I_0 = 0.16$, beam waist of $w_0 = 8 \lambda_c$ and frequency $\omega_0 = 5 \omega_{pe}$.

We ran the code for fifty electron-plasma oscillation periods using a time step of one tenth of the plasma oscillation period, $\Delta t = 0.1 \omega_{pe}^{-1}$. In Figs. 5.1 and 5.2 we have summarized the results from the numerical experiments. Figure 5.1 shows the time evolution of the central peak amplitude for both the solitary and the Gaussian profile. Due to the high initial intensity, the Gaussian beam starts

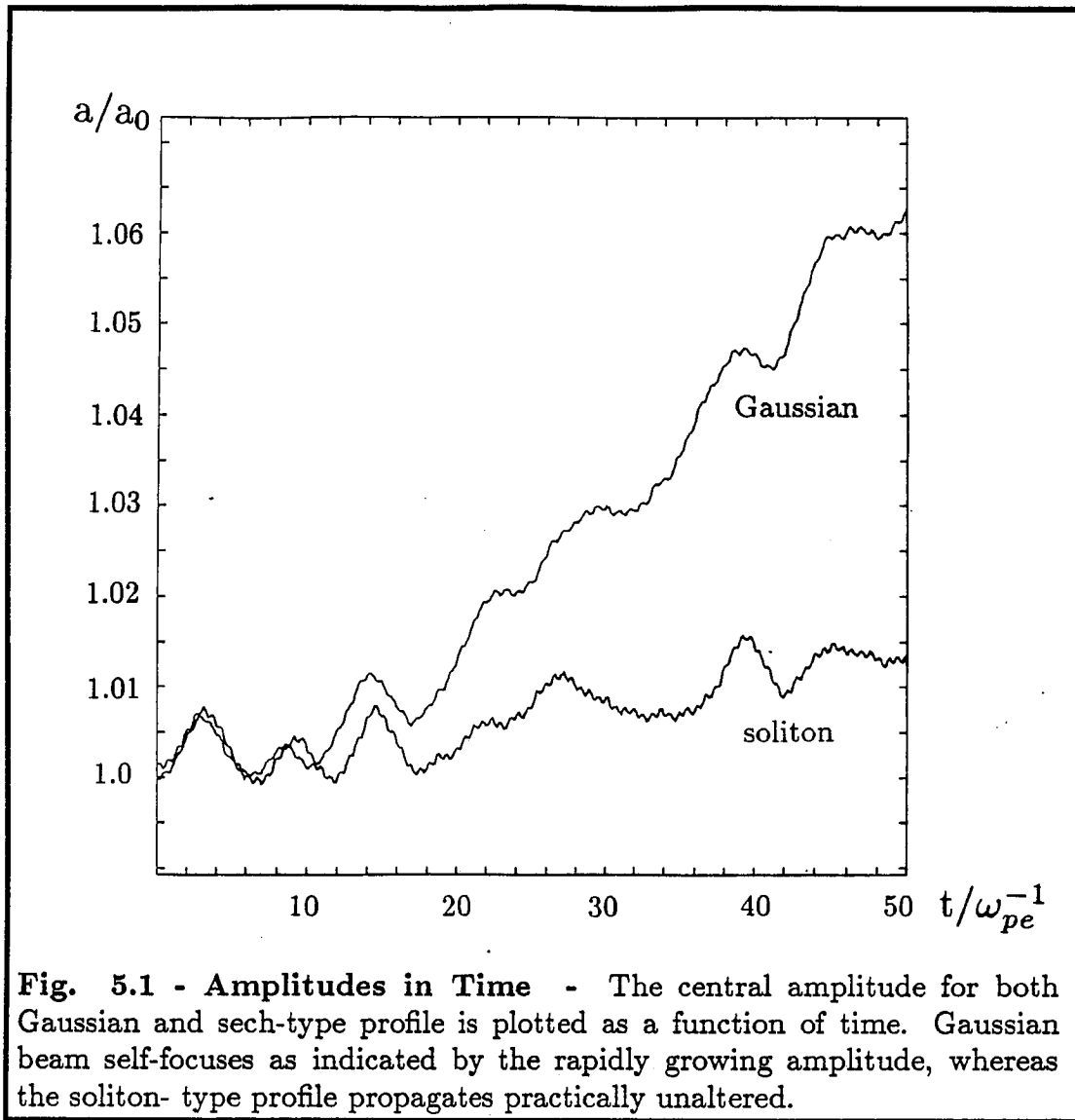


Fig. 5.1 - Amplitudes in Time - The central amplitude for both Gaussian and sech-type profile is plotted as a function of time. Gaussian beam self-focuses as indicated by the rapidly growing amplitude, whereas the soliton-type profile propagates practically unaltered.

to self-focus, as indicated by the rapid increase in the central amplitude. The soliton-type profile, on the other hand, remains constant within 1%. Figure 5.2(a) shows the initial soliton-type profile superimposed on the beam profile after 50 plasma oscillation periods. The profile is seen to retain its shape well. For comparison, in Fig. 5.2(b) we have shown the initial (at $t=0$) and final (at $t=50\omega_{pe}^{-1}$) form of an initially Gaussian beam. The deformation of the profile

is significant.

Based on this numerical experiment we thus conclude that the profile given by the exact solution (Eqs. (3.36) and (3.77)) to the nonlinear equations retains its original shape quite well; if such a profile is produced — either spontaneously in the course of the beam evolution, or initially by crafting the beam — it should remain unaltered as it propagates through the plasma.

5.3 Self-Focusing of a Laser Beam

In this section we first establish the threshold power and intensity for self-focusing of a laser beam from numerical experiments, and then study how the beam behaves after the initial focusing. The theoretical guidelines provided by Section 3.4, however, are not as precise and unambiguous as those provided by Section 3.3 for the previous section. For instance, the theoretical work of Section 3.4 was based on the assumption that the beam will always retain its Gaussian shape. This assumption (or some other, similar assumption about the shape of the beam) is traditionally introduced for convenience. This is not a bad assumption very close to the beam axis, where any beam can be approximated by an inverted parabola (and where our analysis was performed), but there is no physical reason to believe that the beam as a whole would remain Gaussian. Thus it should not come as a great surprise to us if the simulation did, in the course of time, produce a profile deviating from its initial Gaussian shape. In fact, the results of the previous section already suggest that this is indeed the case, although no detailed analysis was carried out yet.

5.3.1 Experiments with Models for Electron Density

In this section the versions of the phase-averaged particle simulation code used will not have explicit, individual electrons. Instead, the electron

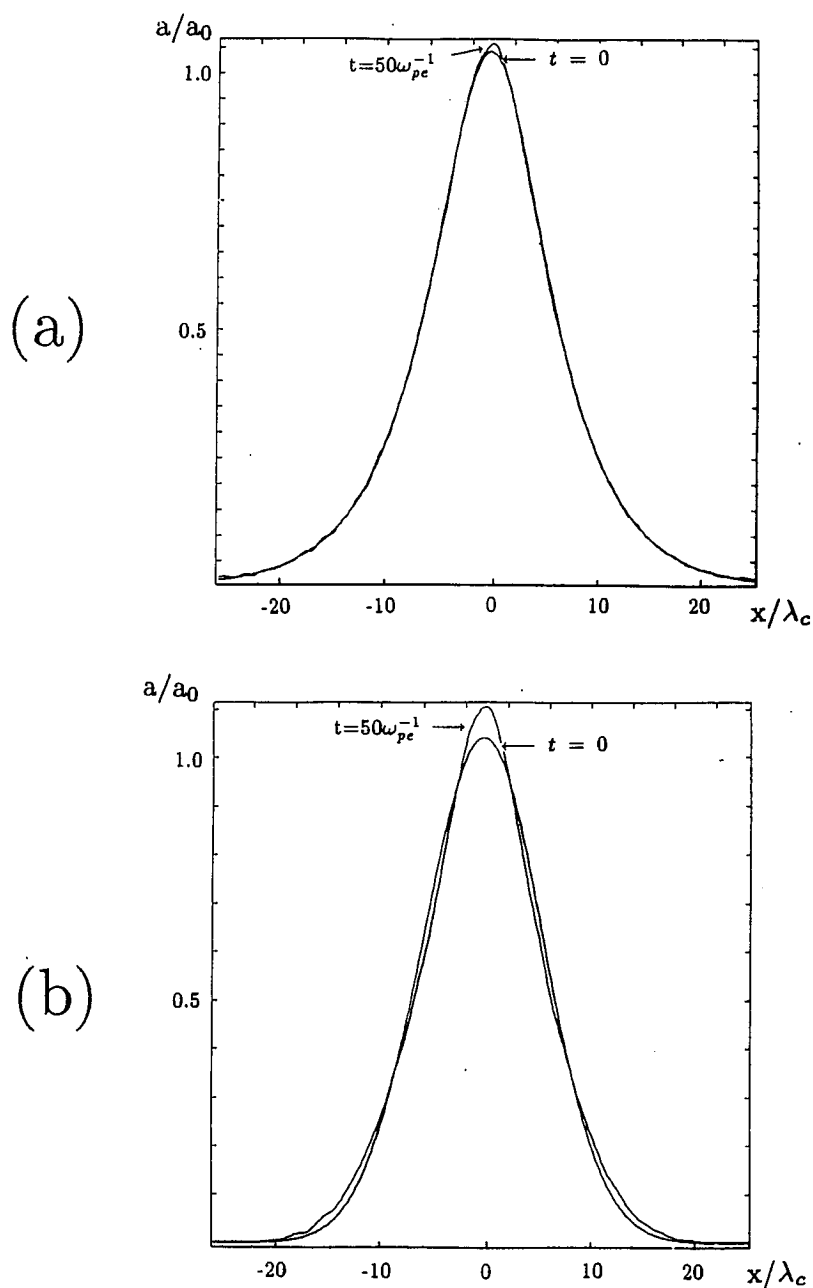


Fig. 5.2 - Gaussian and Asymptotic Beam Profile - (a) The profile of an originally soliton-type beam plotted at $t=0$ and $t=50\omega_p^{-1}$. The beam retains its shape well. (b) The profile of an originally Gaussian beam plotted at $t=0$ and $t=50\omega_p^{-1}$. The profile gets severed.

effects are brought about with the help of various theoretical models. The advantage of this kind of an “intermediate” approach is that we have complete control over which mechanisms are present and which are not.

We start by simulating self-focusing produced by the relativistic electron mass effects only. This is accomplished by keeping the electron density constant throughout the simulation run, $n_e = n_0$. This implies that the ponderomotive and electrostatic effects are then be absent, too. Therefore, for modelling purely relativistic self-focusing, the amplitude and phase equations given by Eqs. (4.45) and (4.46), respectively, should be rewritten as

$$\begin{aligned} \frac{\partial^2}{\partial t^2} = c^2 \nabla^2 a + a \left[\left(\frac{\partial \psi}{\partial t} \right)^2 - c^2 |\nabla \psi|^2 \right] + (\omega_0^2 - c^2 k_0^2) a + \\ 2a \left[\omega_0 \frac{\partial \psi}{\partial t} + c^2 k_0 \right] - \omega_{pe}^2 \frac{1}{\sqrt{1 + \frac{e^2 a^2}{m^2 c^2}}} , \end{aligned} \quad (5.3)$$

and

$$\frac{\partial}{\partial t} \left(a^2 \frac{\partial \psi}{\partial t} \right) = c^2 \nabla \cdot (a^2 \nabla \psi) - 2a \left(\omega_0 \frac{\partial a}{\partial t} + c^2 k_0 \frac{\partial a}{\partial z} \right) . \quad (5.4)$$

Throughout this section the initial beam profile is taken to have Gaussian shape. The code evolving the fields according to the above equations is called FD-SANDH.

Using Eqs. (5.3) and (5.4) in our field solver we carried out a series of computer runs to check the theoretical predictions on the critical power (or intensity) for self-focusing. This was done in the following manner: Choosing a fixed beam waist for the initial Gaussian profile we run the code for various values of the beam intensity. Scanning through the intensity and monitoring the time evolution of the central intensity for each run we can determine approximately what is the critical intensity corresponding to the specific beam waist at which the beam starts to self-focus. The width of the simulation box

quantity determining the evolution of the beam is not the intensity I_0 by itself, but rather the total power of the beam, $P \propto I_0 w_0^2$. Figure 5.3 shows the experimental points from our numerical simulations together with the theoretical predictions from Chapter III. The horizontal axis is the initial beam waist and the vertical axis gives the critical intensity at which the beam is observed to start to self-focus. An experimental point consists of the observed critical intensity multiplied by the square of the corresponding beam waist. The experimental points are indeed observed to lie approximately along a horizontal line, as predicted by the theory, but the magnitude of the critical power is higher than the prediction given in Chapter III. The reason for this discrepancy between the theory and the numerical experiment lies most probably in the near-axis approximation applied in the theoretical approach of Chapter III. As mentioned above, the near-axis expansion implies that we are approximating the beam by an inverted parabola: $e^{-x^2/w^2} \approx 1 - x^2/w^2$, $x^2/w^2 \ll 1$. This is a perfectly legitimate approximation near $x = 0$, but in reality the whole beam, not only the axial part of it, contributes to the self-focusing/defocusing. This is reflected in the mathematical formalism by the fact that the critical quantity determining the beam dynamics is the total power of the beam, not the central intensity itself. It is plausible that the self-focusing of the entire beam has a threshold power higher than that obtained by considering the dynamics of the beam only in the neighborhood of the peak.

Except for the quantitative discrepancy discussed above, the qualitative agreement between the theory and the numerical experiment is remarkable, demonstrating clearly the existence of a threshold or critical power P_{cr} .

We then include the ponderomotive effects. As in the case of the purely relativistic self-focusing, also here we incorporate the ponderomotive (and elec-

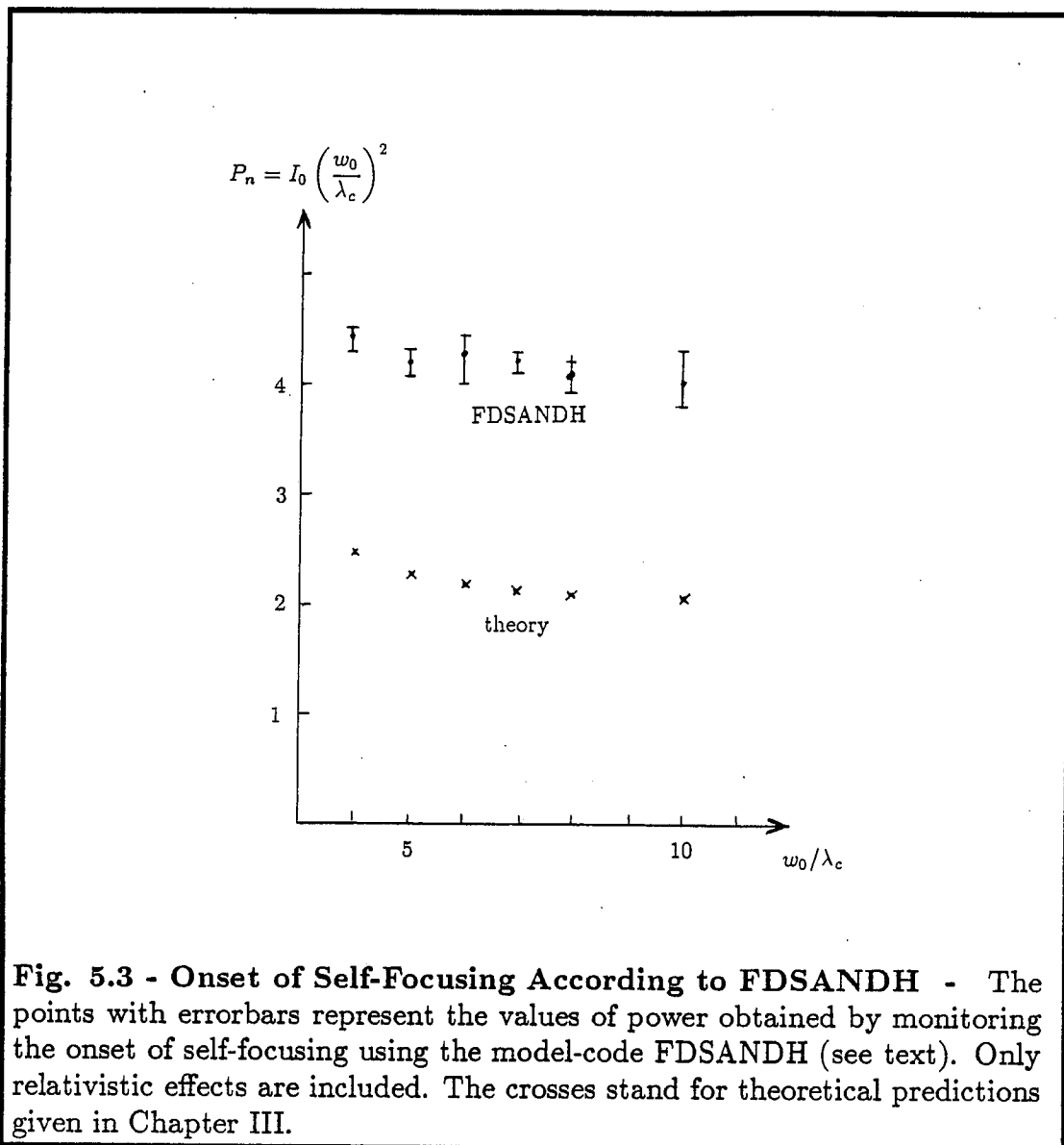


Fig. 5.3 - Onset of Self-Focusing According to FDSANDH - The points with errorbars represent the values of power obtained by monitoring the onset of self-focusing using the model-code FDSANDH (see text). Only relativistic effects are included. The crosses stand for theoretical predictions given in Chapter III.

was always chosen to be about six times the beam width. The total number of grid points was 128 or 256, depending on the width of the beam. The frequency of the laser was varied from $\omega_0 = 3\omega_{pe}$ to $\omega_0 = 5\omega_{pe}$, and the time step was $\Delta t = 0.1\omega_p^{-1}$.

According to the theory, as presented in the Chapter III, the critical

trostatic) effects using a theoretical model. Assuming that the laser-plasma system has reached a stationary state in which the ponderomotive force exerted on the electrons by the laser beam is balanced by the electrostatic force produced by the induced charge separation, we recall the model for electron density from Section 3.2. Equation (3.10) gives the normalized electron density under the combined influence of relativistic and ponderomotive effects, assuming a stationary state described above,

$$N_e = \frac{n_e}{n_0} = 1 + \lambda_c^2 \frac{\partial^2}{\partial x^2} \sqrt{1 + I_n} . \quad (5.5)$$

The field equations for the simulation code now become:

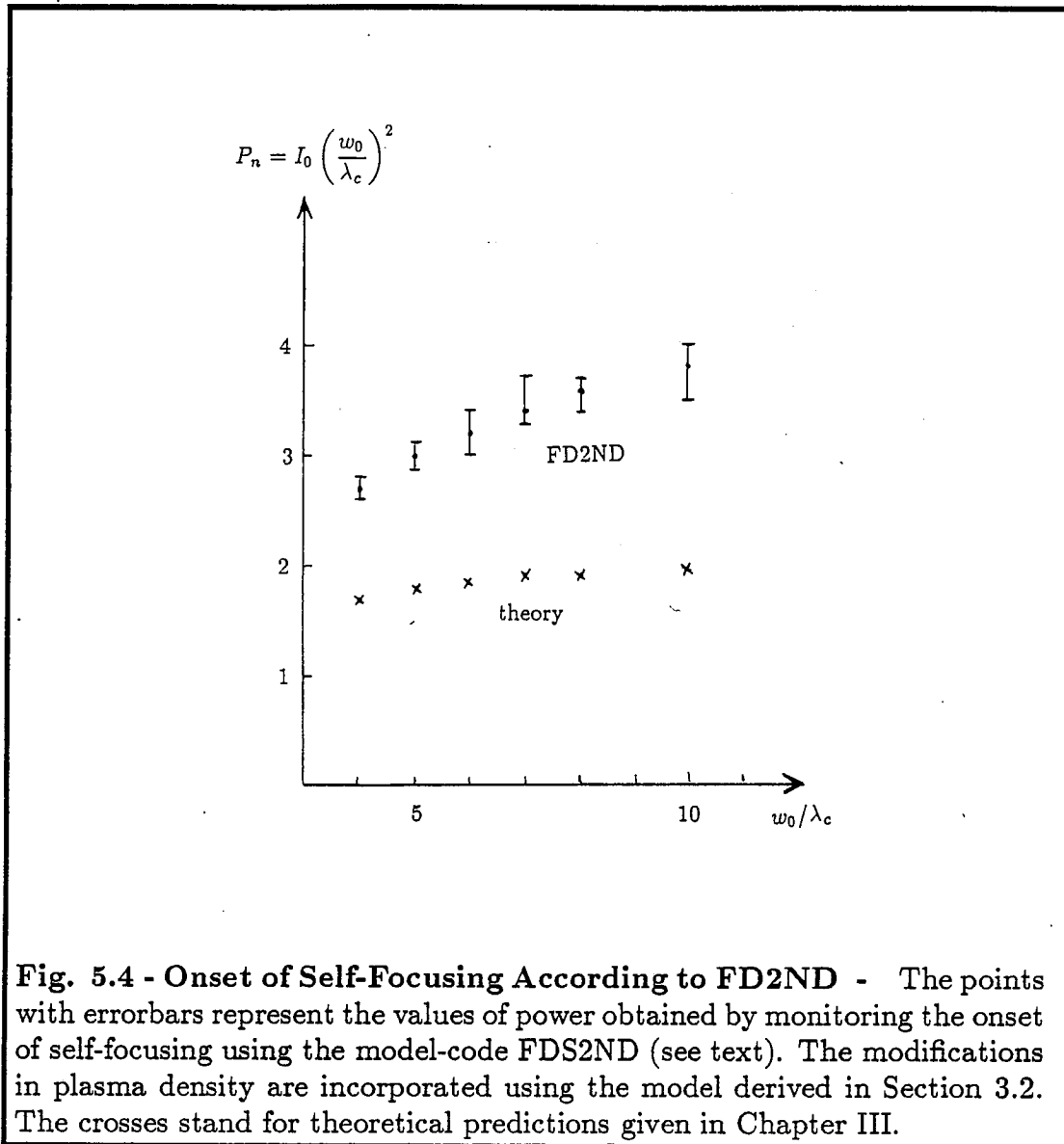
$$\begin{aligned} \frac{\partial^2}{\partial t^2} = & c^2 \nabla^2 a + a \left[\left(\frac{\partial \psi}{\partial t} \right)^2 - c^2 |\nabla \psi|^2 \right] + (\omega_0^2 - c^2 k_0^2) a \\ & 2a \left[\omega_0 \frac{\partial \psi}{\partial t} + c^2 k_0 \right] - \omega_{pe}^2 \frac{1}{\sqrt{1 + \frac{e^2 a^2}{m^2 c^2}}} \left[1 + \lambda_c^2 \frac{\partial^2}{\partial x^2} \sqrt{1 + \frac{e^2 a^2}{m^2 c^2}} \right] , \end{aligned} \quad (5.6)$$

and

$$\frac{\partial}{\partial t} \left(a^2 \frac{\partial \psi}{\partial t} \right) = c^2 \nabla \cdot (a^2 \nabla \psi) - 2a \left(\omega_0 \frac{\partial a}{\partial t} + c^2 k_0 \frac{\partial a}{\partial z} \right) . \quad (5.7)$$

The code evolving the field quantities according to Eqs. (5.6) and (5.7) is called FD2ND.

We repeated the same set of runs as we did for the purely relativistic case. Figure 5.4 shows the results from this numerical experiment together with the theoretical predictions. As in the purely relativistic case, here too the qualitative behavior of the threshold power accords with the theoretical work, but quantitatively there is a discrepancy. The observed critical power is about twice as high as the value given by the theoretical analysis. Again, it seems reasonable to assume that this discrepancy is due to the approximations applied in the theoretical approach. At least for narrow beam radii the presence of the



ponderomotive effects is seen to lower the threshold power for self-focusing. From the equation of motion for the beam radius, Eq. (3.120), the purely relativistic focusing term can be found to be proportional to

$$F_{rel} \propto \sqrt{1 + a^2} , \quad (5.8)$$

whereas the term describing the ponderomotive effects is accordingly given by

$$F_{pm} \propto 2 \frac{\lambda_c^2}{w^2} (a^2 + 3), \quad (5.9)$$

where a common factor $(\frac{1}{w} \frac{a^2}{(1+a^2)^2})$ has been divided out. Thus the ponderomotive effects are seen to be important for narrow beams and for very high intensities, in agreement with the simulation results. For broader beams the observed thresholds are quite close implying that for wide beams the relativistic effects dominate the dynamics. The importance of ponderomotive effects for higher intensities will be discussed when the later evolution of the beam is addressed.

5.3.2 Particle Simulation Experiments

In this section we are running the simulation using the full, phase-averaged electron dynamics. The ions are still taken to be stationary. The essential equations of the code are thus those given by Eqs. (4.44), (4.45) and (4.46). The run is called FDFIB1D.

To begin with, we study how the results from the "model"-runs of the previous section compare with the results given by a full particle simulation. To determine this we ran both FD2ND and FDFIB1D for a beam with beam waist of $w_0 = 4\lambda_c$, frequency $\omega_0 = 5\omega_{pe}$, and intensity $I_0 = 0.16$. The width of the simulation box was $L_x = 25.6\lambda_c$ and the number of grid points $N_g = 128$. The run extended over fifty electron oscillation periods with time step of $\Delta t = 0.1\omega_{pe}^{-1}$. In Fig. 5.5 we plot the output from the computer runs so that in the same frame, on top of each other (to facilitate the comparison), are the corresponding quantities given by the particle simulation code and the model-run. Figure 5.5(a) shows the beam profiles in the end of the run, $t = 50\omega_{pe}^{-1}$, and in Fig. 5.5(b) we have plotted the time histories of the central amplitude.

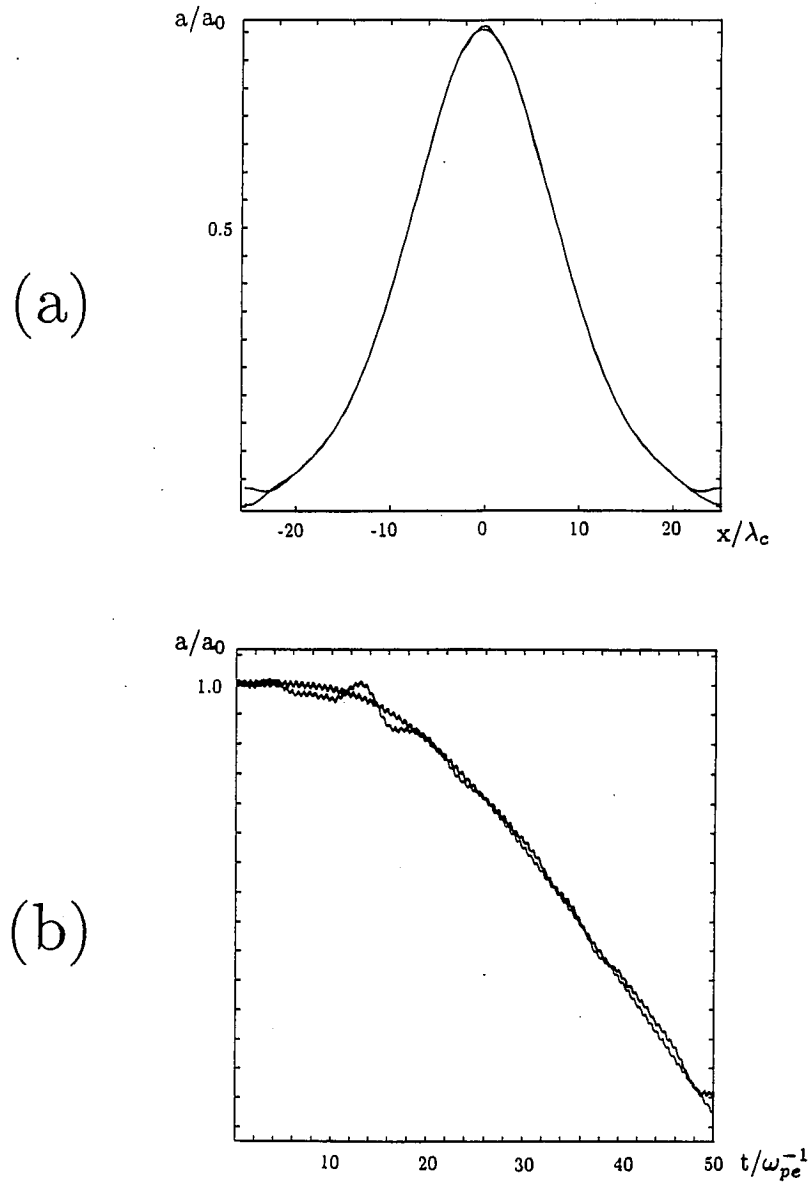
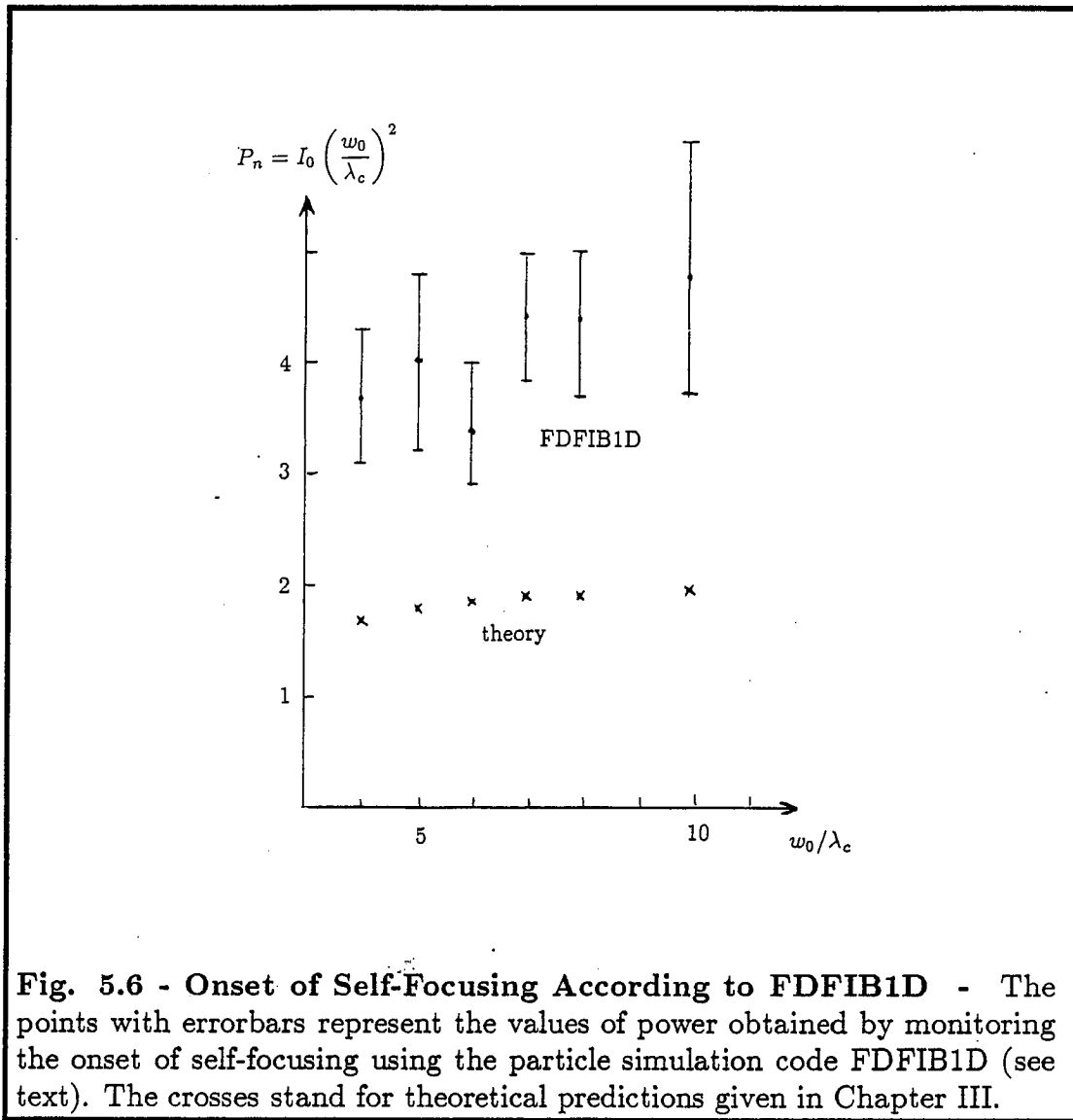


Fig. 5.5 - Comparison of The Model and The Particle Simulation
 - (a) The final ($t=50\omega_p^{-1}$) beam profiles from the model (FD2ND) and particle simulation (FDFIB1D) plotted on top of each other. (b) The time development of the central amplitude as given by FD2ND and FDFIB1D.

The corresponding plots from the different runs are qualitatively very similar, and thus we conclude that the model for electron density derived in Section 3.2 is reasonable. Quantitative differences do arise, however, as the intensity of the beam is increased. The self-focusing is stronger for FDFIB1D-runs, which have individual electrons, and the code produces self-focusing slightly earlier than the runs using the FD2ND-code where the relativistic and ponderomotive effects are incorporated using a model. The reason for these differences is discussed below when comparing the threshold values from various runs.

We now address the question of self-focusing using the particle simulation code. Since the model for electron density derived in the text appeared to be realistic, the model runs of the previous section provide us with guidelines. We thus repeat the simulation runs that we did with the model-codes FDSANDH (only relativistic effects) and FD2ND (both relativistic and ponderomotive effects), scanning through the intensity for fixed beam waist to find the critical case for self-focusing. The simulation results are plotted in Fig. 5.6. Comparing these results to those obtained from the model runs in Section 5.3.1 (see Figs. 5.3 and 5.4), they appear to be a combination of the purely relativistic model and the model incorporating both the relativistic and the ponderomotive effects. The qualitative behavior of the simulation results follows that of the model run that incorporates both the ponderomotive and relativistic effects, but the value of the critical power is closer to the purely relativistic model. This is actually what one should expect. The code FD2ND, which took into account the ponderomotive effects, was based on the assumption of a stationary state in which the electrons were already misplaced according to the laser parameters. In the particle simulation code FDFIB1D, on the other hand, the electrons are not in any way prepared in advance for the incoming laser. Therefore a small but finite time is required for them to drift to the positions corresponding to

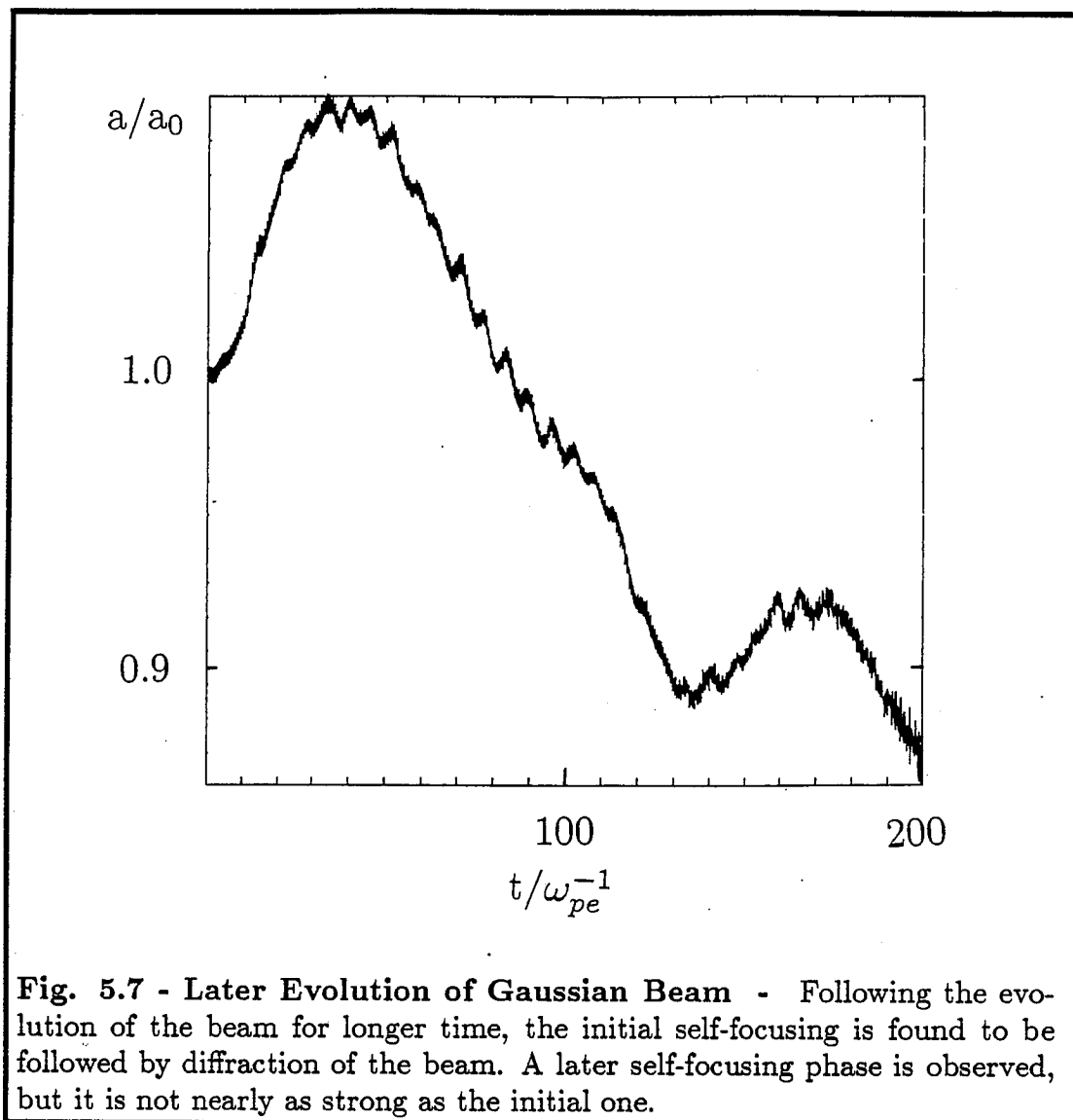


the stationary state (recall the analysis of the ponderomotive time scale carried out in the beginning of Chapter IV) and to bring about the plasma-lens effect necessary for self-focusing. Meanwhile, although the threshold for purely relativistic self-focusing is higher, the process is practically instantaneous (in the time scale of laser oscillation period) as pointed out in Chapter II.

Herein lies also the explanation for the observation why, despite the

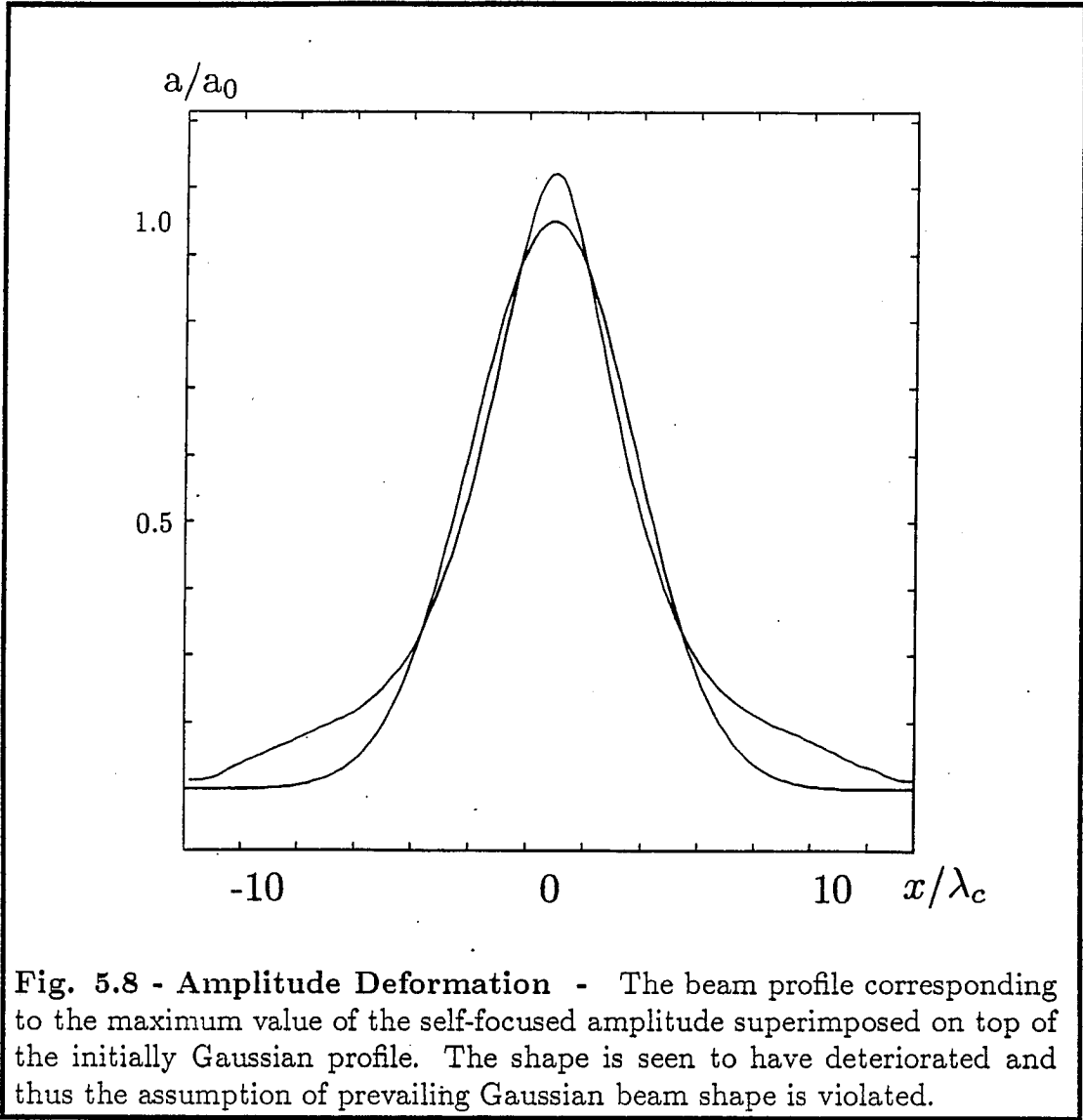
qualitative similarities, the self-focusing was observed to take place earlier using the particle simulation code FDFIB1D than with the model-code FD2ND which, in principle, incorporates all the significant processes: Since the relativistic effects dominate at very early times and FDFIB1D has practically unperturbed electron density in the central region at that time, it provides a stronger lens-effect than the model-run FD2ND in which the electron density is depleted around the axis from the very beginning.

We now address the question of the later evolution of the beam in the case when self-focusing has taken place. In Chapter III we speculated that, after initial focusing, the beam would start to defocus again for one of the two reasons: (1) the beam contracts to such a small radius that the inherent diffraction takes over, or (2) the electrons get depleted from the central region and thus the plasma-lens disappears, leaving the beam propagating in vacuum. This is clearly manifested in all the simulation runs (and in the model runs as well), as demonstrated in Fig. 5.7. After an initial increase in the central amplitude indicating self-focusing, the amplitude will at some point start to decrease. Further, the closer the initial intensity is to the critical intensity for the self-focusing, the sooner the defocusing will take place. In Chapter III we further speculated that this defocusing phase would be followed by another self-focusing phase, and that this pattern would then repeat itself corresponding to an oscillating beam envelope. This, however, seems to take place only for values of power well above the critical value ($P \geq 1.5 \cdot P_{cr}$), and even then the second phase of focusing is not very impressive. This is most probably due to the significant distortion of the Gaussian shape of the beam. In Fig. 5.8 we have plotted the initial beam profile together with the profile corresponding to the maximum self-focused amplitude for the same run as in Fig. 5.7. Unlike in Rayleigh spreading, where the beam always retains its shape, in self-focusing



the inner and outer regions of the beam profile seem to follow different dynamics. In the central region where the intensity is high, the beam self-focuses. In the outer skirts, however, the intensity is too low thus allowing the beam to diffract. Thus the beam gets deformed and does not quite follow the dynamics derived forcing the beam to always remain Gaussian.

It is also interesting to notice that running the model-codes FDSANDH



and FD2ND at this high values of power, the FD2ND-run that incorporates both relativistic and ponderomotive effects produces a similar second hump that was observed in the particle simulation runs. The FDSANDH-runs, carrying only the relativistic terms, on the contrary, failed to produce the secondary hump.

As a final topic we want to address the behavior of the electron density in the presence of self-focusing. The Sagdeev-potential introduced in Sec-

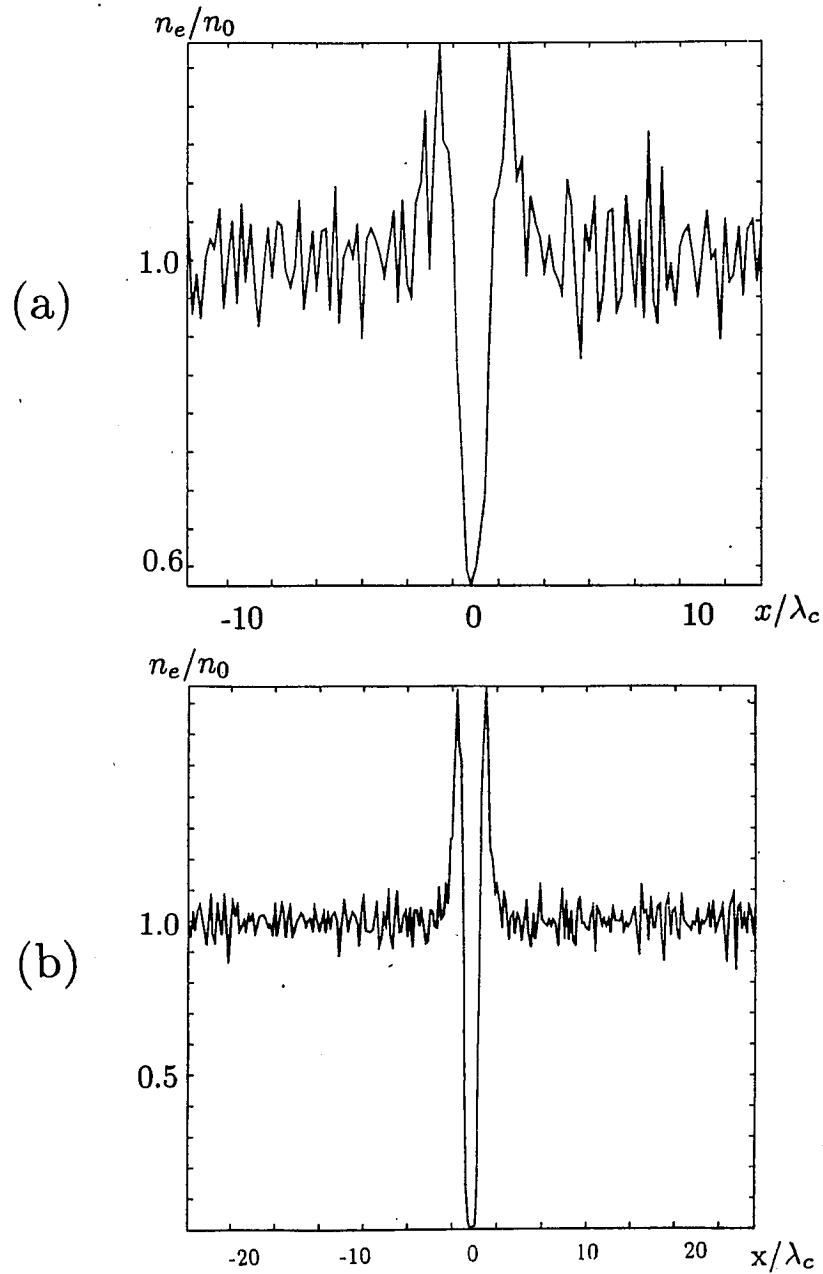
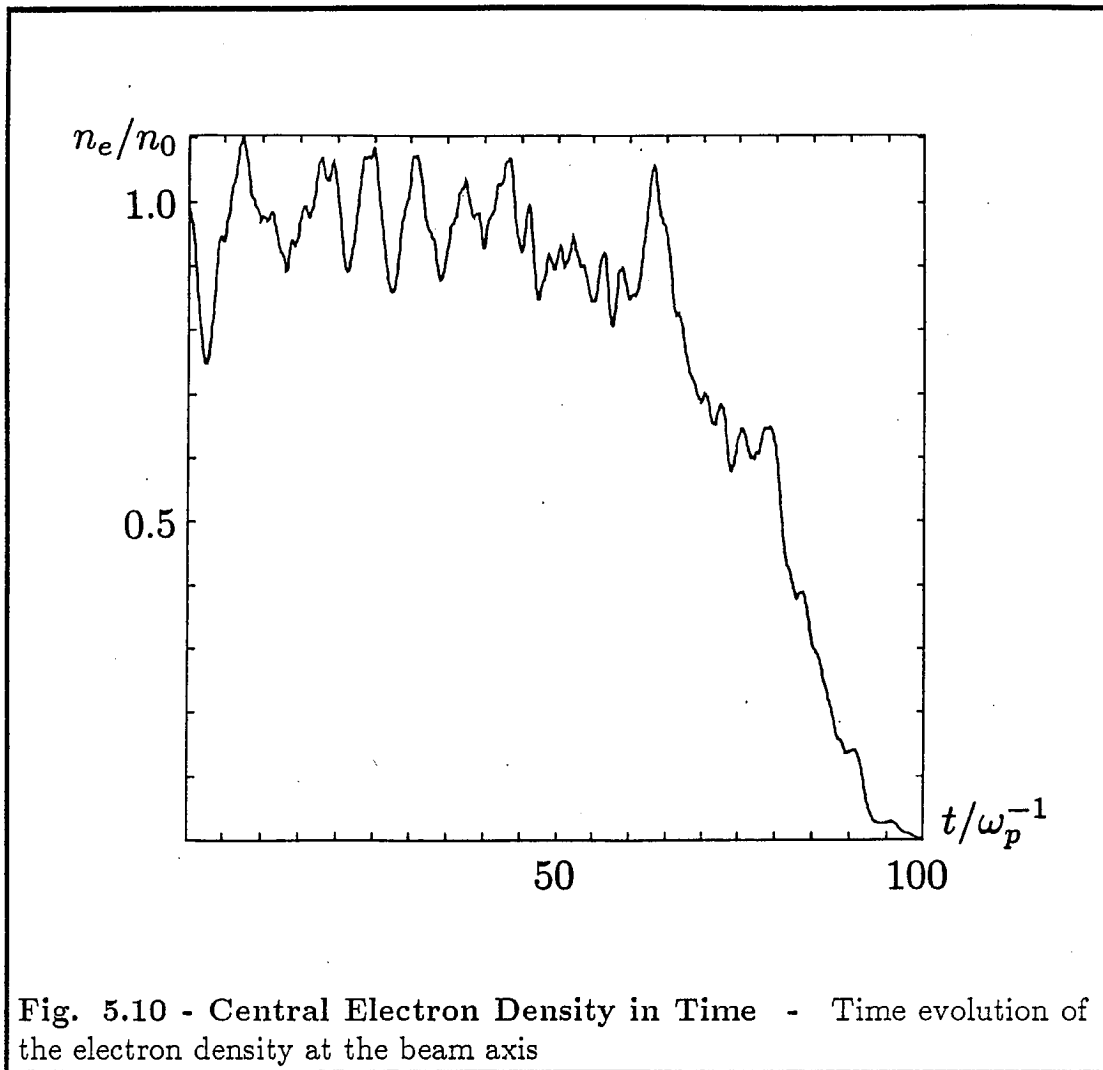


Fig. 5.9 - Electron Density Profiles - (a) The electron density profile after 30 plasma oscillation periods. The initial intensity is $I_0 = 0.64$ and the beam waist is $w_0 = 4\lambda_c$. The self-focused beam intensity corresponding to the electron density shown is $I(t = 30\omega_p^{-1}) = 0.99$. (b) The electron density profile after 100 plasma oscillation periods. The initial intensity is $I_0 = 0.41$ and the beam waist is $w_0 = 8\lambda_c$. The self-focused beam intensity corresponding to the electron density shown is $I(t = 100\omega_p^{-1}) = 1.99$.

tion 3.6 (Eqs. (3.129) and (3.130)) implies that, once the threshold power for self-focusing is exceeded, electron evacuation along the axis will always take place. Experiments with the particle simulation code, however, show something different. According to the simulations the beam power has to be well above the threshold power ($P \geq 2.3 \cdot P_{cr}$) before significant density modifications take place. Figure 5.9(a) shows the electron density after 30 plasma oscillation periods. The intensity of the beam for this run was $I = 0.64$ and the waist of the beam was $w_0 = 4\lambda_c$. A clear density depression along the axis is observed, surrounded by density spikes due to the surplus electrons pushed out of the central region. The depression at this point of the run is about 45% of the equilibrium density. Running the code for longer time and for a beam twice in width, $w_0 = 8\lambda_c$, we can eventually produce practically 100% depletion on the axis as shown in Fig. 5.9(b). One should, however, take this result with caution because by that time the self-focusing has proceeded so far as to produce relativistic field amplitudes, $|\frac{eE}{m\omega_0 c}| > 1$. The plasma current contribution in the simulation code was derived assuming nonrelativistic amplitudes and thus the electron evacuation, as observed running the code up to relativistic amplitudes, is not necessarily reliable. However, a definite tendency for producing a vacuum channel is seen while the field amplitude remains within the limits set by our approximations. In Fig. 5.10 we show the time evolution of the electron density on the beam axis for the case shown in Fig. 5.9(b).

The discrepancy between the theory and simulation in that the electron evacuation was not observed as an inevitable consequence of self-focusing, is due to the incompetence of the model used for the electron density in the theoretical approach. As recalled from Section 3.6, the model for electron density was not automatically protected from becoming negative after all the electrons were depleted. In the theory this was patched up by hand. If we had not done that,



the Sagdeev potential would approach negative infinity for infinitesimal values of the beam radius, i.e. the diffraction term would never start to dominate, and the beam would reach a catastrophic focus. Since it is clear that once the electrons are depleted and a vacuum is formed, there is no physical process to sustain the self-focusing, it was necessary to cut out the negative electron density -effect by writing the potential in two parts (Eqs. (3.131) and (3.132)). This procedure introduced a kink at the minimum of the potential. In reality the potential is naturally smooth and analytic across the minimum, and thus the

predictions given by the theoretical model in the neighborhood of the minimum are not entirely reliable.

Mori *et al.*⁵³ have also carried out a numerical study of nonlinear self-focusing of laser beams in plasmas. They did not, however, observe any electron evacuation for power values approximately an order of magnitude above the threshold value. Comparisons to their work are not, however, necessarily meaningful. The two major differences between the work carried out by Mori *et al.*⁵³ and the work presented here are: (1) the transverse beam profiles in their simulations were not Gaussian but of the form $\cos^2(\pi y/L_0)$, and (2) Mori *et al.* simulated two collinear beams rather than a single laser beam.

Chapter VI

Summary and Discussion

Motivated by the need for novel, ultra-high energy particle accelerators, we have here addressed a fundamental problem: the diffraction of the beam, which causes the reduction of the beam power and unparallel phase front. We have investigated the possibility of overcoming this problem by the nonlinear self-focusing that can take place in plasmas (or certain nonlinear dielectric media). In this work we have considered only very short laser pulses. The length of the laser pulse is sufficiently short ($L_p < 140\omega_p^{-1}$ for a proton plasma)⁴⁵ so that it leaves the ions stationary, and thus ensures that the parametric instabilities associated with the ion dynamics should be absent. This is naturally desirable and perhaps required for any particle accelerator scheme using plasmas.

Investigating the problem first analytically, we derived a model for the electron density in the presence of an intense, nonuniform electromagnetic field by assuming immobile ions and a stationary state in which the ponderomotive force by the laser beam is balanced by the electrostatic force due to the charge separation. We then looked for a possible profile that would propagate in plasma without distorting its shape. Such a profile was obtained in a form of a solitary wave with the amplitude a relation to the width κ_1^{-1} through

$$a(\xi) = 2\kappa \frac{\text{sech}(\kappa\xi)}{1 - \kappa^2 \text{sech}^2(\kappa\xi)} .$$

In the nonrelativistic limit ($a \ll 1$), considering only relativistic electron mass effects, this profile is, within a factor of two, the same as the profile obtained earlier by Schmidt and Horton⁵⁰ for purely relativistic self-focusing.

We investigated the dynamical behavior of the laser-plasma system assuming the above-mentioned stationary state. The beam was taken to have initially a Gaussian intensity profile and, to facilitate the calculations, it was assumed to remain Gaussian as it propagates through the plasma. Using Hamiltonian dynamics and making the paraxial and slowly varying envelope approximations, we arrived at a threshold power for self-focusing given by

$$P_{cr} \approx 10^{10} \left(\frac{\omega_0}{\omega_p} \right)^2 W.$$

Aside from numerical factors, this value compares favorably with earlier results obtained by Schmidt and Horton,⁵⁰ Sprangle *et al.*,⁵¹ and Sun *et al.*⁴⁴ Schmidt and Horton, as well as Sprangle *et al.* considered only relativistic electron mass effects, the first in the nonrelativistic limit, $|\frac{eE}{m\omega_0 c}|^2 \ll 1$. The formulation adopted by Sun *et al.* included both relativistic and ponderomotive effects and was very similar to the one presented here. They, however, obtained the threshold power using numerical integration.

Further, the ray equations were cast in a form analogous to the equation of motion for a classical particle. For beam powers greater than the critical value, the potential exhibits a minimum and thus the later evolution of the beam should consist of oscillations of the beam radius, i.e. the beam would alternate between defocusing and self-focusing phases in the absence of dissipative processes. The equilibrium radius coincides with the value corresponding to a total depletion of the electron along the axis. This is because according to our model for the electron density the self-focusing is unimpeded until vacuum formation sets in resulting in the Rayleigh diffraction.

The above investigation leaves a number of questions. For example,

the model for the electron response had to be patched up by hand at the value corresponding to the vacuum formation. Also the validity of the assumption that the beam would always retain its Gaussian shape is questioned. Even more fundamentally, the theoretical analysis started with the assumption of a stationary state. A computer simulation could reveal if such a state actually exists. Further, any kinetic effects would not be revealed in the theoretical framework since it was based on the fluid equation for the electrons. For these reasons we developed a numerical, phase-averaged particle simulation code suitable for studying laser transport problems in plasma. The code operates on the same principles as a conventional particle simulation code except that the evolution equations are averaged over the short laser oscillation period (and the wavelength) and the code thus follows only the secular changes in the system. By far the shortest wavelength and time scale in the problem are those of the laser, and we are not interested in following them. This approach could be compared to the model for electrostatics by Zakharov.⁶⁴ The code was tested against Rayleigh diffraction in vacuum and the code reproduced the theoretical prediction well.

In this work, only a one-dimensional form of the code was used. We have thus been modeling a beam uniform in the direction of propagation, and the dynamics took place in time. First we tested the asymptotic intensity profile given by Eq. (3.92). For comparison, the same computer run was repeated for an equivalent Gaussian intensity profile. The asymptotic solitary profile proved to retain its shape in the course of time, whereas the Gaussian beam profile was distorted.

In testing the dynamical aspects of the laser-plasma system, we first

removed the individual electrons from the code and represented the plasma response by the model used in the theoretical approach. Performing a series of runs for different beam parameters the threshold power emerged clearly from the data. Thus it was confirmed that the critical quantity for self-focusing is the power of the beam. These runs were then repeated with full particle dynamics and the results were qualitatively the same. Quantitatively, however, there were some differences between the model-runs and the kinetic runs. The threshold power for self-focusing was observed somewhat lower in the kinetic runs than in the model runs and, monitoring the later evolution of the beam, the secondary self-focusing phase was more easily produced in the kinetic run. This secondary focusing phase was, however, a little disappointing in general since it appeared much weaker than the primary one. This seems to be due to the strong deformation of the Gaussian shape of the beam, as indicated by Fig. 5.8.

The phase-averaged particle simulation code developed in Chapter IV to study the problem of self-focusing can be a useful tool for studying other kind of laser-plasma interaction problems as well. In Appendix C we present preliminary results from a study of the evolution of a multi-peaked amplitude profile using the code described in Chapter IV.

The major short-coming of this numerical approach is that it has so far been only one-dimensional. To obtain a more complete picture of the physics involved in the laser-plasma system, we would like to be able to launch a laser pulse of finite length into the plasma. In one-dimensional simulation we are stuck with an infinite, uniform laser beam, which can not provide us with all the dynamical aspects of the system. A two-dimensional simulation would also

allow us to verify the existence of a stationary state, as well as the proposed oscillations of the beam radius. Thus the future work on the problem should include upgrading of the code to two spatial dimensions. This is probably a nontrivial task since it includes implementing a different set of boundary conditions in the direction of propagation. An idea worth pursuing, while doing the upgrade, would be to transform the system into a frame moving at the group velocity of the laser wave. This would naturally include transforming everything including the time and length in the system, and the diagnostics as well as boundary conditions would have to be reconstructed. But provided that a workable solution to these problems can be found, this scheme would have the advantage of monitoring only the interesting time and spatial scales of the laser-plasma system.

Appendices

APPENDIX A

Derivation of the Ponderomotive Force

The equation of motion for electrons under the influence of an electromagnetic field is

$$\frac{d\mathbf{p}}{dt} = -e \left(\mathbf{E} + \frac{1}{c} \mathbf{v} \times \mathbf{B} \right) . \quad (7.1)$$

Assuming circular polarization, the electric field of the wave can be written as

$$\mathbf{E} = E_s(\mathbf{r}) (\cos \phi \hat{\mathbf{x}} - \sin \phi \hat{\mathbf{y}}) , \quad (7.2)$$

where the phase of the wave is given by $\phi \equiv k_0 z - \omega_0 t$ and the wave is assumed to have a nontrivial intensity profile, $E_s(\mathbf{r})$. The magnetic field, as given by the Faraday's law is then

$$\begin{aligned} \mathbf{B} = & -\frac{c}{\omega_0} \left(\frac{\partial E_s}{\partial z} \cos \phi - k_0 E_s \sin \phi \right) \hat{\mathbf{x}} \\ & -\frac{c}{\omega_0} \left(\frac{\partial E_s}{\partial z} \sin \phi + k_0 E_s \cos \phi \right) \hat{\mathbf{y}} \\ & +\frac{c}{\omega_0} \left(\frac{\partial E_s}{\partial y} \sin \phi - \frac{\partial E_s}{\partial x} \cos \phi \right) \hat{\mathbf{z}} . \end{aligned} \quad (7.3)$$

We assume there is no dc current and so the equilibrium velocity vanishes. The equation of motion for the electrons is

$$\frac{d\mathbf{p}}{dt} = -e \left(\mathbf{E} + \frac{1}{c} \mathbf{v} \times \mathbf{B} \right) , \quad (7.4)$$

and so the first order perturbation is given by the electric field only:

$$\frac{d\mathbf{p}^{(1)}}{dt} = -e\mathbf{E} \Rightarrow \mathbf{p}^{(1)} = \frac{e}{\omega_0} (\sin \phi \hat{\mathbf{x}} + \cos \phi \hat{\mathbf{y}}) E_s . \quad (7.5)$$

The first order velocity is thus given by

$$\mathbf{v}^{(1)} = \frac{\mathbf{p}^{(1)}}{m\gamma} = \frac{v_q}{\sqrt{1 + \frac{v_q^2}{c^2}}} (\sin \phi \hat{\mathbf{x}} + \cos \phi \hat{\mathbf{y}}) , \quad (7.6)$$

where $v_q \equiv \frac{eE_s}{m\omega_0}$ is the quivering velocity of the electrons introduced in the end of the chapter II. The second order momentum is given by

$$\begin{aligned} \frac{d\mathbf{p}^{(2)}}{dt} &= \frac{e}{c} \mathbf{v}^{(1)} \times \mathbf{B} \\ &= \frac{e^2 E_s}{m\gamma\omega_0^2} \left[\left(\frac{\partial E_s}{\partial y} \sin \phi \cos \phi - \frac{\partial E_s}{\partial x} \cos^2 \phi \right) \hat{\mathbf{x}} \right. \\ &\quad \left. - \left(\frac{\partial E_s}{\partial y} \sin^2 \phi - \frac{\partial E_s}{\partial x} \sin \phi \cos \phi \right) \hat{\mathbf{y}} \right. \\ &\quad \left. - \frac{\partial E_s}{\partial z} \hat{\mathbf{z}} \right] . \end{aligned} \quad (7.7)$$

We are not interested in the rapid oscillations but rather the secular change in $\mathbf{p}^{(2)}$. Therefore we want to average this equation over the laser oscillation period $T = 2\pi/\omega_0$. In doing that we have to realize that the field quantities in the equation of motion are specified at the instantaneous position of the electron, $\mathbf{r}(t)$. Since the exact form of $\mathbf{r}(t)$ is not known, the equation cannot be integrated as such. We do know, however, the particle trajectory up to the first order in $\frac{v_q}{c}$:

$$\mathbf{r}(t) = \mathbf{r}_0 + \int_0^t \mathbf{v}^{(1)} dt , \quad (7.8)$$

where \mathbf{r}_0 is the initial position of the electron. Calling $\delta\mathbf{r}^{(1)} \equiv \mathbf{v}^{(1)} dt$ we have

$$\delta\mathbf{r}^{(1)} = \frac{eE_s}{m\gamma\omega_0^2} (\cos \phi \hat{\mathbf{x}} - \sin \phi \hat{\mathbf{y}}) , \quad (7.9)$$

and we can express the fields in terms of the known quantities \mathbf{r}_0 and $\delta\mathbf{r}^{(1)}$ using Taylor expansion around \mathbf{r}_0 :

$$\begin{aligned} E_s(\mathbf{r}) &\approx E_s(\mathbf{r}_0) + \delta\mathbf{r}^{(1)} \cdot \nabla E_s|_{\mathbf{r}_0} + O\left(\frac{v_q^2}{c^2}\right) \\ \mathbf{B}(\mathbf{r}) &\approx \mathbf{B}(\mathbf{r}_0) + O\left(\frac{v_q^2}{c^2}\right) . \end{aligned} \quad (7.10)$$

It is sufficient to evaluate the magnetic field at the initial position since the term involving the magnetic field is of the second order in $\frac{v_a}{c}$. The phase factor ϕ will be also given by the initial values, because $\delta\mathbf{r}^1$ does not have a z-component. Using the above expansions in the equation for the second-order momentum we find

$$\begin{aligned}\frac{d\mathbf{p}^{(2)}}{dt} &= -e\delta\mathbf{r}^{(1)} \cdot \nabla E_s|_{\mathbf{r}_0} - \frac{e}{c}\mathbf{v}^{(1)} \times \mathbf{B} \\ &= -\frac{e^2 E_s}{m\gamma\omega_0^2} \left[2\left(\frac{\partial E_s}{\partial x} \cos^2 \phi - \frac{\partial E_s}{\partial y} \sin \phi \cos \phi\right)\mathbf{x} \right. \\ &\quad \left. - 2\left(\frac{\partial E_s}{\partial x} \sin \phi \cos \phi - \frac{\partial E_s}{\partial y} \sin^2 \phi\right)\mathbf{y} \right. \\ &\quad \left. + \frac{\partial E_s}{\partial z} \mathbf{z} \right].\end{aligned}\quad (7.11)$$

Averaging the expression for the second order momentum over the laser oscillation period we obtain

$$\langle \frac{d\mathbf{p}^{(2)}}{dt} \rangle = -\frac{e^2 E_s}{m\gamma\omega_0^2} \left(\frac{\partial E_s}{\partial x} \mathbf{x} + \frac{\partial E_s}{\partial y} \mathbf{y} + \frac{\partial E_s}{\partial z} \mathbf{z} \right), \quad (7.12)$$

or, noting that $(\frac{v_a}{c})^2 = (\frac{eE_s}{m\omega_0 c})^2 \equiv I_n$ and $\gamma = \sqrt{1 + I_n}$,

$$\langle \frac{d\mathbf{p}^{(2)}}{dt} \rangle = -mc^2 \nabla \sqrt{1 + I_n} \equiv \mathbf{F}_p. \quad (7.13)$$

Sometimes the ponderomotive force is given in terms of the ponderomotive potential, χ :

$$\mathbf{F}_p = -\nabla \chi, \quad (7.14)$$

where $\chi \equiv mc^2 \sqrt{1 + I_n}$.

APPENDIX B

Derivation of the Rayleigh Spread in Two Dimensions

We shall here find the behavior of an initially Gaussian beam as it propagates in a vacuum. The analysis is done in two spatial dimensions corresponding to the slab geometry applied in the numerical work of Chapters IV and V. The direction of propagation is labeled by y , and the transverse direction is the x -direction.

The wave equation for the vector potential in vacuum reads

$$\frac{1}{c^2} \frac{\partial^2}{\partial t^2} A - \nabla^2 A = 0 . \quad (7.15)$$

Assuming a stationary state and writing the vector potential in the form

$$A = a(x, y) e^{-i(\omega_0 t - k_0 y)} , \quad (7.16)$$

where a is a complex (in contrast to our choice in the main text), slowly varying amplitude given in the form

$$a = a_0 \exp \left\{ -i \left[\varphi(y) + \frac{k_0}{2q(y)} x^2 \right] \right\} , \quad (7.17)$$

and $\nabla^2 = \frac{\partial^2}{\partial x^2} + \frac{\partial^2}{\partial y^2}$, the wave equation becomes

$$\nabla^2 a + k_0^2 a = 0 , \quad (7.18)$$

where the vacuum dispersion relation, $\omega_0 = ck_0$, was applied. In evaluating the spatial derivatives, only the first derivatives of φ and q are kept because these functions are assumed to be slowly varying. Substituting the ansatz for A into the wave equation we obtain

$$2k_0 \left[\frac{d\varphi}{dy} - \frac{k_0}{2q^2} x^2 \frac{dq}{dy} \right] + i \frac{k_0}{q} - \frac{k_0^2}{q^2} x^2 = 0 . \quad (7.19)$$

For this to be satisfied for all values of x , the terms independent of x should add to zero independently, and similarly, the terms multiplying x^2 should add to zero. We thus arrive at two separate equations:

$$\begin{aligned} 2k_0 \frac{d\varphi}{dy} + i \frac{k_0}{q} &= 0, \text{ and} \\ \frac{dq}{dy} + 1 &= 0. \end{aligned} \tag{7.20}$$

The latter can be directly integrated to yield

$$q(y) = q_0 - y. \tag{7.21}$$

Anticipating the result, we write q in the form

$$\frac{1}{q(y)} = -\frac{1}{R(y)} - i \frac{\lambda_0}{\pi w(y)^2}, \tag{7.22}$$

where R and w are real functions of y . This looks quite strange unless one realizes that a form like this makes the vector potential appear as

$$A = a_0 e^{-r^2/w^2} e^{-\varphi} e^{-ik_0 x^2/R}, \tag{7.23}$$

where each exponential has a well defined, physical meaning: the first exponential, being real, gives the Gaussian shape of the profile, the second exponential gives the phase shift, and the third exponential gives the curving of the phase front with $R(y)$ being the radius of curvature. The initial values for the variables with a physical interpretation are:

$$\begin{aligned} R(y=0) &= \infty \quad \text{for the initially straight phase-front, and} \\ w(y=0) &= w_0. \end{aligned} \tag{7.24}$$

The initial value for $q(y)$ is then $q_0 = i\frac{\pi w_0^2}{\lambda_0}$. The real and imaginary part of expression (21) for q yield the solution for w and R :

$$\begin{aligned} w(y)^2 &= w_0^2 \left[1 + \left(\frac{\lambda y}{\pi w_0^2} \right)^2 \right], \\ R(y) &= y \left[1 + \left(\frac{\pi w_0^2}{\lambda y} \right) \right]. \end{aligned} \quad (7.25)$$

The nature of these solutions becomes much more evident if we define the so called Rayleigh range: $Y_R \equiv \pi w_0^2 / \lambda_0$. The expressions then become

$$\begin{aligned} w(y)^2 &= w_0^2 \left[1 + \left(\frac{y}{Y_R} \right)^2 \right], \\ R(y) &= y \left[1 + \left(\frac{Y_R}{y} \right) \right]. \end{aligned} \quad (7.26)$$

The solution for the phase shift φ is then obtained from the first equation in (20):

$$\begin{aligned} \varphi(y) &= -i \ln \left(1 + \frac{y^2}{Y_R^2} \right)^{1/4} + \frac{1}{2} \arctan \left(\frac{y}{Y_R} \right) \\ &= -i \ln \sqrt{w/w_0} + \frac{1}{2} \arctan \left(\frac{y}{Y_R} \right), \end{aligned} \quad (7.27)$$

where the expression for $w(y)$ was used.

The behaviour of a two-dimensional Gaussian beam propagating in a vacuum is thus given by

$$A = a_0 \sqrt{\frac{w_0}{w}} e^{-x^2/w^2} e^{i(\frac{k_0 x^2}{2R} - \varphi)}. \quad (7.28)$$

The spreading of the beam is seen to take place at the same pace in the three- and two-dimensional cases, because the expressions for $w(y)$ are identical in both cases. The reduction in the magnitude of the central amplitude, however, is slower in the two-dimensional case than in three dimensions: In three dimensions the magnitude of the central amplitude dropped according to $w_0/w(y)$, whereas in two dimensions the amplitude reduces as $\sqrt{w_0/w(y)}$.

APPENDIX C

Profiles Flip-Flopping Between States

We now present some preliminary results from the numerical simulations we did to study the evolution of a multi-peaked amplitude profile. This study was motivated by the theoretical analysis done recently by Kurki-Suonio, Morrison and Tajima⁵⁷ according to which asymptotic profiles with multiple peaks could exist for boundary conditions different from those chosen for the solitary profile derived in Section 3.4.

The analytic expression for the asymptotic, multi-peaked profiles was not obtained in the paper by Kurki-Suonio, *et al.*, but an approximate form can be obtained by integrating Eq. (3.45) with respect to the amplitude a in the neighborhood of the potential minimum:

$$\lambda_s = \int_{a_1}^{a_2} \frac{da}{\sqrt{\mathcal{E} - V(a)}}. \quad (7.29)$$

Here a_1 and a_2 correspond to the same total energy of the system⁵⁷, $\mathcal{E} = -\frac{1}{\lambda_c^2} \sqrt{1 + a_i^2} - \frac{1}{2} C_1 a_i^2$, $i=1,2$. (For the case of the solitary profile $\mathcal{E} = -1/\lambda_c^2$ thus fixing a_1 at the origin). Equation (29) gives us an approximate wavelength λ_s between the peaks in the profile corresponding to the specific amplitudes a_1 and a_2 (see Fig. 7.1).

We ran several computer simulation runs with various parameter values for the multi-peaked amplitude profile. Since none of the runs corresponded to the exact solution for the asymptotic equation, the profiles were not expected to remain undistorted. Indeed, quite interesting evolution was observed to take place: the locations of the peaks and troughs of the profile were seen to

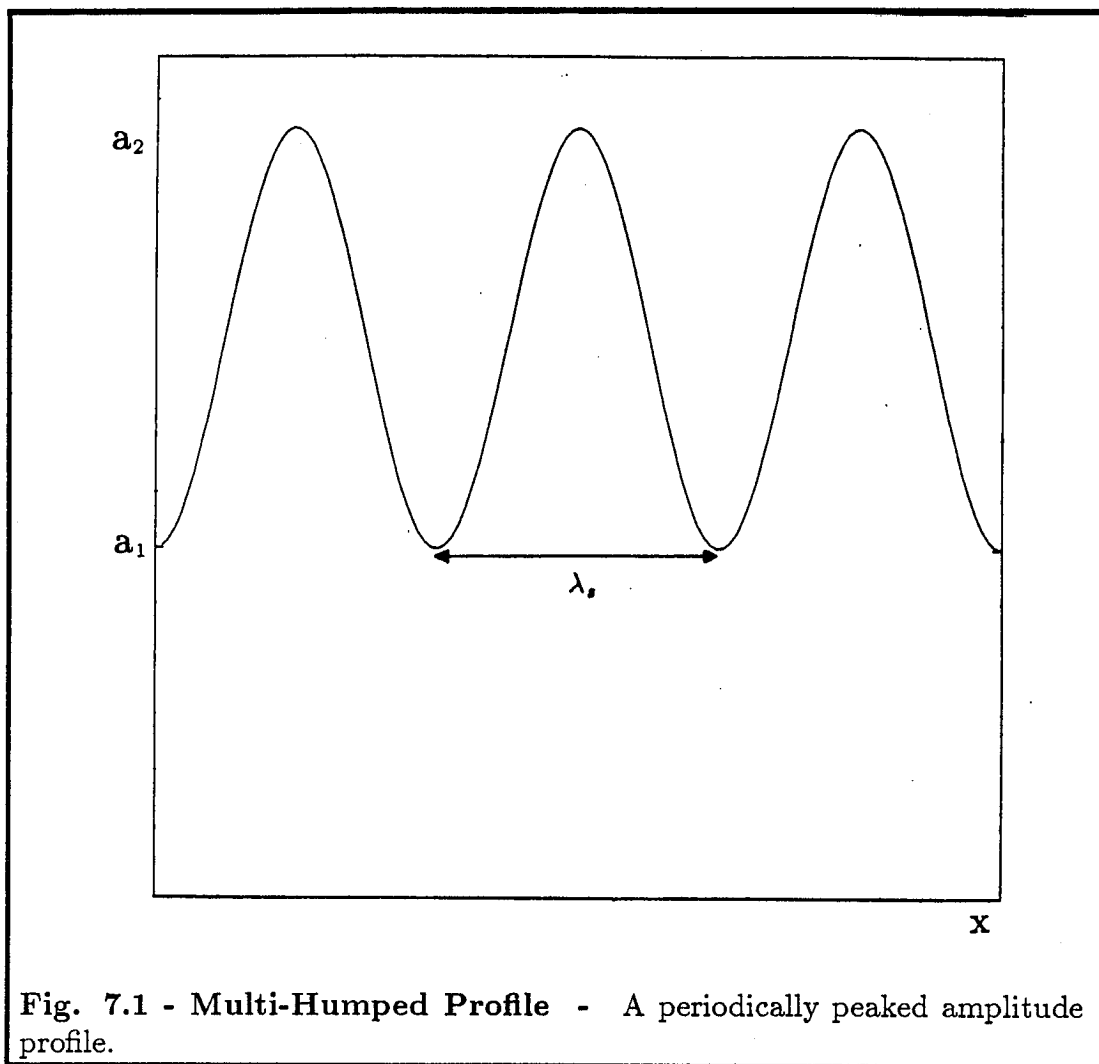


Fig. 7.1 - Multi-Humped Profile - A periodically peaked amplitude profile.

alternate so that for half of the time the peak would be located at the point where the trough was originally and vice versa. Furthermore, the phase shift was observed to exhibit similar behavior but with a $\frac{\pi}{2}$ -phase shift. In Fig. 7.2 we have illustrated the behavior of the field quantities for a specific run with $\lambda_s = 5.12 \lambda_c$, $a_1 = 0.02$, $a_2 = 0.05$.

The time constraints on this project did not allow for detailed theoretical analysis of the problem, but to gain at least some insight on the subject

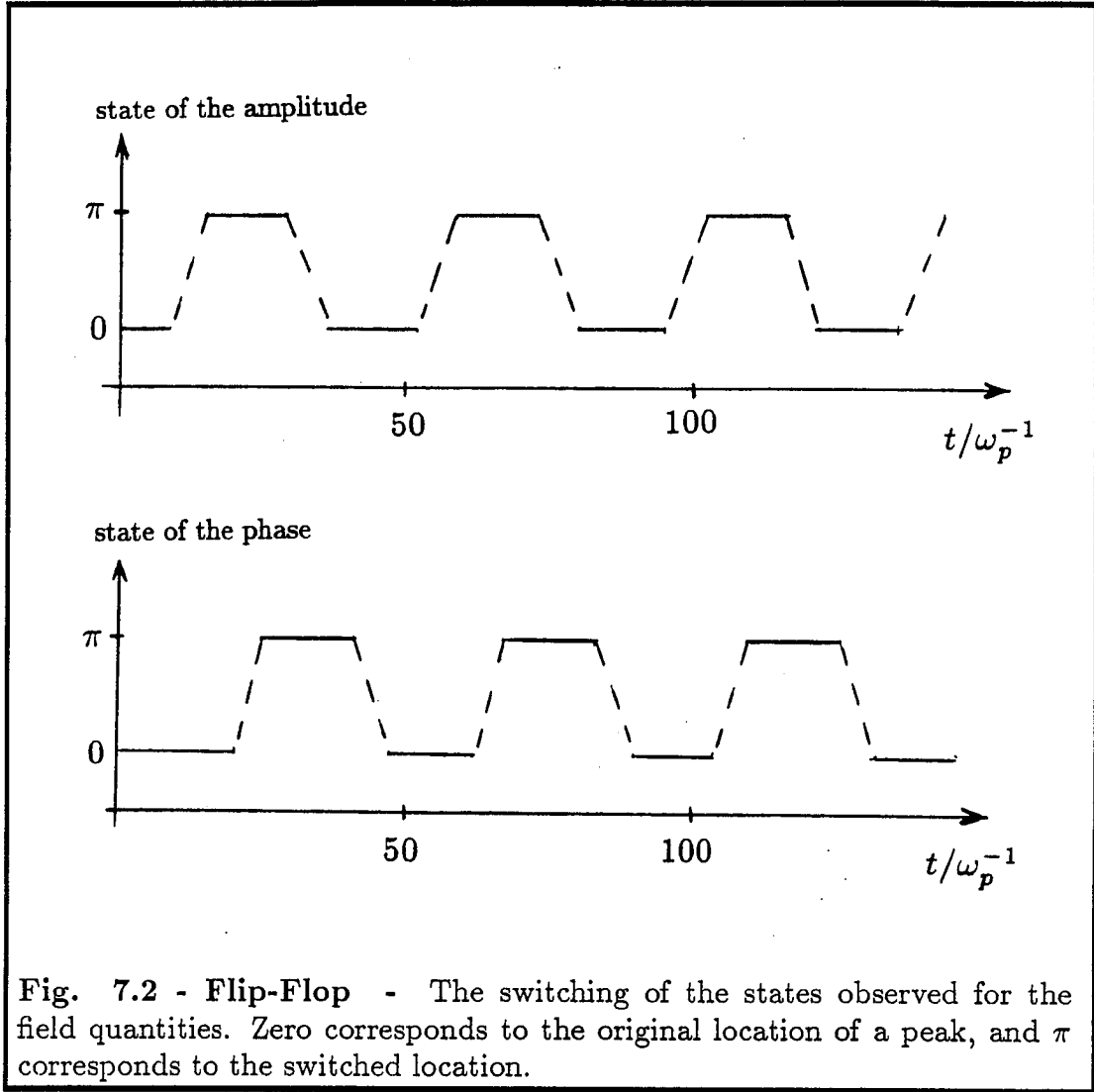


Fig. 7.2 - Flip-Flop - The switching of the states observed for the field quantities. Zero corresponds to the original location of a peak, and π corresponds to the switched location.

and to make sure that what was seen was not a numerical artifact, we studied the relevant field equations for this system at very early times when the process could be taken to be linear. Rewriting Eq. (3.95) in terms of $I \equiv a^2$ it becomes

$$\begin{aligned}
 2k_0 \frac{\partial \psi}{\partial z} - \left(\frac{\partial \psi}{\partial x} \right)^2 - \frac{1}{4} \frac{1}{I^2} \left(\frac{\partial I}{\partial x} \right)^2 + \frac{1}{2} \frac{1}{I} \frac{\partial^2 I}{\partial x^2} = \\
 \frac{1}{\lambda_c^2} \frac{1}{\sqrt{1+I}} \left\{ 1 + \lambda_c^2 \frac{\partial^2}{\partial x^2} \sqrt{1+I} \right\} + k_0^2 - \omega_0^2/c^2.
 \end{aligned}
 \tag{7.30}$$

Linearizing around an initial state given by $I = I_0(x)$, $\psi = 0$,

$$\begin{aligned} I(x, z) &= I_0(x) + I_1(x, z) \\ \psi(x, z) &= \psi_1(x, z), \end{aligned} \quad (7.31)$$

we get

$$\frac{\partial \psi_1}{\partial z} = \frac{1}{2k_0} \left\{ \frac{1}{4I_0^2} \left(\frac{\partial I_0}{\partial x} \right)^2 - \frac{1}{2} \left(\frac{1}{I_0} - 1 + \frac{1}{2} I_0 \right) \frac{\partial^2 I_0}{\partial x^2} \right\}, \quad (7.32)$$

where we have assumed $I_0 \ll 1$ and we have neglected all the terms involving I_1 compared to terms containing I_0 only on the right hand side. Also, the dispersion relation as given by Eq. (3.100) was used.

According to Eq. (32) the phase shift should thus be driven by the gradients of the initial amplitude profile. In the code we have specified the initial profile as

$$a_0(x) = \alpha - \beta \cos(k_s x), \quad (7.33)$$

where $\alpha = \frac{1}{2}(a_1 + a_2)$ and $\beta = \frac{1}{2}(a_2 - a_1)$. For this profile the equation for ψ_1 becomes

$$\begin{aligned} \frac{\partial \psi_1}{\partial z} &= \frac{1}{4k_0} \left\{ \frac{1}{2I_0^2} k_s^2 \beta^2 [2\alpha \sin(k_s x) - \beta \sin(2k_s x)]^2 + \right. \\ &\quad \left. \left(1 - \frac{1}{2} I_0 - \frac{1}{I_0} \right) 2k_s^2 \beta [\alpha \cos(k_s x) - \beta \cos(2k_s x)] \right\}. \end{aligned} \quad (7.34)$$

Therefore, at the locations where the amplitude peaks ($\cos(k_s x) = -1$) the phase shift should start evolving according to

$$\frac{\partial \psi_1}{\partial z} \approx \frac{1}{2k_0} \frac{k_s^2 \beta}{a_2}. \quad (7.35)$$

Accordingly at the trough locations ($\cos(k_s x) = +1$) the phase shift should be given by

$$\frac{\partial \psi_1}{\partial z} \approx -\frac{1}{2k_0} \frac{k_s^2 \beta}{a_1}. \quad (7.36)$$

We ran a few cases varying the separation parameter $k_s = \frac{2\pi}{\lambda_s}$ for the amplitude profile. The simulation results together with the theoretical predictions are summarized in Fig. 7.3. Figure 7.3(a) shows the behavior of the phase shift at the maximum amplitude location, and Fig. 7.3(b) shows the corresponding result for the minimum amplitude location. The scaling in the simulation results is observed to follow that of the theory, and even the numerical values are surprisingly close to the theoretical estimates.

Phenomenologically, what is taking place here seems to be the following: The optical beam has initially a flat phase front and a multi-humped amplitude profile as indicated in Fig. 7.4. The spatial gradients of the amplitude profile drive a deformation of the phase front in such a way that the phase front curvature will be reminiscent of the amplitude profile, i.e. a maximum on the phase front will form where the amplitude peaks etc. (see Fig. 7.4(b)). The curvature of the phase front will now drive the dynamics of the amplitude profile (as indicated by the arrows in Fig. 7.4(b)) so that the profile flattens out and eventually forms new peaks at the locations of the former minima. The new amplitude peaks act back on the phase, and the cycle continues. The system thus flip-flops between two states exhibiting thus some kind of a bistability or breathing.

As mentioned, these results are very preliminary and simplistic. The flip-flop behavior between two states that the amplitude exhibits could be of enormous importance to optical switching; the bistability could lead to an optical analog of an electronic transistor. Therefore this phenomenon deserves a careful and detailed theoretical analysis.

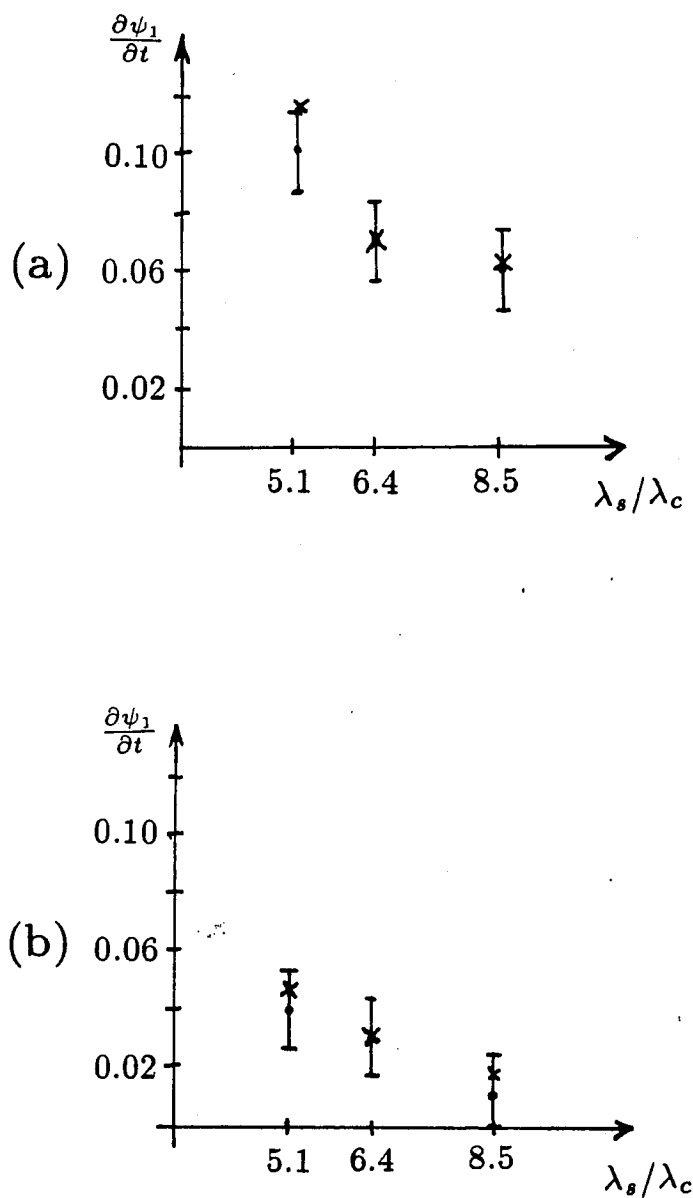


Fig. 7.3 - Simulation Results - The observed growth rate of the phase shift together with the theoretical value. (a) at the location of a peak amplitude value, (b) at the location of a trough.

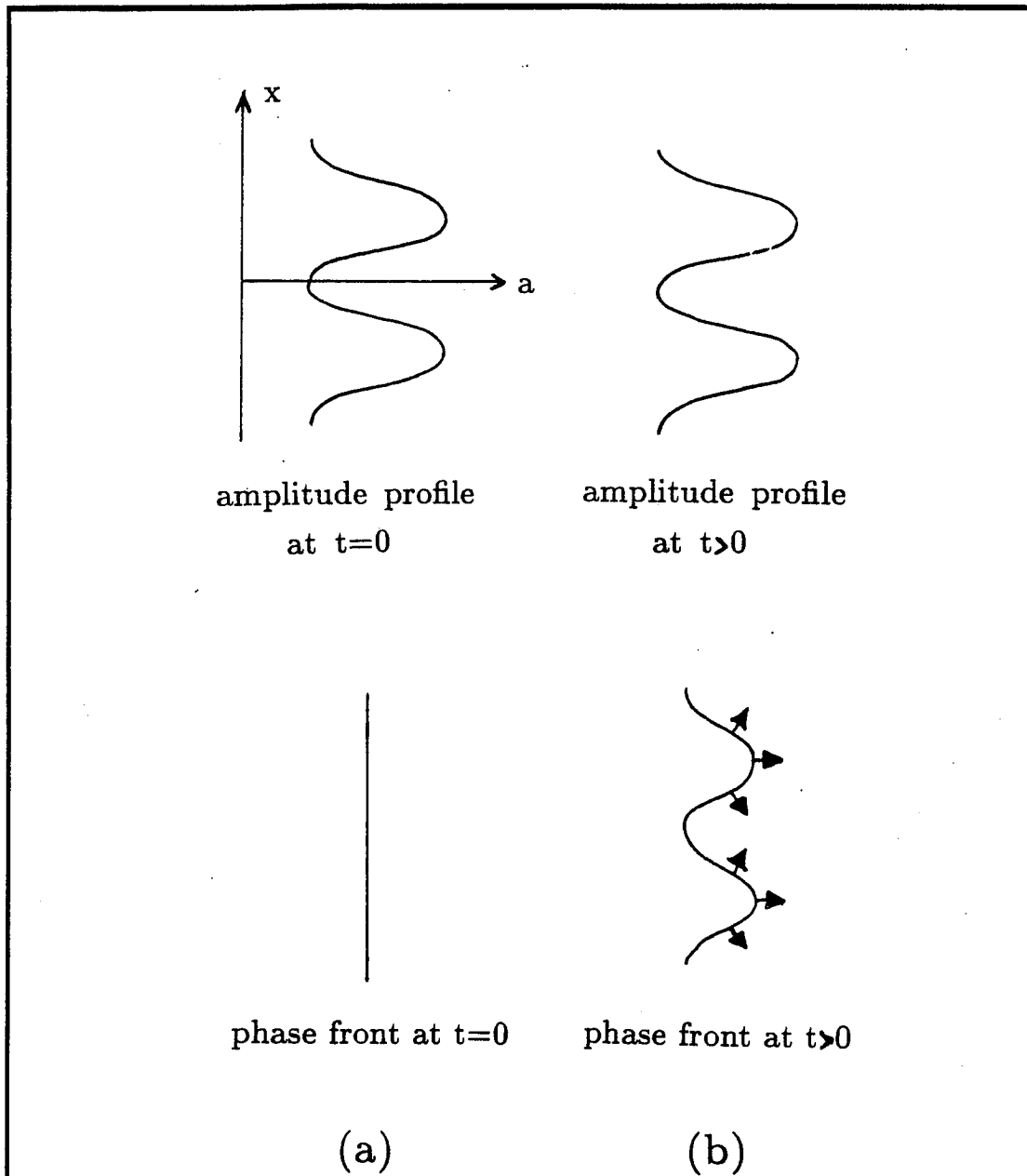


Fig. 7.4 - Interplay of the amplitude and phase - A multi-humped amplitude profile distorts an originally flat phase front. The curved phase front acts back on the amplitude causing periodical structure of self-focusing and defocusing regions.

References

1. J.D. Cockcroft and E.T.S. Walton, Proc. Roy. Soc. A **136**, 619 (1932).
2. E.O. Lawrence and N.E. Edlefsen, Science **72**, 376 (1930).
3. E.O. Lawrence and M.S. Livingston, Phys. Rev. **37**, 1707 (1931).
4. E.O. Lawrence and M.S. Livingston, Phys. Rev. **38**, 834 (1931).
5. E.O. Lawrence and M.S. Livingston, Phys. Rev. **40**, 19 (1932).
6. D.W. Kerst, Phys. Rev. **58**, 841 (1940).
7. D.W. Kerst, Phys. Rev. **60**, 47 (1940).
8. E.M. McMillan, Phys. Rev. **68**, 143 (1945).
9. V.I. Veksler, J. Physics (USSR) **9**, 153 (1945).
10. R. Wideröe, Arch. Electrotechn. **21**, 387 (1928).
11. Ginzton, Hansen, and Kennedy, Rev. Sci. Instr. **19**, 89 (1948).
12. J.L. Bobin, Europhysics News, **19**, 129 (1988).
13. R. Palmer, J. Appl. Phys. **43**, 3014 (1972).
14. N. Rostoker and M. Reiser, *Collective Accelerators*, Harwood Publishers, New York 1979.
15. P. Chen, J.M. Dawson, R.W. Huff, and T. Katsouleas, Phys. Rev. Lett. **54**, 693 (1985).
16. P. Chen, J.J. Su, J.M. Dawson, K.L.F. Bane, and P.B. Wilson, Phys. Rev. Lett. **56**, 1252 (1986).
17. J.B. Rosenzweig Phys. Rev. Lett. **58**, 555 (1987).
18. J.B. Rosenzweig, D.B. Cline, B. Cole, H. Figueroa, W. Gai, R. Konecny, J. Norem, P. Schoessow, and J. Simpson, Phys. Rev. Lett. **61**, 98 (1988).
19. T. Tajima, W. Horton, S. Nishikawa, and T. Nishikawa, to be published in *Laser and Particle Beams*.

20. P. Chen and R. Noble in *Relativistic Channeling*, Eds. R.A. Carrigan and J.A. Ellison, Plenum Press, New York 1987.
21. T. Tajima and M. Cavenago, *Phys. Rev. Lett.* **59**, 1440 (1987).
22. T. Tajima, and J.M. Dawson, *Phys. Rev. Lett.* **43**, 267 (1979).
23. C. Joshi, W.B. Mori, T. Katsouleas, J.M. Dawson, J.M. Kindel, and D.W. Forslund, *Nature (London)*, **311**, 525 (1984).
24. T. Tajima, *Laser and Particle Beams* **3** Part 4, 351 (1985).
25. W. Horton and T. Tajima, *Phys. Rev. A*, **31**, 3937 (1985).
26. W. Horton and T. Tajima, *Phys. Rev. A*, **34**, 4110 (1986).
27. C.J. McKinstrie and D.F. DuBois, *Phys. Rev. Lett.* **57**, 2022 (1986).
28. E. Esarey, A. Ting, and P. Sprangle, *Appl. Phys. Lett.* **53**, 1266 (1988).
53. W.B. Mori, C. Joshi, J.M. Dawson, D.W. Forslund, and J.M. Kindel, *Phys. Rev. Lett.* **60**, 1298 (1988).
30. C. Joshi, C.E. Clayton, and F.F. Chen, *Phys. Rev. Lett.* **48**, 874 (1982).
31. C.E. Clayton, C. Joshi, C. Darrow, and D. Umstadter, *Phys. Rev. Lett.* **54**, 2343 (1985).
32. C.E. Clayton, C. Joshi, C. Darrow, and D. Umstadter, *Phys. Rev. Lett.* **55**, 1652 (1985).
33. M.N. Rosenbluth and C.S. Liu, *Phys. Rev. Lett.* **29**, 701 (1972).
34. C.S. Liu and M.N. Rosenbluth, *Phys. Fluids* **17**, 1211 (1974).
35. K. Mima, T. Ohsuga, H. Takabe, K. Nishihara, T. Tajima, E. Zaidman, and W. Horton, *Phys. Rev. Lett.* **57**, 1421 (1986).
36. T. Tajima, *Nature (London)*, **327**, 285 (1987).
37. T. Tajima, in *Proc. 12th Int. Conf. High Energy Acc.*, Eds. F.T. Cole and R. Donaldson (Fermi Nat. Acc. Lab., Batavia, Ill., 1983), p. 470.
38. W. Demtröder, *Laser Spectroscopy*, Springer-Verlag, Berlin, 1982.

39. V. Stefan, B.I. Cohen, and C. Joshi, *Science* **243**, 494 (1989).
40. E.L. Lindman and M.A. Strosio, *Nuclear Fusion* **17**, 619 (1977).
41. R.Y. Chiao, E. Garmire, and C.H. Townes, *Phys. Rev. Lett.* **13**, 479 (1964).
42. S.A. Akhmanov, A.P. Sukhurov, and R.V. Khokhlov, *Sov. Phys. Uspekhi* **10**, 609 (1968).
43. C.E. Max, *Phys. Fluids* **19**, 74 (1974).
44. G.-Z. Sun, E. Ott, Y.C. Lee, and P. Guzdar, *Phys. Fluids* **30**, 526 (1987).
45. D.C. Barnes, T. Kurki-Suonio, and T. Tajima, *IEEE Trans. on Plasma Science* **PS-15**, 154 (1987).
46. F.W. Perkins and E.J. Valeo, *Phys. Rev. Lett.* **32**, 1234 (1974).
47. R.S. Craxton and R.L. McCrory, *J. Appl. Phys.* **56**, 108 (1984).
48. C.E. Max, J. Arons, and A.B. Langdon, *Phys. Rev. Lett.* **33**, 209 (1974).
49. D.A. Jones, E.L. Kane, P. Lalouis, P. Wiles, and H. Hora, *Phys. Fluids* **25**, 2295 (1982).
50. G. Schmidt and W. Horton, *Comments of Plasma Phys. Controlled Fusion* **9**, 85 (1985).
51. P. Sprangle, C.-M. Tang, and E. Esarey, *IEEE Transactions on Plasma Science* **PS-15**, 145 (1987).
52. F.S. Felber, *Phys. Fluids* **27**, 1410 (1980).
53. W.B. Mori, C. Joshi, J.M. Dawson, D.W. Forslund, and J.M. Kindel, *Phys. Rev. Lett.* **60**, 1298 (1988).
54. C.J. McKinstrie and D.A. Russell, *Phys. Rev. Lett.* **61**, 2929 (1988).
55. I.S. Gradshteyn and I.M. Ryzhik (eq. 2.224) *Table of Integrals, Series, and Products*, Academic Press, New York, 1980.
56. Private Discussion with Dr. P.J. Morrison.

57. T. Kurki-Suonio, P.J. Morrison, and T. Tajima, Submitted to Physical Review A (March 1989).
58. P. Kaw, G. Schmidt, and T. Wilcox, Phys. Fluids **16**, 1522 (1973).
59. F.S. Felber and D.P. Chernin, J. Appl. Phys. **52**, 7052 (1981).
60. E. Persico, E. Ferrari, and S.E. Segre, *Principles of Particle Accelerators*, W.A. Benjamin, Inc. (New York, 1968).
61. Private communication with Dr. Mima.
62. A.B. Langdon and B. Lasinski, Phys. Rev. Lett. **34**, 934 (1975).
63. A.B. Langdon and B. Lasinski, Phys. Fluids **26**, 582 (1983).
64. V.E. Zakharov, Sov. Phys. JETP **35**, 908 (1972).
65. L.M. Degtyarev, I.M. Ibragimov, R.Z. Sagdeev, G.I. Solov'ev, V.D. Shapiro, and V.I. Shevchenko, JETP Lett. **40**, 1282 (1984).
66. D. Russell, D.F. Dubois, and H.A. Rose, Phys. Rev. Lett. **60**, 581 (1988).
67. T. Tajima, *Computational Plasma Physics*, Chapter 6, Addison-Wesley (Reading, Massachusetts 1988).

VITA

Taina-Kaisa Susanna Kurki-Suonio was born in Rovaniemi, Finland, on December 29, 1959, the daughter of Kaija Rönkkö and Olavi Rönkkö. After graduating from Rovaniemen Keskustan Lukio in 1978 she entered the University of Helsinki. She received the degree of Luonnontieteiden Kandidaatti in February 1981, and the degree of Filosofian Kandidaatti in December 1986, both from the University of Helsinki. During years 1981-82 she was employed as a teaching assistant in the Department of Physics. During summers 1980, 81, and 82 she worked as a research assistant for the Geological Survey of Finland. In August 1983, she received a Rotary International Fellowship for graduate studies at the Massachusetts Institute of Technology. On June 9, 1984 she married Hannu Antero Kurki-Suonio. In September 1984 she transferred from M.I.T. to the Graduate School at The University of Texas at Austin. She has authored or coauthored three scientific papers that have been submitted to refereed journals.

Permanent Address:

Taivaanvuohentie 14 C 19
SF-00200 Helsinki
Finland

This dissertation was typed by the author and her husband.